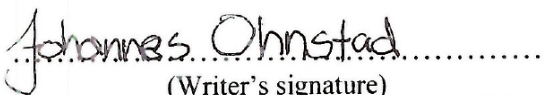




University of
Stavanger

Faculty of Science and Technology

MASTER'S THESIS

Study program/ Specialization: Master in Design and Materials/ Mechanical Engineering	Spring semester, 2013 Restricted access,5years
Writer: Johannes Ohnstad	 (Writer's signature)
Faculty supervisor: Hirpa G.Lemu External supervisor(s): Tommy Svartvatn	
Title of thesis: Experimental study of indentation related to slips design for well intervention plug	
Credits (ECTS): 30	
Key words: Slips(mechanical gripping element) Contact Mechanics, Indentation tests, Well intervention plug	Pages: 75 + enclosure: 60 Stavanger, June 14,2013 Date/year

PREFACE

This master thesis marks the final work of the 2 year Master's degree program in mechanical engineering at the University of Stavanger. The thesis has been written during the spring of 2013 in collaboration with the well technology company E Plug and the University of Stavanger.

I would especially like to thank my supervisors Hirpa Lemu and Tommy Svartvatn who have contributed with guidance, inspiration and input during work with the thesis. I would also like to thank chief engineer at UiS Jan Kåre Bording for providing useful comments and input during the later stages of the thesis work. Thanks to senior engineer at UiS Ahmad Yaaseen Amith for with measurement equipment. Special thanks to my sister Elisabeth for reading preliminary drafts and giving advice and input on the final structure of the thesis. I would like to thank the people who have helped out with many of the practical aspects of thesis, the guys in the workshop at UiS providing material and help to build equipment for the test rig, the guys at Teo Teknikk for providing a suitable load measurement cell on relatively short notice.

I would especially like to thank my parents and family for motivation and moral support during my five year long quest to become an engineer.

Thank you Susanne for keeping up with me during long hours of thesis work and for moral support throughout the thesis.

ABSTRACT

On behalf of the well technology E plug, an experimental study has been conducted on the subject of indentation related to a mechanical component called slips. Slips are a type of metal wedge element with sharpened teeth profiles designed for the purpose of anchoring plugs and other types of downhole equipment in an oil well. Anchoring is achieved by sharpened teeth profiles on the surface of the slips indenting the wall of the production tubing, which in turn causes a radial gripping force that provides resistance to plug movement. E plug has experienced some technical difficulties in determining the ideal geometry for the teeth profiles on their slips, which is used on their well intervention plug, the TorcPlug®.

The goal of the thesis has been to find a correlation between applied load, indentation pressure, surface area, indenter angle and depth of penetration. This, in turn could prove beneficial in design of teeth profiles for the TorcPlug®. Based on the theory studied on the subject of indentation, seven indenters were tested during a series of indentation tests. The indenters had different geometries which purpose was to resemble the teeth profiles on the slips. The indentation tests were performed at E Plug's workshop.

A hypothesis related to indentation pressure, indenter hardness and depth of penetration for each of the indenters was developed before testing. The hypothesis for all except one of the indenters was based on a theory called the slip line field theory. The indenters were made of the steel grade AISI 4140, heat treated to a hardness value of 50-51HRc. The steel which indentations were made on was chosen in order to resemble the mechanical properties of production tubing and was also of the steel grade AISI 4140. However a grade with different mechanical properties and a hardness value of around 18-22HRc. Indentation tests were performed with a hydraulic press. The plastic impression left on the indented steel was measured by the use of a microscope at UiS, measured results were then compared and analyzed together with load data.

The test results showed that the slip line field theory did not accurately predict the indentation pressure or the depth of penetration for 60° and 120° angled wedge shaped indenters. The deviation between theoretical and measured values is likely due to the assumption of plane strain (2-dimensionality) not being fulfilled which is an important assumption in slip line field theory. However, a large collection of measured data in relation to geometric properties of the indentations at a wide range of loading has been produced. Regression curve analysis has been performed on the measured data and an iterative equation based on the curves that produces approximately correct values has been suggested.

A successful method of calculating indentation pressure, depth of penetration and plastic surface area at a given load has been discovered for a pyramid shaped indenter with a 90° face angle. The theoretical calculations matched the test results by a margin of less than one percent on the lowest load to three percent on the highest load. A mathematical model for calculating the indentation pressure for axi-symmetric pyramid shaped indenters of different angles has been presented. The model is called the expanding cavity model. The indentation pressure calculated by using the model is supported by physical data from the indentation tests.

The two most effective indenters in terms of depth of penetration in relation to the applied load were the pyramid and 60° wedge indenters. At loads up to around 1100kg the pyramid is the most effective in terms of penetration. Between 1100-1450kg there is a transition area where the 60° wedge indenter becomes more effective than the pyramid.

Unfortunately the indenters that were tested for the purpose of demonstrating the relation between surface area and indentation pressure failed as a result of excessive deformation during testing. The deformation of these indenters can be accounted to an incomplete heat treatment which led to a lower total hardness value. Two of the other indenters that were tested experienced minor deformation at the first stage of testing. The deformation of these two indenters gradually worsened as the applied load was increased during the later stages of testing.

For future design considerations the teeth profiles chosen for slips application should have a hardness value of at least two and a half times that of the indented metal (tubing). Preferably the hardness ratio should be even higher if possible. The profiles should have the same volume in order to achieve equal hardness from heat treatment procedures.

A proposed design for a slip element has been produced. Teeth profiles chosen are similar to the pyramid indenter which during the course of the study has been found to be the most suited indenter profile for slips application.

GLOSSARY OF TERMS AND ABBREVIATIONS

Indentation:	The act of cutting into an edge/surface with tooth like notches or angular incisions
Indenter:	The object which performs the indentation
Production Tubing:	Production steel pipe. The final string of pipe run in a producing oil well.
Packing element:	A rubber sealing element that forms a fluid-tight seal.
Downhole:	General term that is used in reference to operations, tools and activities in an oil well.
Well intervention:	A well intervention is any operation carried out on a well, during, or at the end of its productive life, that alters the state of the well and or well geometry, provides well diagnostics or manages the production of the well.
Slickline:	Metal wire used to lower tools in different well operations.
Bridge plugging:	A term used for isolation of a zone in an oil reservoir.
Completion:	Completion is a generic term used to describe the assembly of downhole tubulars and equipment required to enable safe and efficient production from an oil or gas well.
ID:	Inner diameter
OD:	Outer diameter
HRC:	Rockwell hardness
mm:	millimetres
N:	Newton, kgm/s^2
g:	Gravity acceleration constant $9,81\text{m/s}^2$
kg:	Kilograms

J_2 :	Second deviatoric stress invariant
$\sigma_1, \sigma_2, \sigma_3$:	Principal stresses in the state of combined stress
K:	Yield stress of a material in pure shear
Y:	Yield stress of material in tension/compression
τ_{\max} :	Maximum shear stress, Tresca criterion
ϵ :	Strain component
α – line:	α -slip line, 45° to the directions of principal stress
β – line:	β -slip line, 45° to the directions of principal stress
$\Delta\phi_\alpha$:	Angular change on an α -slip line
$\Delta\phi_\beta$:	Angular change on an β -slip line
p :	Indentation pressure/normal pressure acting on a slip-line
$\Delta\phi_{PRQ}$:	Angle between three slip-lines in an penetrating slip line field
H:	Thickness of indented plate
L:	Length of the indenter
α :	Semi angle of wedge/half angle
Ψ :	Angle associated with the α -angle in wedge indentation
P_w :	Load per unit width, usually in N/mm
h :	Hypotenuse wedge impression
P :	Load on indenter, usually in kilograms
L_i :	Width of impression
l :	Length of indenter perpendicular to the indenter face
A_s :	Surface area of indenter or plastic surface
d :	Diagonal length of pyramid impression
h_p :	Depth of penetration, pyramid
D_{mean}	Average diagonal length

Y_f :	Flow stress, yield stress or the associated flow stress related to work-hardening
σ_r :	Radial component of stress
a :	Core radius expanding cavity model
c :	Boundary radius expanding cavity model
ν :	Poissons ratio
ϵ_R :	Representative strain at a given flow stress
E :	Elastic modulus
E^* :	Combined elastic modulus
β :	Inclination from the face of the indenter to the surface
σ_H :	Hardness stress N/mm ²
I_r :	Indentation ratio

TABLE OF CONTENTS

Preface	iii
Abstract	iv
Glossary of Terms and Abbreviations	vi
Table of Contents	ix
List of figures	xii
List of tables	xiv
1 Introduction	1
1.1 Scope.....	3
1.2 Report structure.....	3
2 Theory	4
2.1 Governing equations for yield stress.....	5
2.2 Slip-line field theory	6
2.2.1 Rigid-perfectly plastic solid	6
2.2.2 Plane-strain deformation	7
2.2.3 Governing equations of plane strain	7
2.2.4 Hencky's relation	8
2.3 Plane strain indentation	11
2.4 Flat punch indentation	11
2.5 Indentation by flat punch as a function of plate geometry	14
2.6 Indentation by wedge formed indenter.....	15
2.7 Deformation of the Indenter	17
2.8 Mechanical properties of tubing.....	18
3 Experimental	19
3.1 Material properties.....	19
3.2 Guidelines and equipment.....	20
3.3 Indenter geometries & load calculations	22
3.4 Adjustments	22
3.5 Square	23
3.6 Rectangle	24
3.7 Wedge 60°.....	25
3.8 Wedge 120°	28
3.9 Pyramid.....	30
3.10 Double wedge 60°	32
3.11 Setup & execution	33

4	Results	35
4.1	Deformation of the indenters	35
4.2	Observations & adjustments.....	37
4.3	Wedge 60°	38
4.4	Increased loading of wedge 60°.....	39
4.5	Wedge 120°	41
4.6	Increased loading wedge 120°.....	42
4.7	Double wedge 60°	44
4.8	Increased loading double wedge 60°	47
4.9	Pyramid.....	49
4.10	Increased loading pyramid	50
5	Discussion of results	52
5.1	Deviation between theoretical and measured values.....	52
5.1.1	Wedge 60°.....	52
5.1.2	Wedge 120°.....	54
5.1.3	Double wedge 60°	55
5.1.4	Pyramid.....	56
5.2	Regression curve analysis.....	57
5.3	Depth of penetration in relation to applied load.....	58
5.4	Expanding cavity model.....	60
5.5	Plastic impression analysis.....	64
5.6	Probable reasons for deviations	65
5.7	Deformation.....	65
5.8	Potential sources of error in results	66
5.9	Design considerations	67
5.10	Proposed slips design	68
5.11	Relevance of the testst results and study	70
6	Conclusions.....	71
7	Suggestions for further work	73
8	References.....	74
	Literature list	74
	Figure referances.....	75

APPENDIX A. Indentation Test Procedure	76
A.1. Equipment list.....	76
A.2. Equipment setup	78
A.3. Guidelines	79
A.4. Load calculations.....	79
A.5. Square	81
A.6. Rectangle	83
A.7. Wedge 60°	85
A.8. Wedge 120°	87
A.9. Pyramid.....	89
A.10. Double Wedge 60°	87
A.11. Load cell technical sheet.....	89
APPENDIX B. $\Delta\phi PRQ$-values	90
APPENDIX C. Material certificates.....	92
C.1. Mechanical properties indented steel	92
C.2. Mechanical properties indenter steel before heat treatment	93
C.3. Heat treatment procedure for indenters	95
C.4. Load measurement cell certificate	96
APPENDIX D. Measured values	97
D.1. Wedge 60°	97
D.2. Wedge 120°	99
D.3. Double Wedge 60°	100
D.4. Pyramid.....	104
APPENDIX E. Regression curves	106
E.1. Wedge 60°	106
E.2. Wedge 120°	109
E.3. Double Wedge 60°	111
APPENDIX F. Plastic impression analysis.....	113
APPENDIX G. Proposed slips element design drawings & Wedge adjustment	113
APPENDIX H. Load cell data and measurement photos	118
APPENDIX I. Pre-study report.....	118

LIST OF FIGURES

Figure 1: TorcPlug® in iso view and its placement inside the production tubing.[1]	1
Figure 2: A slips element prototype that was tested on the TorcPlug®.[2]	2
Figure 3: A complete slips model before it is expanded into the tubing wall. [3]	2
Figure 4: Illustration of a slips element inside the production tubing.[2]	4
Figure 5: Simple illustration of the slips-teeth indentation of the tubing wall.[2]	5
Figure 6: Stress versus strain curve for rigid-perfectly plastic solid.[4]	6
Figure 7: Stress element for a plain strain deformation.[5]	7
Figure 8: Illustration of the stress components and the slip lines.[6]	9
Figure 9: Mohr's circle for plain strain.[6]	9
Figure 10: Net of straight lines and centered fan.[2]	11
Figure 11: Plane strain indentation by a flat punch.[2]	12
Figure 12: Slip-line field at yield stress for indentation of plate of finite depth ($2a=L$).[7]	14
Figure 13: Slip line pattern for two dimensional wedge penetrating a rigid-perfectly plastic.[2]	15
Figure 14: Penetration of rigid perfectly-plastic metal by wedge with different semi-angles [8]	17
Figure 15: Assembly drawing of equipment setup.[2]	21
Figure 16: Square flattop indenter.[2]	23
Figure 17: Rectangle flattop indenter.[2]	24
Figure 18: Wedge 60° indenter.[2]	25
Figure 19: ψ -angle for a wedge semi angle of 30°.[8]	26
Figure 20: Wedge 120° indenter.[2]	28
Figure 21: ψ -angle for a wedge semi angle of 60°.[8]	29
Figure 22: Pyramid indenter.[2]	30
Figure 23: Double wedge 60° indenter.[2]	32
Figure 24: Equipment setup.[2]	34
Figure 25: Surface of steel plate with net of lines.[2]	34
Figure 26: Deformed rectangular and square indenters.[2]	35
Figure 27: Deformed triangle indenter.[2]	36
Figure 28: photo of 60° and 120° wedges after the first series of testing.[2]	36
Figure 29: Width and length measurements of wedge 60° indentations.[2]	38
Figure 30: Measured average width and standard deviations.	39
Figure 31: Wedge 60° indenter after testing with increased loading.[2]	40
Figure 32: Width and length measurements for wedge 120° indentation.[2]	41
Figure 33: Measured average width and standard deviation.	42
Figure 34: Measured average width increased loading series.	43
Figure 35: Wedge 120° after testing with increased loading.[2]	43
Figure 36: Width and length measurements of the first double wedge profile.[2]	44
Figure 38: Width and length measurements of the second double wedge profile.[2]	44
Figure 38: Measured average width and standard deviation for double wedge 60°	45
Figure 39: Difference between average width profile 1&2	46
Figure 40: Measured average width, increased loading series	47
Figure 41: Double wedge 60° after testing with increased load. [2]	48
Figure 42: Measurement of diagonals for pyramid indentation.[2]	49
Figure 43: Dmean and standard deviation for pyramid indentations	50
Figure 44: Dmean 7,5% increased load versus Dmean series 1-3.	51
Figure 45: Pyramid indenter after testing with increased loading.[2]	51
Figure 46: Measured average width compared theoretical average width.	52
Figure 47: Measured width compared to theoretical width wedge 120°	54
Figure 48: Measured average width compared to theoretical width for double wedge 60°	55

Figure 49: Dmean versus the theoretically calculated values.....	56
Figure 50: Regression curve analysis	57
Figure 51: Depth of penetration versus applied load first three test series	59
Figure 52: Pyramid and increased loading wedge series compared	59
Figure 53: Cavity model of a pyramid/cone indentation.[10].....	60
Figure 54: Slip element seen from isometric view with pyramid profiles on the top surface.[2]68	
Figure 55: Slip element seen in front view with pyramid profiles and tail groove.[2]	69
Figure 56: Ramp formed underside of the slip element with tail groove.[2]	69

LIST OF TABLES

Table 1: Yield stress, ultimate tensile strength and elongation of different API grades.[9].....	18
Table 2: Mechanical properties of AISI 4140 indenter steel before heat treatment.	19
Table 3: Mechanical properties of AISI 4140 steel plate.	20
Table 4: Chemical composition.....	20
Table 5: Assembly list.....	21
Table 6: Measured average values and standard deviation for different parameters	38
Table 7: Increased loads	39
Table 8: Average measured length and width.....	40
Table 9: Average data for wedge 120°	41
Table 10: Average measured data for increased loading series	42
Table 11: Average data for double wedge 60°	45
Table 12: Difference between average data for profile 1&2	46
Table 13: Table of data increased loading series, double wedge 60°	47
Table 14: Average measured data for Pyramid indentations.....	49
Table 15: Average measure values 7,5% increased loading.....	50
Table 16: Measured width compared to the theoretical width increased loading	53
Table 17: Measured width compared to the theoretical width increased loading series	54
Table 18: Measured width compared to the theoretical width for increased loading series	55
Table 19: Dmean compared to theoretically predicted values.....	56
Table 20: Mechanical properties for indenter and indented steel plate.....	62
Table 21: <i>Ir</i> ratio for the first three test series	64

1 INTRODUCTION

The oil and gas industry is constantly looking for safer, faster and more efficient ways of producing hydrocarbons both offshore and onshore. It is in the general interest of the field operators to reduce downtime and increase efficiency related to installation and maintenance. In doing so the costs of lost production and high day-rates for offshore rigs are reduced. This gives a powerful drive to develop better and smarter downhole-equipment for well operations such as completion and well intervention.

E Plug is a Norwegian based well technology company founded in 2008 by a group of engineers and technicians with many years of experience from working in the oil industry. The company is currently in the latter stages in the development of their main product, the TorcPlug® seen in Figure 1 below.

TorcPlug® is an electrical multiple set and release plugging device developed through a new patented method of transferring downhole forces without the use of explosives or pressurized chambers. It can be run on an electrical line or a slick line that uses a downhole battery package. TorcPlug® has various applications with regards to well intervention operations such as leak detection, pump through operations and bridge plugging. The main benefits with TorcPlug® is the multiple set and release feature which reduces the number of runs and provides a more cost efficient and time saving operation. Time is saved since the plug does not need to be pulled from the well and re-dressed between each run.



Figure 1: TorcPlug® in iso view and its placement inside the production tubing.[1]

TorcPlug® is set at the desired depth in the production tubing by using a torque created by an electrical motor. The torque creates an axial force that expands the slips and packing element outwards and anchors the plug to the tubing ID. Slips are a type of metal wedge element with sharpened teeth that digs into the metal of the tubing and is used for anchoring of various downhole tools. They are usually made of steel and have a surface with hardened teeth which

are designed to indent the tubing wall. A slips element prototype tested on the TorcPlug® can be seen in Figure 2.



Figure 2: A slips element prototype that was tested on the TorcPlug®.[2]

The axial force that expands the slips elements outwards and causes indentation on the tubing ID, is generated by what is called an upper and lower slips cone. The cones are shaped to match the back of the slips and form a ramp that drives the slips outward and into the tubing when the setting force is applied. The outward expansion of the slips and the following indentation of the tubing by the teeth provide a radial gripping force that anchors the plug to the tubing ID. The TorcPlug® is designed with five slips element distributed around the circumference of the plug. A complete model of slips with upper and lower slips-cone is shown in Figure 3 below.

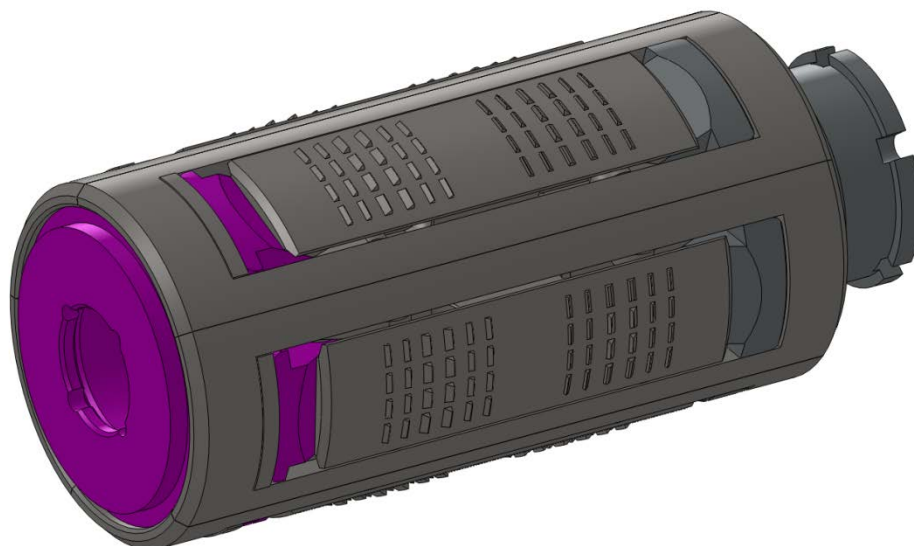


Figure 3: A complete slips model before it is expanded into the tubing wall. The coloured area illustrates the lower slipscone. [3]

The plug is run in the oil well with an open ball valve which is located in front of the slips and packing element, seen in Figure 1. This allows for equal pressure on both sides of the plug. When setting depth is reached, the slips are expanded and the plug is anchored to the tubing ID, a fluid tight seal is formed following compression of the rubber packing element. The ball valve is then closed and a substantial differential pressure is created below and above the slips and packing element. In operation the plug must be able to withstand very high differential pressures both from above and below the slips and packing element. The pressure rating of the TorcPlug® is 517 bar differential pressure. It is therefore of vital importance that the slips teeth indent the tubing wall deep enough to provide sufficient resistance to axial plug movement. A useful animation of setting mechanism and application can be seen at E Plugs homepage [1].

1.1 SCOPE

E plug have experienced some technical difficulties in determining the ideal geometry for the teeth profiles on the slips which is to be used on the TorcPlug®. E Plug therefore wished that a study was carried out on the subject of indentation in relation to indenter profiles that could prove to be beneficial in the design and use as teeth profiles for slips. A mathematical framework that could accurately describe the different mechanisms involved in an indentation process was the goal of the thesis. This involved aspects such as accurately predicting the depth of penetration in relation to the applied force. The difference in pressure needed to produce an indentation related to surface area and angle of the indenter, necessary indenter hardness and the amount deformation left on the indented material. An experimental part of the study involved a series of tests with indenters of different geometries. The tests were carried out based on various hypotheses developed from studied literature on the subject of indentation. Test results were studied, analysed and compared to theoretical values.

From E Plugs perspective this study could aid in the process of determining the ideal geometry of the teeth profiles as well as provide useful insight to different design considerations. The TorcPlug® is currently only designed for application in wells with 5 1/2" O.D production tubing, the mathematical framework could allow for easier to up-scaling of the slips elements, should the TorcPlug® be up-scaled for use in wells with larger tubing diameter.

1.2 REPORT STRUCTURE

The rest of the thesis is organized as follows. Chapter 2 discusses the relevant theory of indentation and contact mechanics. Governing equations describing yield stress, plain strain condition and the slip-line field theory is presented. The experimental work is presented in chapter 3 where topics like material properties, indenter geometries, examples of load calculations, equipment, test setup and execution is discussed. Test results are presented in chapter 4 in the form of graphs and tables. In chapter 5 the test results are compared to the theoretically predicted values. Possible reasons for trends, deviations, analysis, a new model and design considerations are discussed. A proposed slips design is presented at the end of the chapter. The thesis report is concluded with conclusions and suggestions for future work in chapter 6 and 7.

2 THEORY

Normally, in structural problems, one design against yielding and plastic deformation, but in the case of indentation, yielding and plastic deformation is a desired condition. In design of slips for the TorcPlug®, the wish is for the teeth to have a shape and geometry that effectively causes yielding and penetration. At the same time the deformation needs to be highly localized so the structural integrity of the tubing remains intact. Placement of a slips element relative to the production tubing is shown in Figure 4.

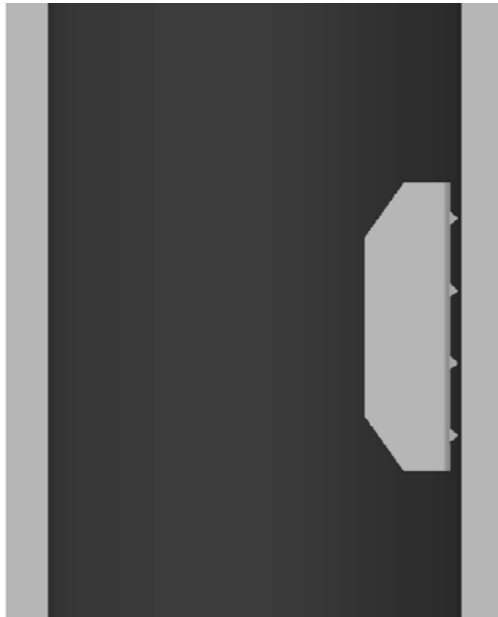


Figure 4: Illustration of a slips element inside the production tubing.[2]

From the literature studied on the subject of indentation and contact mechanics, the general consensus is that an indentation process can be divided into three ranges of loading: purely elastic (below yield), elastic-plastic (contained mode) and fully plastic (uncontained mode).

The purely elastic mode of indentation occurs at loading below the yield stress of the indented material and the deformation process is reversible. The elastic mode of indentation is described by the Hertzian equations of contact mechanics.

The elastic plastic, contained mode of indentation occurs at a loading lying between yield stress and 3 times the yield stress of the indented material. In this range of loading the deformation and plastic flow is contained by the elastic part of the material, the plastic zone is small and fully contained by material which remains elastic, there is no large scale impression visible on the indented material.

The fully plastic, uncontained mode occurs at a value about 3 times the yield stress depending on the geometry of the indenter and friction at the interface. The deformation at this loading is fully plastic where displaced material is free to escape to the side of the indenter by plastic flow. The uncontained mode of deformation is described by a theory known as slip-line field theory.

The range of loading which is relevant for the problem in this thesis is the fully plastic mode. The desired effect of the teeth profiles indenting the tubing wall is that they penetrate the wall to a sufficient depth in order to create enough friction between the slips and the wall so that the plug is anchored in place, as illustrated in Figure 5. This deformation process is of a largely plastic nature.

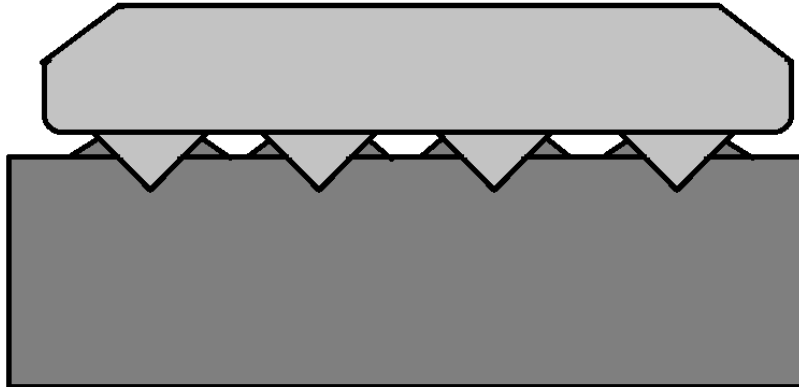


Figure 5: Simple illustration of the slips-teeth indentation of the tubing wall.[2]

2.1 GOVERNING EQUATIONS FOR YIELD STRESS

From the theory of material science and mechanics we know that the plastic behavior of a metal commences when stresses acting on the metal exceeds the yield stress (Y). The governing equations of yield in a stress field where two solids are in contact is given by either von Mises' (shear) strain-energy criterion or by Tresca's maximum shear strain criterion. The yield stress is determined by the yielding of the more ductile material, given in a simple tension/compression test. The difference in the predictions of yield between the two criterions is discussed in chapter 2.4.

Von Mises's shear strain-energy criterion:

Mathematically this yielding criterion is given by Equation(2.1):

$$J_2 = \frac{1}{6} [(\sigma_1 - \sigma_2)^2 + (\sigma_2 - \sigma_3)^2 + (\sigma_1 - \sigma_3)^2] = k^2 = \frac{1}{3} \cdot Y^2 \quad (2.1)$$

Where J_2 is the second deviatoric stress invariant, $\sigma_1, \sigma_2, \sigma_3$ are the principal stresses in the state of combined stress, k and Y denotes the value of the yield stress in pure shear and tension/compression respectively.

Tresca's maximum shear strain criterion:

Mathematically this yielding criterion is given by Equation(2.2):

$$\tau_{\max}\{|\sigma_1 - \sigma_2|, |\sigma_2 - \sigma_3|, |\sigma_3 - \sigma_1|\} = 2k = Y \quad (2.2)$$

2.2 SLIP-LINE FIELD THEORY

The most common way of analyzing a plastic indentation process is by constructing a slip-line field. This is a graphical approach, which illustrates the flow pattern from point to point in the deforming metal and is referred to as slip-line field analysis. The term should not be confused with slip-lines or slip-bands which can be observed when examining metal samples under a microscope. The slip lines refer to planes of maximum shear stress which are 45° to the directions of principal stress and are denoted as α, β -lines. The analysis is based upon a deformation field that is geometrically consistent with the shape change. The assumptions for construction of slip-line field are usually:

- Metal is isotropic and homogeneous.
- The metal is treated as rigid-perfectly plastic.
- Plane strain deformation.
- Temperature effects, strain rate, and time are not considered.
- Constant shear stress at the interface boundary. Usually, either a frictionless condition or sticking friction is assumed.

2.2.1 Rigid-perfectly plastic solid

In the rigid-perfectly plastic solid model seen in Figure 6, the elastic component of strain is neglected. The plastic deformations are so severe that the plastic strains are large compared to the elastic strains. This approximation can only be made when the yield stress of the metal is exceeded and the nature of the process involves plastic flow and the plastic material has freedom to flow in some direction. The flow stress is treated as constant meaning the effect of work hardening is neglected. If an easy direction of flow is available and the elastic strains can be neglected in the plastic zone, there still exists a boundary layer/ transition region between the elastic and plastic zone where elastic and plastic strains are comparable, the smaller this region is the better the approximation becomes.

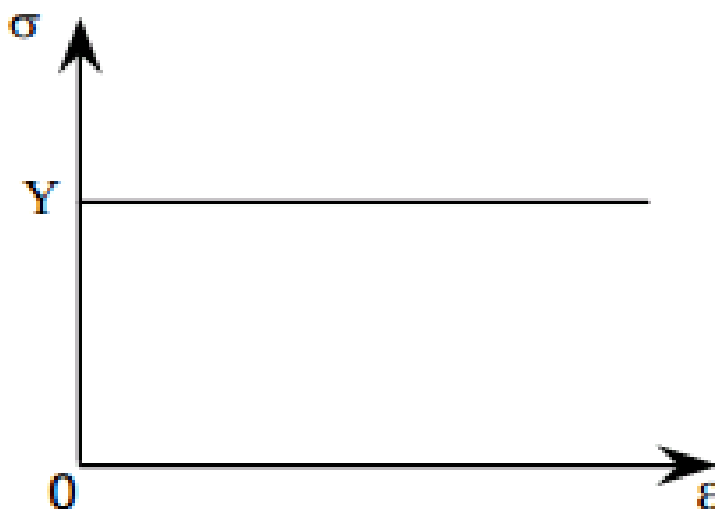


Figure 6: Stress versus strain curve for rigid-perfectly plastic solid.[4]

2.2.2 Plane-strain deformation

Indentation is approximated as a plane-strain deformation condition. The properties of plane strain deformation are that the metal flow is always parallel to a given plane, i.e. there is no displacement or motion of metal in the direction perpendicular to the plane of flow. From this assumption, metal flow occurs in planes parallel to the x-y plane in reference to coordinate system in Figure 7. No movement of metal occurs in the z direction. A plane strain deformation therefore becomes two-dimensional. The length of the indenter in z-direction is assumed the same length as the plate being indented, or infinitely long.

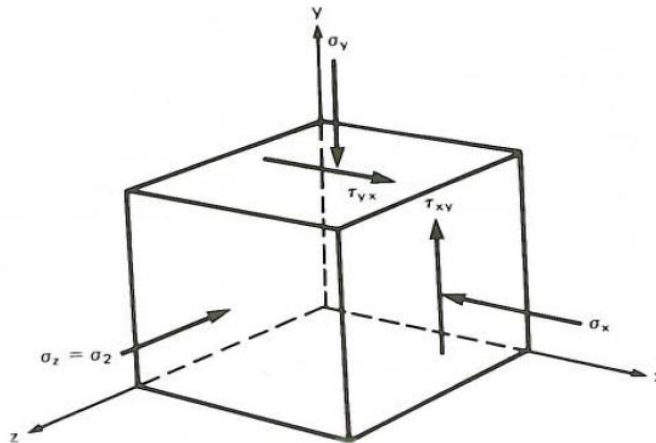


Figure 7: Stress element for a plain strain deformation.[5]

2.2.3 Governing equations of plane strain

A plain strain condition gives the strain components in Equation (2.3):

$$\begin{aligned}
 \epsilon_{zz} = \epsilon_{xz} = \epsilon_{yz} &= 0 \\
 \epsilon_{xx} = \frac{\partial u}{\partial x}, \quad \epsilon_{yy} = \frac{\partial v}{\partial y} &\rightarrow \epsilon_{xx} = -\epsilon_{yy} \\
 \epsilon_{xy} &\neq 0
 \end{aligned} \tag{2.3}$$

$$\tau_{zy} = \tau_{xz} = 0$$

$$\sigma_2 = \sigma_{zz} = \frac{1}{2}(\sigma_1 + \sigma_3) \tag{2.4}$$

Thus σ_2 is a principal stress, so at yield σ_2 must be the mean or hydrostatic stress at any point in the field of deformation. Inserting Equation (2.4) into (2.1) leads to the following expression of the Von Mises criterion in Equation (2.5) :

$$\left[\left(\sigma_1 - \frac{1}{2}(\sigma_1 + \sigma_3) \right)^2 + \left(\frac{1}{2}(\sigma_1 + \sigma_3) - \sigma_3 \right)^2 + (\sigma_1 - \sigma_3)^2 \right] = 6k^2 = 2 \cdot Y^2 \tag{2.5}$$

$$\rightarrow \frac{3}{2}(\sigma_1 - \sigma_3)^2 = 6k^2 = 2 \cdot Y^2$$

Where the expression for k and Y is described in Equations (2.6) & (2.7):

$$k = \frac{(\sigma_1 - \sigma_3)}{2} \quad (2.6)$$

$$2k = \frac{2}{\sqrt{3}}Y \quad (2.7)$$

The expression for the principal stresses is described in Equation (2.8):

$$\sigma_1 = \sigma_2 + k \quad \sigma_3 = \sigma_2 - k \quad (2.8)$$

In plain strain deformation the intermediate stress is always σ_2 . The mean stress σ_2 has no influence upon yielding, it is the constant shear stress k which causes yielding. Yielding occurs when shear yield stress, k is reached and the yield criterion for this situation is shown in Equation (2.9):

$$k^2 = \frac{(\sigma_{xx} - \sigma_{yy})^2}{4} + \tau_{xy}^2 \quad (2.9)$$

Plain strain deformation causes a state of stress that can be considered as a pure shear deformation with a superimposed hydrostatic stress that can vary from point to point in the region of deformation.

2.2.4 Hencky's relation

In plain strain the equilibrium Equations(2.10) become:

$$\begin{aligned} \frac{\partial \sigma_{xx}}{\partial x} + \frac{\partial \tau_{xy}}{\partial y} &= 0 \\ \frac{\partial \sigma_{yy}}{\partial y} + \frac{\partial \tau_{xy}}{\partial x} &= 0 \end{aligned} \quad (2.10)$$

Analyzing a curvilinear element in the x-y plane on which shear stress and hydrostatic stresses acts upon, the x- and y-directions do not correspond with the direction of the α, β -lines. As illustrated in Figure 8, the α, β -slip lines are $\pm 45^\circ$ to the principal stresses σ_1, σ_3 where $\sigma_1 > \sigma_3$.

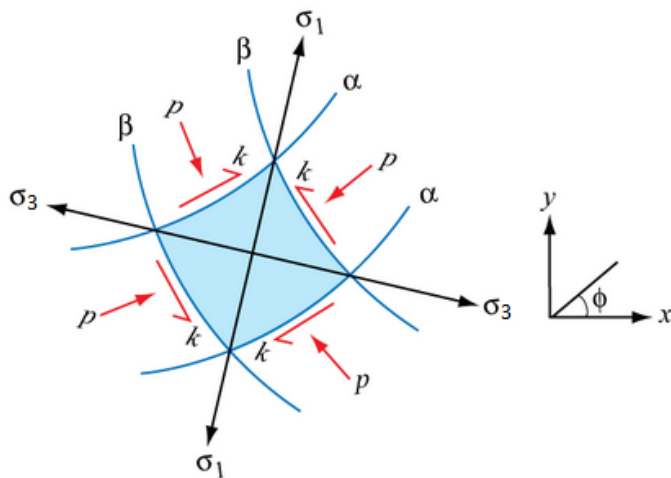


Figure 8: Illustration of the stress components and the slip lines.[6]

The angle of rotation between α, β -lines, ϕ , is considered positive for counterclockwise movement from x - and y -axis. If an α -line makes an angle ϕ with the x -axis, the β -line must then make an angle of $\phi + 90^\circ$ with respect to the x -axis. Clockwise and counterclockwise movement from an α to β line always passes the direction of one of the maximum principal stresses.

The stress state on Mohr's circle looks as shown in Figure 8:

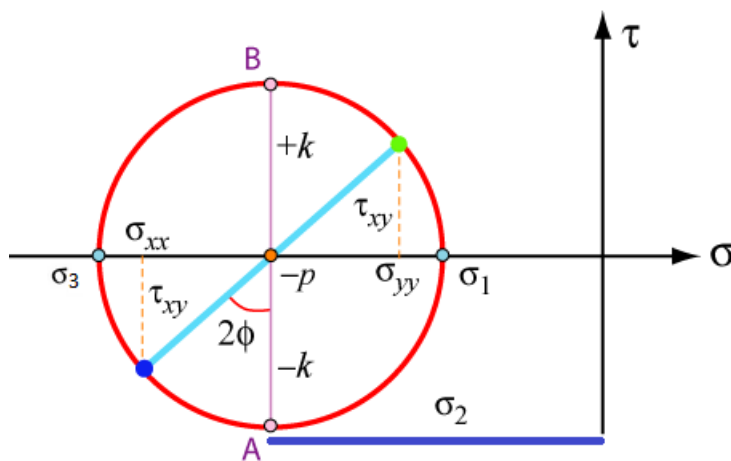


Figure 9: Mohr's circle for plain strain.[6]

The points A-B in Figure 9 represent the stress states along the α, β -lines.

From Mohr's circle we get the relation:

$$\begin{aligned}\sigma_{xx} &= \sigma_2 - k \sin 2\phi \\ \sigma_{yy} &= \sigma_2 + k \sin 2\phi \\ \tau_{xy} &= k \cos 2\phi\end{aligned}\tag{2.11}$$

Combining Equations (2.11) with the equilibrium Equations (2.10) gives:

$$\begin{aligned}\frac{\partial \sigma_{xx}}{\partial x} + \frac{\partial \tau_{xy}}{\partial y} &= -\frac{\partial \sigma_2}{\partial x} - 2k \cos 2\phi \frac{\partial \phi}{\partial x} - 2k \sin 2\phi \frac{\partial \phi}{\partial y} = 0 \\ \frac{\partial \sigma_{yy}}{\partial y} + \frac{\partial \tau_{xy}}{\partial x} &= \frac{\partial \sigma_2}{\partial y} + 2k \cos 2\phi \frac{\partial \phi}{\partial y} - 2k \sin 2\phi \frac{\partial \phi}{\partial x} = 0\end{aligned}\tag{2.12}$$

For $\phi = 0$, the α, β -lines coincides with the x-y-axes at a particular position, the equations above then reduces to:

$$\begin{aligned}\frac{\partial}{\partial x}(\sigma_2 - 2k\phi) &= 0 \\ \frac{\partial}{\partial y}(\sigma_2 + 2k\phi) &= 0\end{aligned}\tag{2.13}$$

Integrating the Equations (2.13) leads to:

$$\begin{aligned}\sigma_2 - 2k\phi &= C_1 = \text{constant along } \alpha - \text{line} \\ \sigma_2 + 2k\phi &= C_2 = \text{constant along } \beta - \text{line}\end{aligned}\tag{2.14}$$

If σ_2 is replaced with $-p$ which is the normal pressure acting on the slip line then Equations (2.14) become:

$$\begin{aligned}\Delta p &= 2k\Delta\phi_\alpha \text{ on an } \alpha - \text{line} \\ \Delta p &= -2k\Delta\phi_\beta \text{ on a } \beta - \text{line}\end{aligned}\tag{2.15}$$

These are the equilibrium equations expressed along a slip line and were first derived by Hencky and are therefore known as Henckys relation.

2.3 PLANE STRAIN INDENTATION

There are two types of slip-line fields which are of special interest when solving indentation problems. One is a net of straight lines shown left in Figure 10 and the other is the centered fan to the right. In the net of straight lines the value of the normal pressure p is the same throughout the field since there is no curvature. For the centered fan the value of $\sigma_2(p)$ is the same for a radial line, but changes when moving from one radial line to another along the curvature. Combinations of these two fields are used for solving a number of problems.

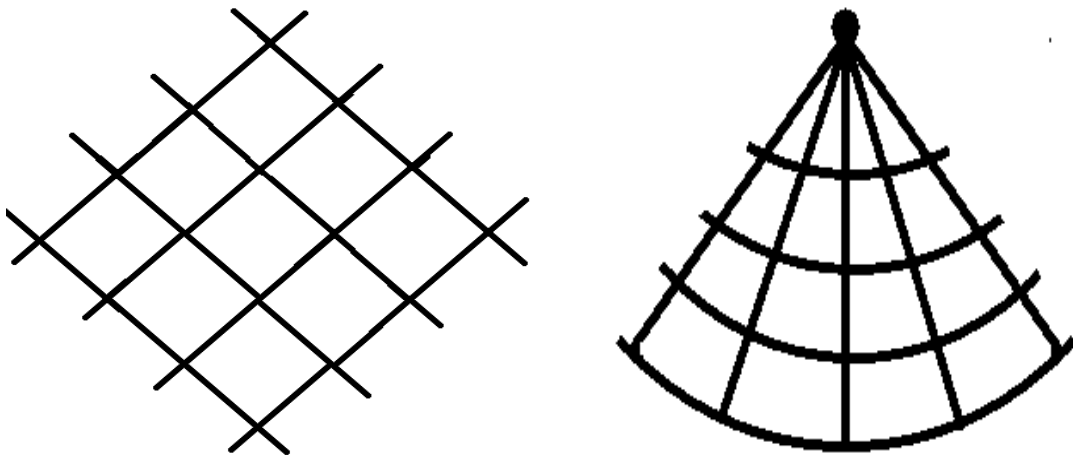


Figure 10: Net of straight lines and centered fan.[2]

2.4 FLAT PUNCH INDENTATION

Considering a plain strain indentation of a rigid perfectly-plastic, semi-infinite plate by a flat punch-indenter, as seen in Figure 11. The indenter is considered undeformable and friction at the interface between the metal and the indenter is assumed negligible. At a load below the yield stress the deformation is given by the elastic equations. As the load on the indenter increases beyond the yield stress of the material the region under and around the punch becomes plastic. The plastic area increases in size until the whole area is in a fully plastic state and the indenter starts to penetrate the metal surface. The pressure on the face of the indenter when this happens is determined by combining the net of straight lines and centered fan.

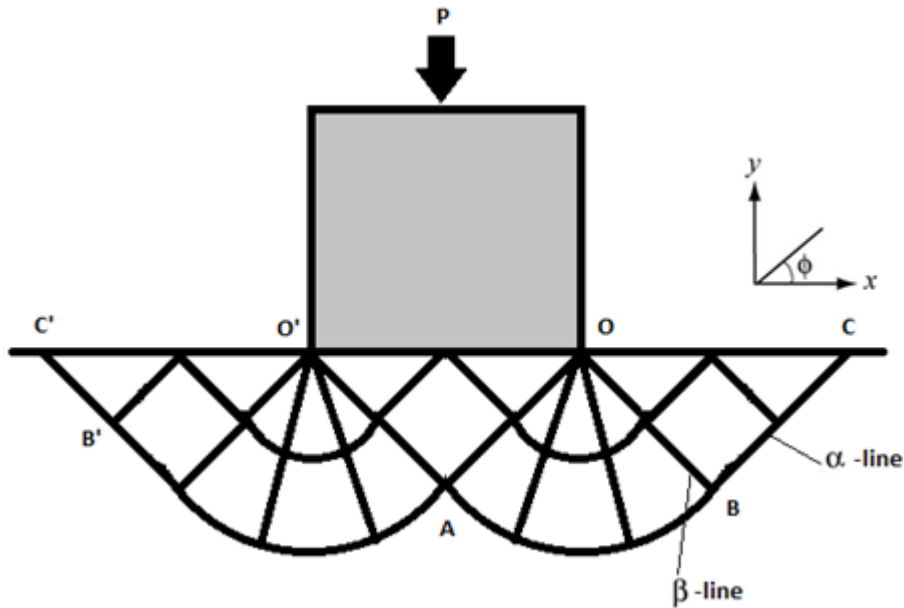


Figure 11: Plane strain indentation by a flat punch.[2]

The solution is symmetric on both sides of the indenter and the slip lines meet the free surface at 45° .

Stress state along the line OC in Figure 10 is expressed in Equations (2.16):

$$\begin{aligned}
 \sigma_{yy} &= \sigma_1 = 0 \\
 \sigma_{xx} &= \sigma_3 \\
 \sigma_{zz} &= \sigma_2 = \frac{\sigma_3}{2}
 \end{aligned}
 \tag{2.16}$$

The line CBAO' is an α -line while OA and OB are β -lines. The triangle OBC is a net of straight lines which gives the following stresses everywhere in the triangle described in Equations (2.17):

$$\begin{aligned}
 \sigma_1 &= 0 \\
 \sigma_2 &= -k \\
 \sigma_3 &= -2k
 \end{aligned}
 \tag{2.17}$$

By moving clockwise from B to A in Figure 10 along the α -line through an angle change $\Delta\phi_\alpha = -\frac{\pi}{2}$

The value of σ_2 at A is described in Equation (2.18):

$$\sigma_{2A} = \sigma_{2B} + 2k\Delta\phi_\alpha = -k + 2k\left(-\frac{\pi}{2}\right) = -k(1 + \pi) \quad (2.18)$$

The value of σ_2 in the triangle AOO' is equal everywhere as this region is made up of straight lines and the stress state is compressive in principal directions. The pressure under the indenter p which is expressed by the line OO' in Figure 10 is given by Equation (2.19):

$$p = -\sigma_{yy} = -\sigma_3$$

$$\sigma_3 = \sigma_{2A} - k = -k(1 + \pi) - k = -2k\left(1 + \frac{\pi}{2}\right) \quad (2.19)$$

$$p = 2k\left(1 + \frac{\pi}{2}\right)$$

From the derived Von Mises' criterion in Equation(2.7), chapter 2.2.2 it was shown that:

$$2k = \frac{2}{\sqrt{3}}Y = 1,15 \cdot Y \quad (2.7)$$

The expression for p in relation to the yield stress is then given by Equation (2.20):

$$p = 2,96 \cdot \text{Yield stress} \quad (2.20)$$

If the Tresca criterion is used, Equation(2.2) from chapter 2.1:

$$2k = Y \quad (2.2)$$

The expression for p when using the Tresca criterion in Equation (2.19):

$$p = 2,57 \cdot \text{Yield stress} \quad (2.21)$$

In theory full scale plastic flow and subsequent indentation occurs when the pressure on the face of the indenter is 2,6-3,0 times the yield stress of the material depending on which yield criterion is used. Von Mises criterion predicts a 15% higher indentation pressure than the Tresca criterion.

The slip-line field theory gives an estimate of indentation pressure p as a function of the material yield stress.

2.5 INDENTATION BY FLAT PUNCH AS A FUNCTION OF PLATE GEOMETRY

The theory and calculations for plain strain indentation by a flat undeformable punch and the associated slip-line field were described in the previous chapter. The theory however seems to be applicable above a certain thickness of the indented plate. When the ratio $\frac{H}{L}$ between the thickness of the plate (H) divided by the width of the indenter (L) is less than 4,37, the slip-line field for the flat punch takes on another shape. The shape of the new field is shown in Figure 12 below ($2a=L$). If the ratio between thickness H and width is equal, $\frac{H}{L} = 1$, the indentation pressure is described in Equation (2.22):

$$p = 2k\Delta\phi_{\alpha} = 2k \quad (2.22)$$

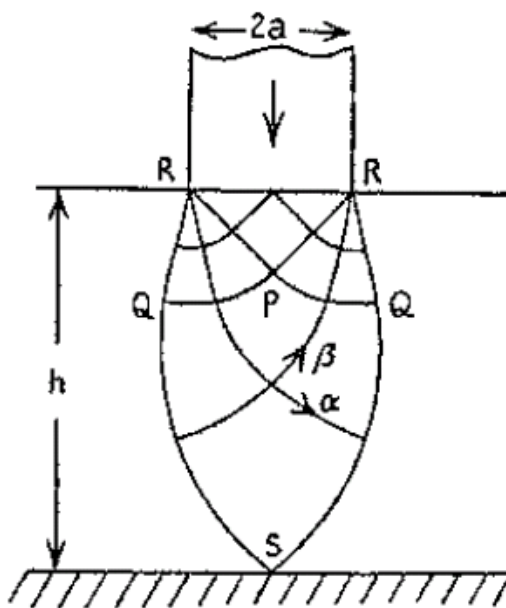


Figure 12: Slip-line field at yield stress for indentation of plate of finite depth ($2a=L$).[7]

As the $\frac{H}{L}$ ratio increases, the angle PRQ shown in the slip-line field in Figure 12 also increases.

For a ratio $1 \leq \frac{H}{L} \leq 4,37$ the indentation pressure is given by Equation (2.23):

$$p = 2k\Delta\phi_{PRQ} \quad (2.23)$$

When $\frac{H}{L} > 4,37$ the PRQ angle is around $77,3^\circ$ and the slip line field becomes the same as described in chapter 4.1.

A complete table of $\Delta\phi_{PRQ}$ values at different $\frac{H}{L}$ ratios can be found in APPENDIX B.

2.6 INDENTATION BY WEDGE FORMED INDENTER

The solution for a wedge shaped indentation builds on the same assumptions as for the case of a flat punch, i.e. the metal is rigid-perfectly plastic, the wedge indenter considered undeformable and the friction is negligible. The field, as seen in Figure 13 is made up by a net of straight lines and a centered fan with an angle ψ . The ψ angle is directly related to the semi angle of the wedge α . The metal flows plastically in the two symmetrical regions from C to D in Figure 13.

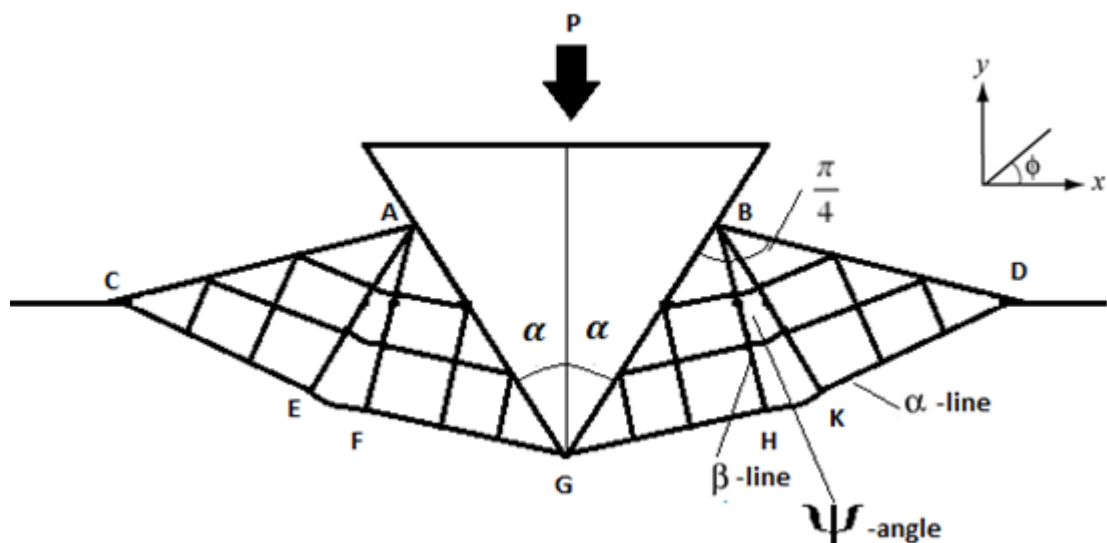


Figure 13: Slip line pattern for two dimensional wedge penetrating a rigid-perfectly plastic material. [2]

The angle ψ is related to the semi angle α by the relation in Equation (2.24):

$$\cos(2\alpha - \psi) = \frac{\cos \psi}{1 + \sin \psi} \quad (2.24)$$

The face of the wedge BG seen in Figure 11, meets the slip-lines at 45° , similarly the slip-lines meet the free surface BD at 45° . The stress state in the triangle BDK is described by Equations (2.25):

$$\begin{aligned} \sigma_1 &= 0 \\ \sigma_2 &= -k \\ \sigma_3 &= 2k \end{aligned} \quad (2.25)$$

Where σ_3 is compressive. Following the α -line from the triangle BDK at the free surface to the triangle GBH in Figure 13, the angle turned is $\Delta\phi_\alpha = -\psi$. The normal pressure to the face of the wedge GB (β -line) is given by Equation (2.26):

$$p = -\sigma_{2GB} = -(\sigma_2 + 2k\Delta\phi_\alpha) = k + 2k\psi = k(1 + 2\psi) \quad (2.26)$$

Since the wedge is symmetrical the indentation pressure p is according to Equation (2.27):

$$p = 2k(1 + \psi) \quad (2.27)$$

Applying the Von Mises criterion the Equations (2.27) becomes:

$$p = 1,15 \cdot Y(1 + \psi) \quad (2.28)$$

The indentation pressure for fully plastic penetration increases with an increasing wedge semi-angle α . If the semi-angle of the wedge is 90° Equation (2.28) becomes equal to the flat punch Equation (2.18) described in chapter 2.4.

The Load per unit width of the wedge is given by Equation (2.29):

$$P_w = 2 \cdot p \cdot h \cdot \sin \alpha \quad (2.29)$$

Where h is the hypotenuse of the impression (GB line in Figure 12), p indentation pressure and semi angle α .

Equation (2.29) above gives the same as results as Equation (2.30) :

$$P_w = \frac{P}{L_i} \quad (2.30)$$

Where P is the load on the wedge and L_i is the width of the impression.

The relation between indentation pressure, semi-angle α and the angle ψ is shown in Figure 14.

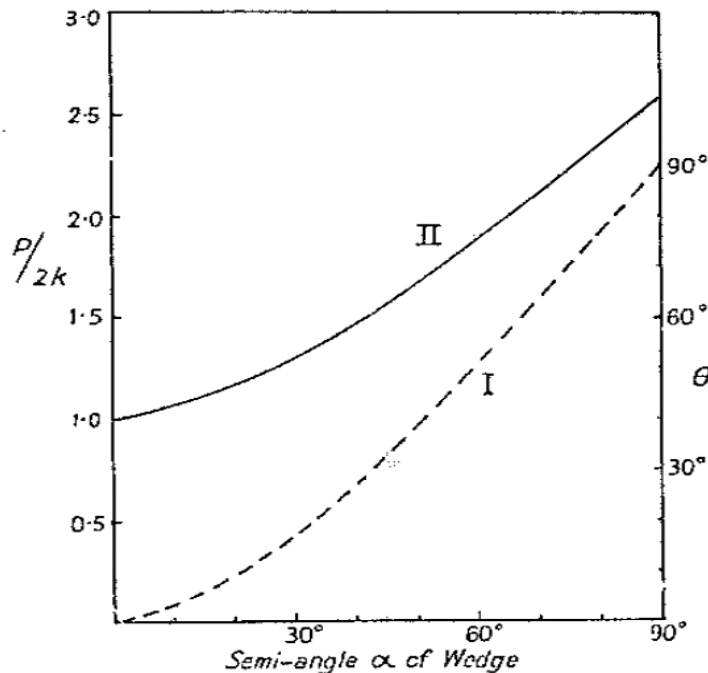


Figure 14: Penetration of rigid perfectly-plastic metal by wedge with different semi-angles. The full line II is indentation pressure in relation to semi-angle. Dotted line I is the semi angle of the wedge related to slip-line angle (θ is denoted as ψ in this text). [8]

2.7 DEFORMATION OF THE INDENTER

In order for the indenter itself to become plastically deformed, the normal pressure between indenter and indented metal will need to exceed the yield stress of the indenter material. When considering an indenter of an arbitrary material indenting a metal plate, full plasticity is reached in the indented metal when the normal pressure is around 3 times that of the yield stress of the metal, depending on indenter geometry. If the normal pressure during indentation is higher than 1,1 times the yield stress of the indenter material there is a big chance that the indenter will experience some plastic deformation.

According to Tabor (1950)[2], the indenter should be at least two and a half times as hard as the indented metal or harder to avoid any permanent deformation.

2.8 MECHANICAL PROPERTIES OF TUBING

The mechanical properties of production tubing used in oil wells are in general defined by the American Petroleum Institute (API) standards. There are many standard steel grades of tubing: H-40, H-55, C-75 and L-80 etc. The numbers in the API grading signifies the minimum yield stress in the units of a thousand psi. The letters in the API grade refers to the chemical composition and treatment of the steel e.g. C and L grades are heat treated to remove martensite. Each grade has an area of application which is dependent on the well scenario. Mechanical properties for a wide range of API tubing grades are shown in Table 1, with minimum and maximum values for yield stress, ultimate tensile strength and elongation.

Table 1: Yield stress, ultimate tensile strength and elongation of different API grades.[9]

API Grade	Yield Stress, psi		Minimum Ult. Tensile, psi	Minimum Elongation, %
	Minimum	Maximum		
H-40	40,000	80,000	60,000	29.5
J-55	55,000	80,000	75,000	24.0
K-55	55,000	80,000	95,000	19.5
N-80	80,000	110,000	100,000	18.5
L-80	80,000	95,000	95,000	19.5
C-90	90,000	105,000	100,000	18.5
C-95	95,000	110,000	105,000	18.5
T-95	95,000	110,000	105,000	18.0
P-110	110,000	140,000	125,000	15.0
Q-125	125,000	150,000	135,000	18.0

Tubing joints are generally around 9meters long (30 ft) with a threaded connection on each end. Typically the outside diameter of the tubing is specified in inches. The inside diameter is defined by the wall thickness by the tubing's weight per feet, e.g. 7 inch O.D tubing can be 26lbs/feet, wall thickness of 0,362inches.

3 EXPERIMENTAL

A series of indentation tests were performed with seven steel indenters of different geometric properties. The indenters were indented into a steel plate by the use of a hydraulic press. The goal of the tests was to compare theoretically calculated values to the measured values and observe how each of the different geometries effectively indented the steel plate.

A hypothesis for load, indentation pressure and depth of penetration for each of the geometries was formulated on the basis of the theory presented in chapter 2. Indenter geometries were chosen in order to observe how small differences in surface area and angle would affect measured results and to see which geometries could be considered applicable for use as slips teeth. The steel grade of the plate which indentations were made on was chosen because of the resemblance in mechanical properties to many production tubing grades.

An indenter with two similar indenter-profiles 2mm apart from each other, similar in geometry to one of the single indenters, was tested to observe how the measured values would compare to the single indenter.

A test procedure was developed before the tests were executed. The test procedure can be found in APPENDIX A.

3.1 MATERIAL PROPERTIES

The indenters and the steel plate where of the same steel grade AISI 4140. AISI 4140 is a chromium-molybdenum steel alloy much used in the oil industry.

The indenters were machined from a AISI 4140 quenched and tempered round bar with the initial mechanical properties shown in Table 2:

Table 2: Mechanical properties of AISI 4140 indenter steel before heat treatment.

Ultimate tensile strength	909,1 N/mm ²	131,82KSI
0,2%proof stress (Yield stress)	781,3 N/mm ²	113,29KSI
Elongation at failure	63%	
Red. of area	21,9%	
Hardness	30HRc	

The indenters went through a series of heat treatment procedures in order to achieve a martensitic microstructure with greater hardness. Hardness after heat treatment was measured to be 50-51HRc. The initial mechanical properties shown in Table 2 changed during heat treatment as well as hardness value. According to a research paper by R.S De Fries [3], the Yield stress for heat treated AISI 4140 with a hardness of 50HRc is 222KSI (1531 N/mm²). Complete material and heat treatment certificates can be found in Appendix (C.2 & C.3).

Similar to the indenters, the steel plate was also quenched and tempered AISI 4140 steel grade, however, with different mechanical properties. Mechanical properties and basic chemical composition are shown in Table 3&4.

Table 3: Mechanical properties of AISI 4140 steel plate.

Ultimate tensile strength	752 N/mm ²	109,06KSI
0,2%proof stress (Yield stress)	586,3 N/mm ²	85,02KSI
Elongation at failure	65%	
Red. of area	23%	
Hardness	20HRc	

Table 4: Chemical composition.

	C	Si	Mn	P	S	Cr	Mo
Weight %	0,42	0,28	1,03	0,008	0,001	1,06	0,27

Complete material certificate can be found in Appendix (C.1)

The plate which the indentations were made on was delivered as a round disc 16"(406,5mm) in diameter and 1"(25,4mm) thick. The disc was cut into multiple smaller rectangles with dimensions 100x200mm roughly, more appropriate for testing.

Hardness values in Table 2&3 have been converted from Brinell hardness to HRc values by the use of a conversion calculator [4].

3.2 GUIDLINES AND EQUIPMENT

Selected guidelines which seemed relevant for the execution of the tests were taken from ASTM-standard "*The standard test method for rapid indentation hardness testing for metallic materials*", [5]. The guidelines involved topics such as: Spacing between each indentation and edge of the plate, angle tolerance for load line, tolerance of depth measurement device and surface treatment of indented material.

The tests were performed to the best of ability in accordance to selected guidelines from this standard. Selected set of guidelines can be found in the test procedure in Appendix (A.3)

Equipment list:

- 30tonn-Hydraulic press.
- Six AISI 4140 indenters, 50HRC.
- AISI 4140 rectangular steel plates, 18-22HRC-ca 200x100x25,4mm.
- Indenter holder for placement of indenters, AISI 4140 steel.
- AEP-TS, 7,5tonn load measurement cell with logger.
- Dial test indicator, 1 μ m accuracy with needle point and setup rig.
- Digital calliper.
- Photo camera.
- Additional tools, plates and bolts for rig up of load measurement cell.
- Mounting cylinder.

Equipment setup:

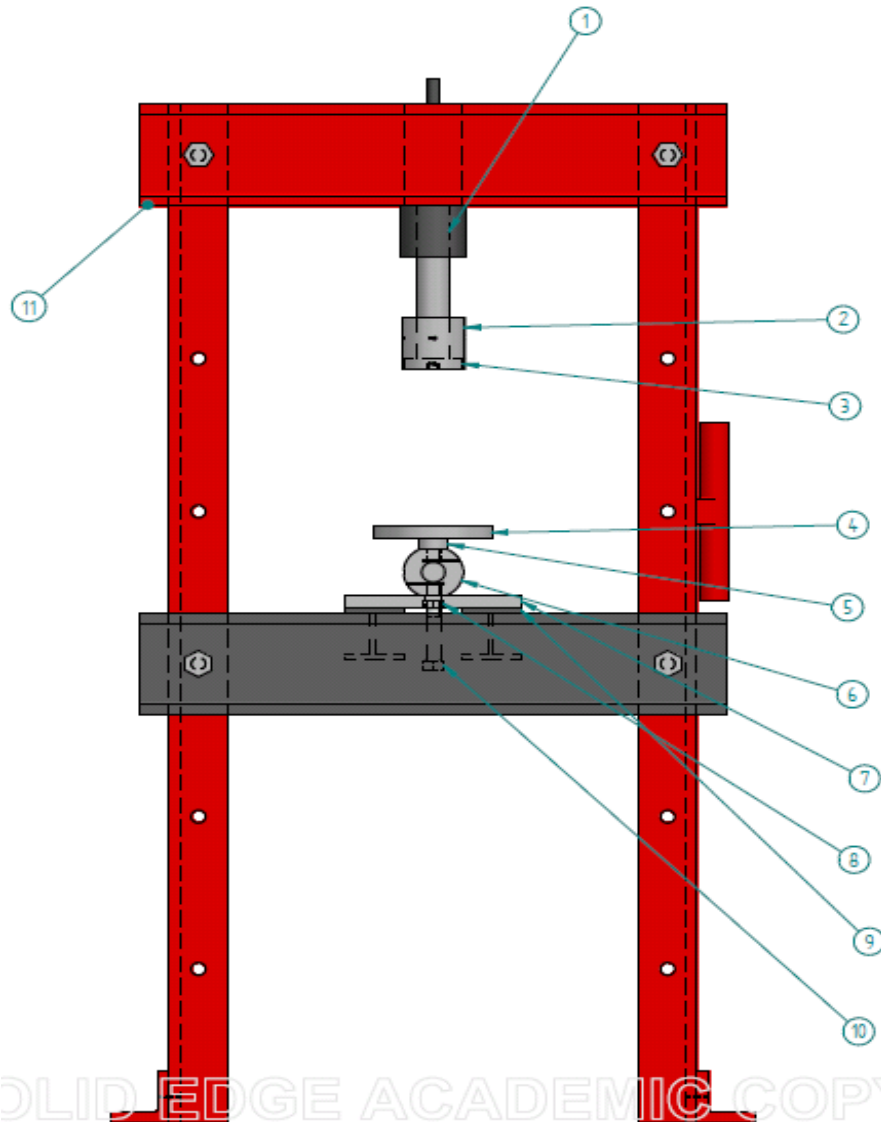


Figure 15: Assembly drawing of equipment setup.[2]

Table 5: Assembly list.

1. Piston-Hydraulic press	7. Mounting plate with 25mm hole
2. Mounting cylinder	8. Support beams (H-profile)
3. Indenter holder	9. Threaded Bolt-M24x2
4. Steel plate, rectangular	10. Fastening nut-M24x2
5. End piece	11. Hydraulic press-30t
6. TS-7,5t load cell (compression)	

3.3 INDENTER GEOMETRIES & LOAD CALCULATIONS

Calculations of the indentation pressure and applied loads are based on the on the slip-line field theory presented in chapter 2, even though the indenters are three-dimensional.

This was done knowing it would likely cause some discrepancy between theoretical and measured results. The expectation was that the differences between theoretical and measured values would not be too high. The indenters have been considered as undeformable for all calculations and the Von Mises yield criterion is applied. The effect of surface friction was not considered in the calculations. For the square and rectangular indenters the depth of penetration related to indentation pressure is hard to predict theoretically. Measurements for depth of penetration versus applied load were to be plotted graphically. Detailed production drawings for every indenter can be found in the test procedure in APPENDIX A.

3.4 ADJUSTMENTS

Errors were done with regards to the yield stress of the indented steel plate and the effect of work-hardening was interpreted wrong. The yield stress used in the calculations of indentation pressure and applied loads was taken from Sverdrup Steels homepage [6]. Sverdrup Steel reports the yield stress to be 551 N/mm^2 (80 KSI) for the indented steel. When reviewing the material certificate the actual measured value was $586,3 \text{ N/mm}^2$ (85,02KSI). The theoretical indentation pressure was multiplied with additional 8% to take the effect of work-hardening into account. This error was done due to a misunderstanding of the literature from Tabor (1950) [2], regarding work-hardening.

Fortunately the two errors did not accumulate big numerical errors in regards to applied loads. The incorrect yield stress of 551 N/mm^2 multiplied with additional 8% equals $595,1 \text{ N/mm}^2$ which is a 1,48% higher value than $586,3 \text{ N/mm}^2$ which is given in the material certificate. The calculations are therefore approximately the same as if the indented steel was treated as a rigid-perfectly plastic material where the effect of work-hardening is neglected.

3.5 SQUARE

The square indenter is shown in Figure 16 below. It has a top surface area of 4x4mm with and a height of 3,5mm. Ratio between the thickness of the plate H and width of the indenter L is $\frac{H}{L} = 6,35$. The equation for the indentation pressure is taken from the theory of indentation by flat punch described in chapter 2.4. The applied load was found by multiplying the surface area of the top of the square with the indentation pressure and divide by the gravitational constant g, as described in Equation (3.1).

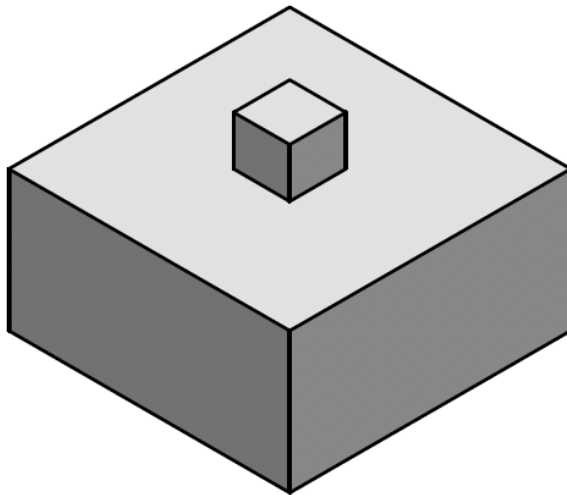


Figure 16: Square flattop indenter.[2]

Equation (2.20) for the indentation pressure with the von Mises criterion applied:

$$p = 2k \left(1 + \frac{\pi}{2} \right) = 2,96 \cdot Yield \quad (2.20)$$

Calculated value of the indentation pressure with work-hardening included:

$$p = 2,96 \cdot 551 \frac{N}{mm^2} \cdot 1,08 = 1761,4 \frac{N}{mm^2}$$

Note: 1,48% Higher value than actual, see chapter 3.4

Surface area of the indenter:

$$A_i = 4 \cdot 4 = 16mm$$

Indentation load in Kilograms:

$$P = \frac{1761,4 \cdot 16}{9,81} = 2873kg \quad (3.1)$$

3.6 RECTANGLE

The rectangular indenter is shown in Figure 17 below. It has a top surface area of 6x4mm and a height of 3,5mm. Ratio between the thickness of the plate H , and width of the indenter L is $\frac{H}{L} = 4,23$. This is just below the limit of 4,37 given in chapter 2.5 which gives a different type of slip-line field compared to the flat punch. The equation for the indentation pressure is taken from the theory of indentation by a flat punch as a function of plate geometry described in chapter 2.5. The applied load was found by multiplying the surface area of the top of the square with the indentation pressure and dividing by g , as described in Equation (3.1).

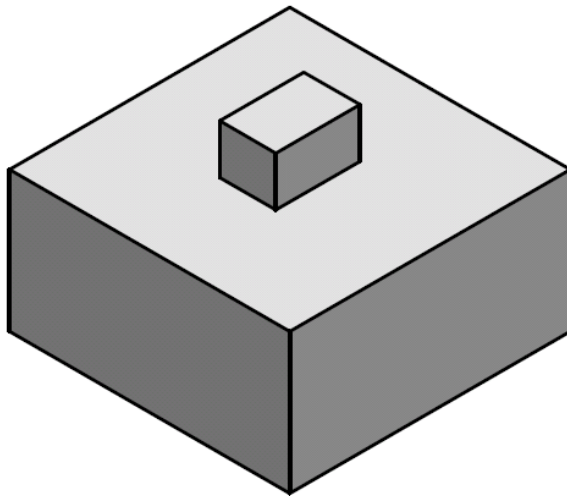


Figure 17: Rectangle flattop indenter.[2]

The indentation pressure is then given by Equation (2.23):

$$p = 2k\Delta\phi_{PRQ} \quad (2.23)$$

Where $\Delta\phi_{PRQ} = 40^\circ = \frac{2}{9}\pi$

The angle $\Delta\phi_{PRQ}$ was found in Hosford (1983) Ref [7], a complete table of $\Delta\phi_{PRQ}$ can be found in APPENDIX B.

Solving Equation (2.23) with the von Mises criterion applied:

$$p = 2k \left(1 + 2 \cdot \frac{2}{9}\pi \right) = 2,756 \cdot Yield \quad (2.23)$$

Calculated value of the indentation pressure with work-hardening included:

$$p = 2,756 \cdot 551 \frac{\text{N}}{\text{mm}^2} \cdot 1,08 = 1640 \frac{\text{N}}{\text{mm}^2}$$

Note: 1,48% Higher value than actual, see chapter 3.4

Surface area of the indenter:

$$A_i = 6 \cdot 4 = 24mm$$

Indentation load in Kilograms:

$$P = \frac{1640 \cdot 24}{9,81} = 4012kg \quad (3.1)$$

3.7 WEDGE 60°

The wedge 60° indenter is shown in Figure 18 below. The face of the wedge is an equilateral triangle with all angles equal to 60° and all three sides having equal length of 4,04mm. The height of the apex is 3,5mm with a length perpendicular to the face of the wedge being 4mm. The equation for the indentation pressure is taken from the theory of indentation by wedge formed indenter described in chapter 2.6.

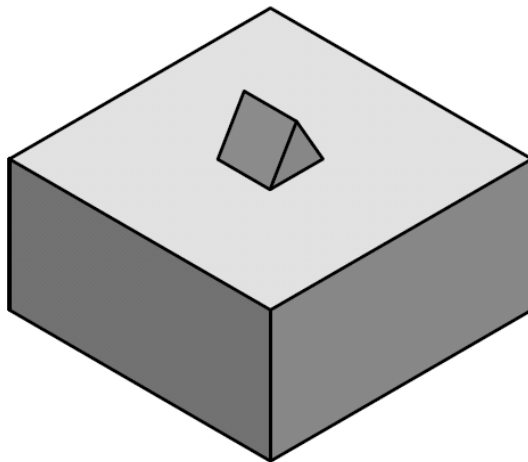


Figure 18: Wedge 60° indenter.[2]

For indentation by a wedge the indentation pressure is given by Equation (2.27):

$$p = 2k(1 + \psi) \quad (2.27)$$

Where angle ψ , is related to the semi angle of the wedge which is 30°. By using the diagram found in Tabor (1950) [2] where the relation between indentation pressure, semi-angle α and the angle ψ is graphically illustrated. The ψ angle was found to be:

$$\psi = 15^\circ = \frac{\pi}{12}$$

This is shown graphically in Figure 19, below.

The indentation pressure with the von Mises criterion applied, Equation (2.27) becomes:

$$p = 2k \left(1 + \frac{\pi}{12} \right) = 1,451 \cdot Yield \quad (2.27)$$

Calculated value of the indentation pressure with work-hardening included:

$$p = 1,451 \cdot 551 \frac{N}{mm^2} \cdot 1,08 = 863,5 \frac{N}{mm^2}$$

Note: 1,48% Higher value than actual, see chapter 3.4

Load per unit width of the indentation was calculated from Equation (2.29):

$$P_w = 2 \cdot p \cdot h \cdot \sin \alpha \quad (2.29)$$

For load calculations P_w is multiplied by the length of the indenter which is 4mm, at a given height below the apex. The pressure at the apex of the wedge is in theory infinite, load calculations therefore start at a height 0,5mm below the apex and down to the bottom of the wedge. This way the load is proportional to a given depth of penetration relative to the indentation pressure p .

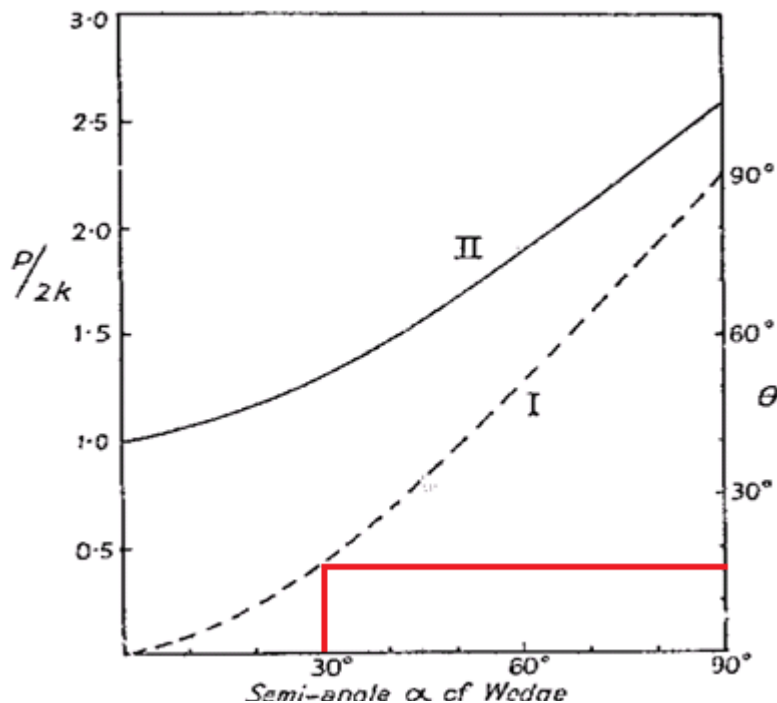


Figure 19: ψ -angle for a wedge semi angle of 30°. [8]

Example of the load calculation for a depth of penetration 0,5 mm:

The hypotenuse at penetration depth of 0,5mm is found to be 0,578mm, semi angle $\alpha = 30^\circ$,
 $p = 863,5 \frac{\text{N}}{\text{mm}^2}$.

Equation (2.29) then becomes:

$$P_w = 2 \cdot 863,5 \frac{\text{N}}{\text{mm}^2} \cdot 0,578\text{mm} \cdot \sin 30^\circ = 499,1 \frac{\text{N}}{\text{mm}} \quad (2.29)$$

Indentation load in kilograms is shown in Equation (3.2):

$$P = \frac{P_w \cdot l}{g} = \frac{499,1 \frac{\text{N}}{\text{mm}} \cdot 4\text{mm}}{9,81} = 203\text{kg} \quad (3.2)$$

Calculations shown above were done for all depths of penetration down to the bottom of the wedge. For complete load tables for every depth, see test procedure in Appendix (A.7).

3.8 WEDGE 120°

The wedge 120° indenter is shown in Figure 20 below. The face of the wedge is isosceles triangle with a top angle of 120° and two equal bottom angles of 30°, two sides have equal length of 4mm, while the bottom width is about 6,93mm. The height from the apex to the bottom is 3,5mm, but the triangle height is 2mm. Maximum penetration depth of the wedge is therefore 2mm. From 2mm to the bottom the indenter becomes a rectangle, the length perpendicular to the face of the wedge is 4mm. Equations for the indentation pressure is given from the theory of indentation by wedge formed indenter described in chapter 2.6

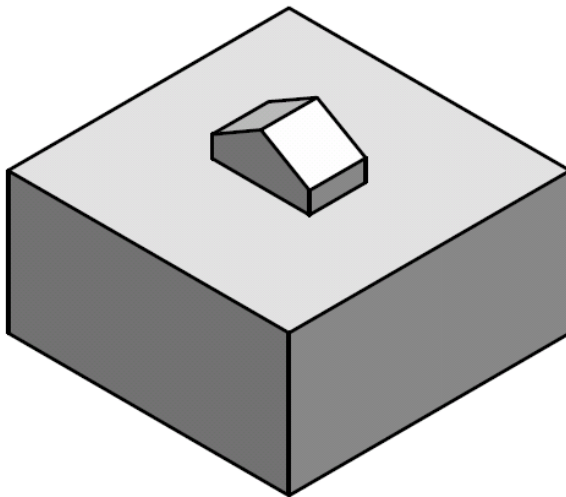


Figure 20: Wedge 120° indenter.[2]

For indentation by a wedge the indentation pressure is given by:

$$p = 2k(1 + \psi) \quad (2.27)$$

Where angle ψ is related to the semi angle of the wedge which is 60°. By using the same diagram as for the wedge 60° found in Tabor (1950) [2], the ψ angle was found to be:

$$\psi = 50^\circ = \frac{5\pi}{18}$$

This is shown graphically in Figure 21.

The indentation pressure with the von Mises criterion applied, Equation (2.27) becomes:

$$p = 2k \left(1 + \frac{5\pi}{18} \right) = 2,154 \cdot \text{Yield} \quad (2.27)$$

Calculated value of the indentation pressure with work-hardening included:

$$p = 2,154 \cdot 551 \frac{\text{N}}{\text{mm}^2} \cdot 1,08 = 1281,8 \frac{\text{N}}{\text{mm}^2}$$

Note: 1,48% Higher value than actual, see chapter 3.4

Load calculations were performed in the exact same way as described for the Wedge 60° in chapter 3.6. For complete load tables for every depth, see test procedure in Appendix (A.8.).

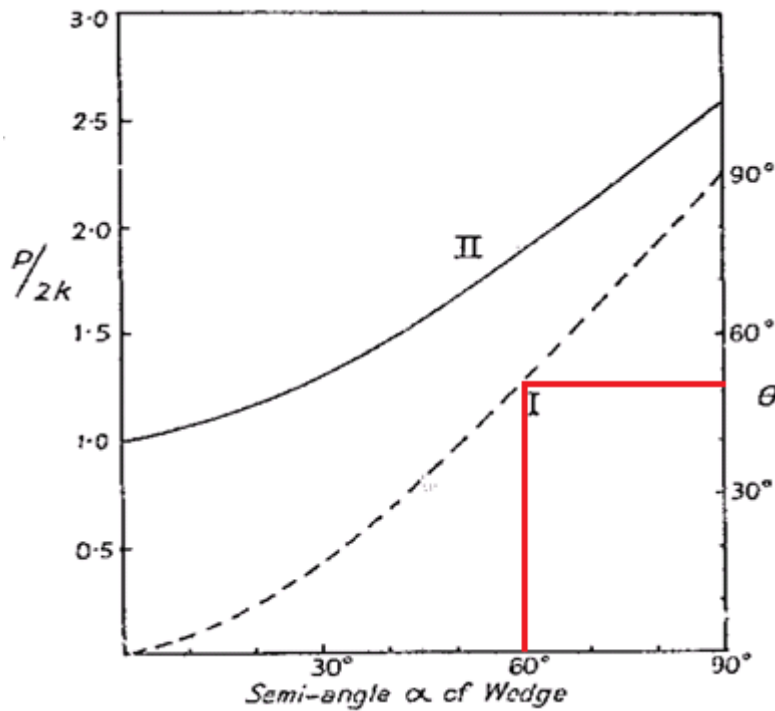


Figure 21: ψ -angle for a wedge semi angle of 60°. [8]

3.9 PYRAMID

The pyramid indenter is shown in Figure 22 below. The pyramid is four sided with a 7x7mm base area and a height from bottom to tip of 3,5mm. The face angle of the pyramid is 90° and the diagonal angle is 110°.

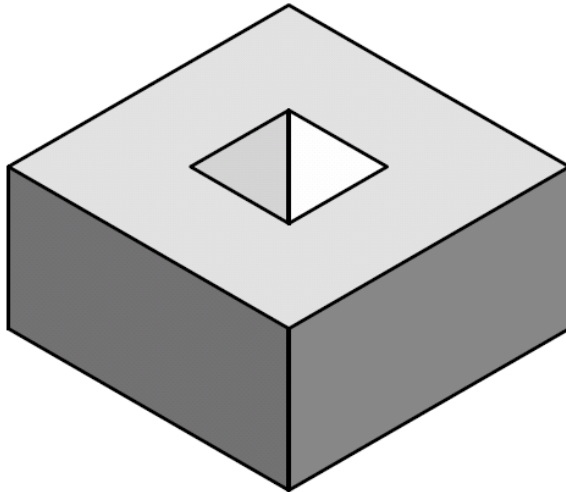


Figure 22: Pyramid indenter.[2]

Indentation pressure for the pyramid cannot be predicted with slip-line field theory. The deformation and plastic flow pattern is three dimensional where as for the wedge the deformation is two dimensional. Experiments with a Vickers pyramid indicates that the value of the indentation pressure is around $3,3 \cdot Yield$, according to Tabor(1950)[2]. The Vickers pyramid has a face angle of 136°, while the pyramid indenter has a face angle of 90°.

In theory the indentation pressure decreases with a smaller semi-angle, however, experiments have shown that for a pyramid indentation the pressure increases with a smaller angle according to Tabor (1950)[2]. A conservative approach to the load calculations is therefore taken with predicted indentation pressure shown in Equation (3.3):

$$p = 3,4 \cdot Yield \quad (3.3)$$

Calculated value of the indentation pressure with work-hardening included:

$$p = 3,4 \cdot 551 \frac{N}{mm^2} \cdot 1,08 = 2023,3 \frac{N}{mm^2}$$

Note: 1,48% Higher value than actual, see chapter 3.4

The tip of the pyramid is considered in the same way as the apex of the wedge, the pressure is in theory infinite and causes yielding at the smallest loads. For load calculations the surface area of the pyramid is considered exponentially growing, starting at 1mm^2 with the depth of penetration calculated from the diagonal of the impression and half the pyramid face angle which is 45° .

Relation between surface area (A_s) and diagonal (d) is seen in Equations (3.4) & (3.5):

$$A_s = \frac{d^2}{2 \sin 45^\circ} \quad (3.4)$$

$$d = \sqrt{A_s \cdot 2 \sin 45^\circ} \quad (3.5)$$

The depth of penetration is calculated from diagonal (d) half the diagonal angle which is 55° , seen in Equation (3.6):

$$h_p = \frac{d}{\tan 55^\circ} \quad (3.6)$$

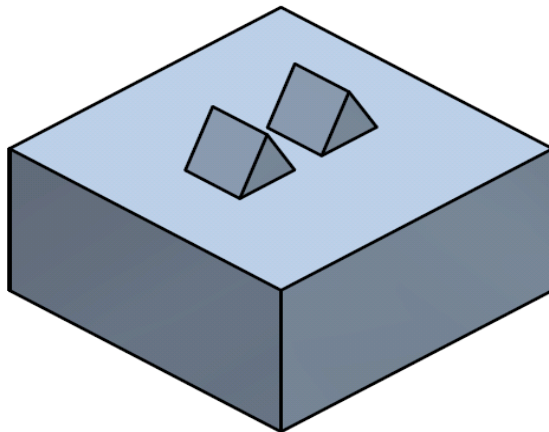
The indentation load in kilogram calculated for a surface area of 1mm^2 with work-hardening included is shown in Equation (3.7) below:

$$P = \frac{p \cdot A_s}{g} = \frac{2023,3 \frac{N}{\text{mm}^2} \cdot 1\text{mm}^2}{9,81} = 206\text{kg} \quad (3.7)$$

The calculations shown above were done for all surface areas down to 49mm^2 . For complete load tables, see test procedure in Appendix (A.9)

3.10 DOUBEL WEDGE 60°

The double wedge 60° indenters are shown in Figure 23. The two indenters have exactly the same dimensions as the wedge 60° indenter, but are 2mm apart at the bottom. The double wedge was chosen for testing to observe how two similar indentations close to each other affect the rate of penetration and geometry of the plastic impression. In theory the volume displaced by a wedge is equal to the volume of penetration; the volume is distributed equally to each side of the wedge and could have some impact on the measured results. This is called the pile up effect.



1,48% Higher value than actual, see chapter 3.4

Figure 23: Double wedge 60° indenter.[2]

Since the two indenters have exactly the same dimensions as the wedge 60° the indentation pressure is considered the same, as seen in Equation (2.27):

$$p = 2k \left(1 + \frac{\pi}{12} \right) = 1,451 \cdot Yield \quad (2.27)$$

The applied load is however doubled compared to the single indenter. Complete load tables are found in the test procedure in Appendix (A.10)

3.11 SETUP & EXECUTION

The tests were performed at E Plugs workshop and lasted a full week. Dimensions of the indenters were checked and verified against the production drawings with a digital calliper upon delivery. A seventh indenter that was originally deselected for testing had been included in the delivery from the company that produced the indenters. This indenter had a triangular shape and was also tested.

The equipment was setup according to the test procedure with a few minor adjustments, as shown in Figure 24. The load cell was constrained axially from underneath to a steel support beam using a threaded M24 bolt (and nut). The support beam was constrained laterally with a simple clamp. The load cell was connected to a laptop via the USB port. The included software provided live monitoring of the applied load. An adjustable vice was placed on the side of the piston of the hydraulic press. The vice allowed for accurate placement of the steel plate relative to the piston and indenter, effectively making a bigger area of the steel plate available for making indentations.

Before testing, a net of lines was drawn on the surface of the steel plate as shown in Figure 25. This was done for guidance to make sure the indentations were made on a straight line and not too close to each other. See guidelines in test procedure, Appendix (A.3)

The surface of the steel plate was checked with a spirit level to make sure the surface was horizontally level with the load cell and piston. The indenters were placed in the specially designed test holder and then accurately centered under the piston. Extra caution was taken in order to ensure that the indenter was centered and levelled before the loads were applied.

Each test was logged with the load cell. The data measured by the cell was extracted into an excel sheet for each test by the software. Test duration for each test was approximately 120 seconds with the goal of holding the target load for at least 10seconds. This was done to ensure more or less equal loading time for each test because of the time it took to reach the target load with the hydraulic press. The hydraulic press was manually operated.

Due to a minor leakage of the hydraulic press there were some difficulties in holding the target load over a longer duration of time. This sometimes resulted in a peak load a bit higher than the target load.



Figure 24: Equipment setup.[2]



Figure 25: Surface of steel plate with net of lines.[2]

4 RESULTS

The tests were performed with loading as specified in the test procedure. After the first series of testing, a review of the results was done for both the indenter and indentations by visual inspection with a digital calliper. Depth measurements were originally planned to be done with a dial test indicator, this however proved to be impossible due to size of the indentations and the thickness of the needle attached to the dial test indicator. Geometric properties of the indentations like width and length was measured between each series with the calliper. Although the measurements done with the calliper were rough, they gave a fair estimate of the geometric properties.

4.1 DEFORMATION OF THE INDENTERS

During inspection, after the first series of testing, it was discovered that the square, rectangular and triangular indenters had plastically deformed during testing, as shown in Figure 26 below. The original dimensions of the square and rectangle became distorted as the volume of the indenters seems to have been compressed. A bulging effect occurred at the mid-section of the area while the base and top surface became smaller. Inspections done with the stereo microscope at UIS later indicates that the deformation of the indenters occurred during the first test. The plastic area of the indentations left on the steel plate is smaller than the surface area of the square and rectangle. The only conclusion that could be drawn was that the heat treatment did not provide sufficient hardness throughout the whole volume of the rectangle and square, and as a result the indenters plastically deformed in a compressive manner.

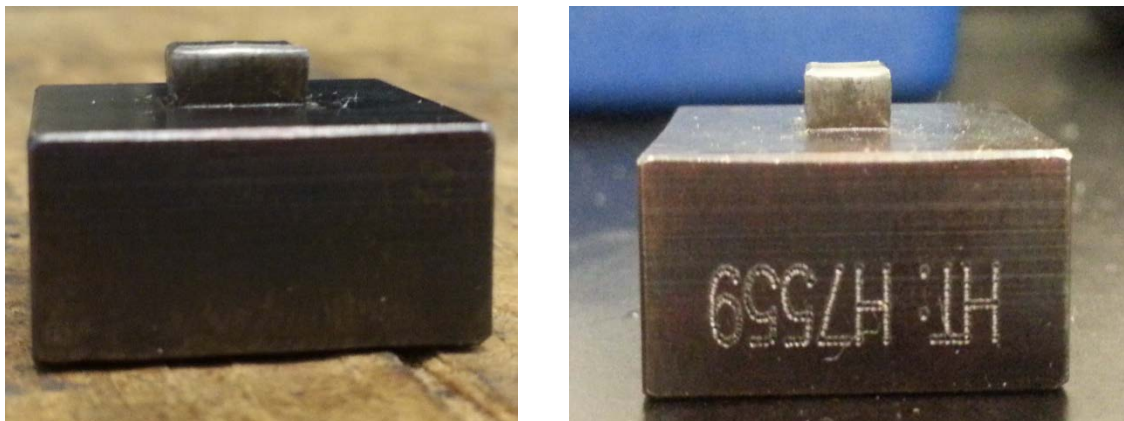


Figure 26: Deformed rectangular and square indenters.[2]

The triangular indenter shown in Figure 27 was originally deselected for production and testing because the shape of the indenter was considered structurally too weak for testing. This proved to be the case during testing as the tip of the triangle bent even at the lightest loads.



Figure 27: Deformed triangle indenter.[2]

No further testing was performed with the three indenters due to the severe deformation.

Inspection of the four other indenters revealed that two of them, namely the 60° and 120° wedges have experienced some moderate deformation. This can be seen in Figure 28 below. The apexes of the wedges in both cases have partial deformation, the 120° wedge being the most severe. Both indenters had experienced a rounding near the edges of the apex which could indicate that the indenters were slightly unbalanced during the early stages of loading. The deformation however, had not led to any other dimensional changes of the indenters except in the apex. The pyramid and double wedge 60° experienced little to no deformation at all from the first series of testing.

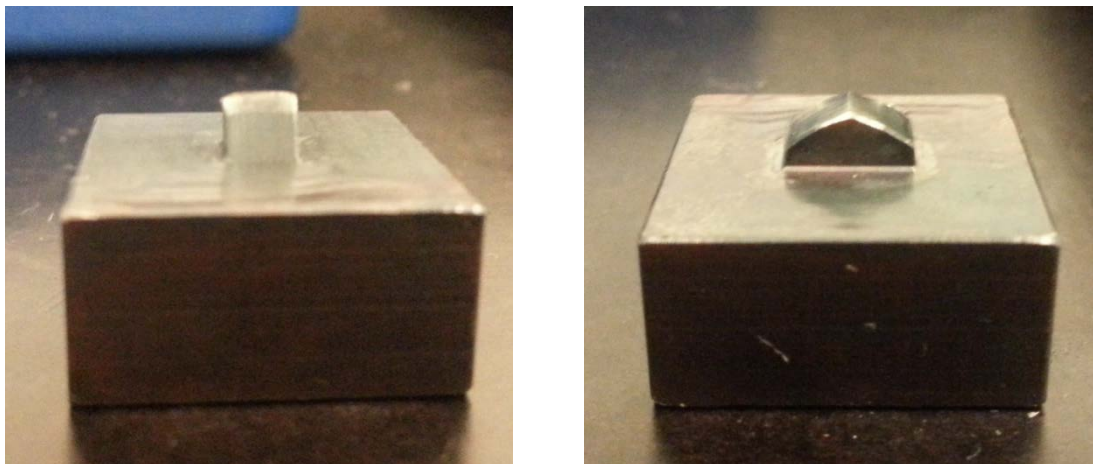


Figure 28: photo of 60° and 120° wedges after the first series of testing.[2]

4.2 OBSERVATIONS & ADJUSTMENTS

After the first series of testing it became clear that the two dimensional load calculations based on the slip-line field theory, which assumes plain strain and a rigid-perfectly plastic metal did not accurately match the experimental results. There were big differences between the theoretically predicted width and depth of penetration and the measured values for all indenters except the pyramid.

A total of three test series were conducted as specified in the test procedure using the four indenters that did not suffer severe deformation. In order to check the effect of reduced surface friction between indenter and material, one of the series was performed with an oil film applied to the surface of the steel. However, the results did not give any indication of surface friction being the reason for the big difference between theoretical and measured values. Measurements of the indentations were more or less identical to the first two series. The first three series of testing has therefore been studied and compared to each other, even though the third series was performed with an oil film applied to the surface.

Upon completing the first three series of testing with the same indentation loads, the load for the 4th series was increased to about 3 times the yield pressure for all indenters except the pyramid. This was done because literary sources like Johnson (1985) [8], states: *"The "uncontained" mode of deformation, when the plastic breaks out to the surface occurs when the pressure under the indenter reaches a value around 3 times the yield stress of the material depending on geometry of the indenter and friction"*. By increasing the load so that the indentation pressure became 3 times that of the yield stress, the expectation was that the differences between theoretical and measured values would diminish.

After testing was completed the plastic areas of the indentations were inspected with a stereo microscope with incorporated measurement and photo capabilities at UiS. Each indentation was photographed at a 2M magnification and the geometries of the indentations were measured with the incorporated measurement software. Photographs with attached measured values were then compiled in an Excel spreadsheet along with the loading data from the load cell for each series of testing. Load and measured data for every test, including the ones performed with increased loading were finally collected in a new spreadsheet for evaluation and study.

Measurements of the width of the wedge indentations were done by measuring five or more horizontal lines across the length of the indentations, as shown in Figure 28. The average value of the five measured lines was then used as the effective width. The reason for doing it this way is because the width of the indentation is not uniform over the whole length of the impression. A general trend for all the wedge indentations seems to be that the width of the impression is shortest at the middle which can be seen in Figure 29. The length measurement was done as shown in Figure 29, where one measuring line was drawn at the middle of the width.

The effective load is taken as the peak load from the entire duration of the test.

4.3 WEDGE 60°

The 60° wedge was initially tested with an indentation pressure of 1,451 times the yield stress, calculated in chapter 3.6. One series of testing consisted of seven tests. The typical plastic area left from the indentation for the wedge 60° is shown in Figure 29. As mentioned earlier in section 4.1, the indenter experienced some deformation during the first test series. No further deformation occurred during the second and third series of testing

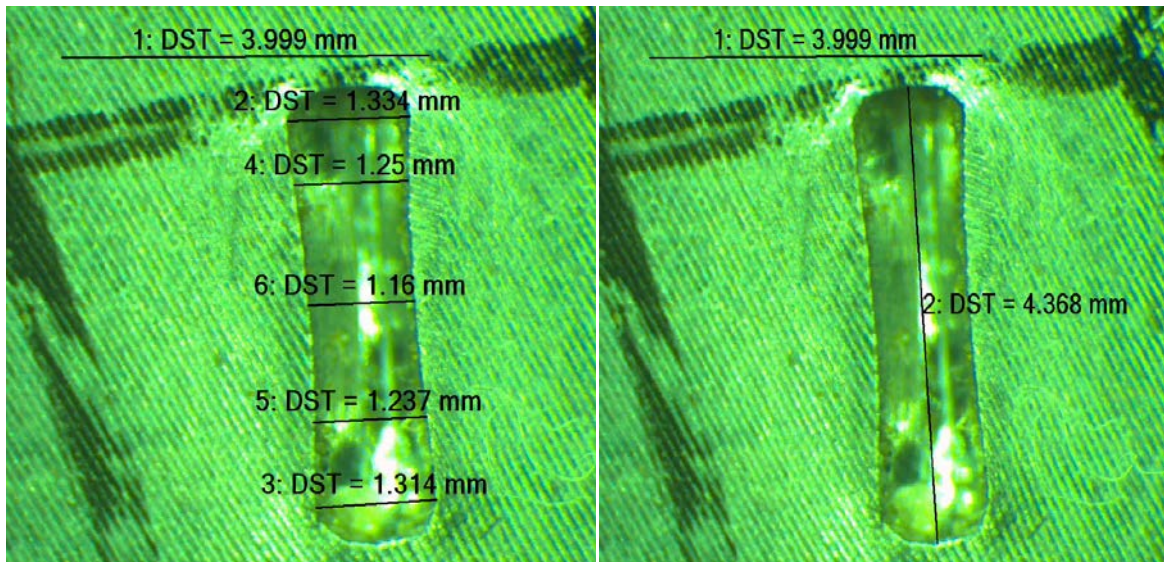


Figure 29: Width and length measurements of wedge 60° indentations.[2]

The width and length of the impressions from all three test series was collected and analysed in an excel spreadsheet along with the peak load for each test. The depth of penetration was then calculated from the measured width since the angle of the impression must be approximately the same as the wedge angle. An average for every parameter was calculated along with the standard deviation between the values of the three series and the average value. The average data is shown in Table 6 below. Complete set of data can be found in Appendix (D.1).

Table 6: Measured average values and standard deviation for different parameters

Load[kg]							
Theoretical	203	407	610	814	1017	1220	1424
Average	209,2	412,5	619,9	831,8	1024,3	1235,6	1434,3
Width[mm]							
Average	0,277	0,442	0,610	0,803	0,973	1,200	1,349
Standard deviation	0,018	0,015	0,009	0,033	0,030	0,102	0,073
Length[mm]							
Average	3,041	3,717	4,064	4,194	4,263	4,312	4,345
Standard deviation	0,250	0,128	0,035	0,024	0,100	0,061	0,065
Depth[mm]							
Average	0,240	0,383	0,528	0,696	0,843	1,039	1,169

The measured average width of the impressions has been plotted against load in Figure 30 below.

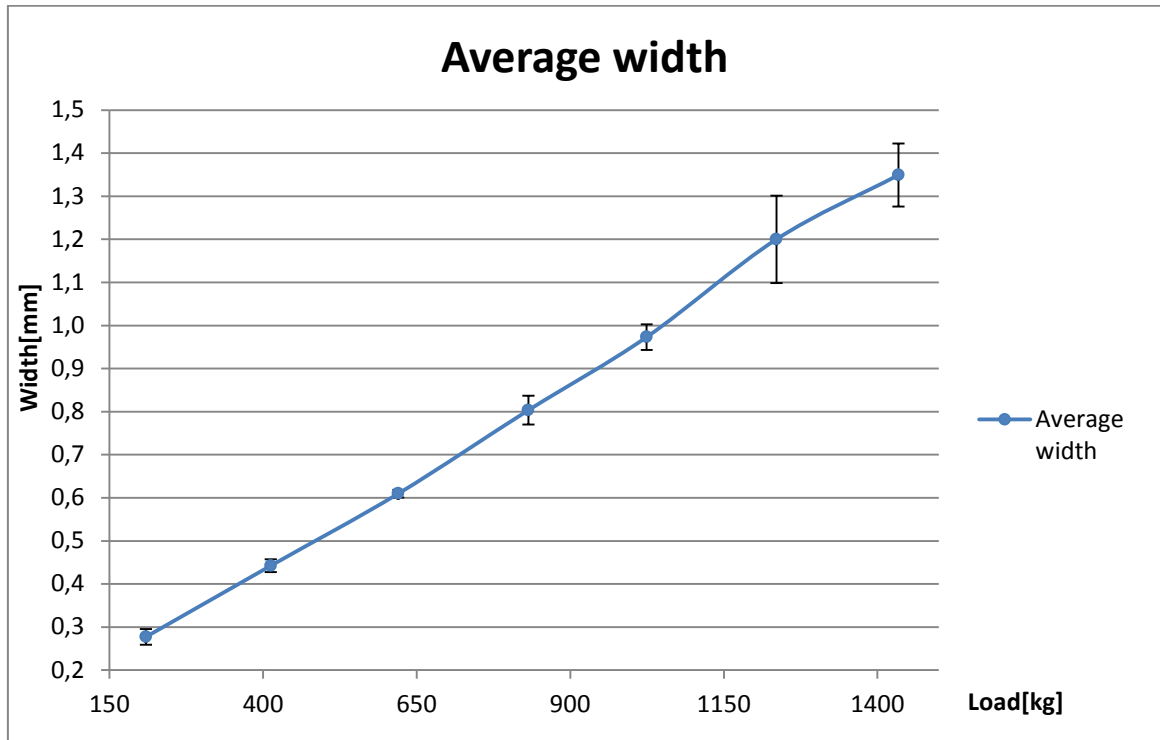


Figure 30: Measured average width and standard deviations.

4.4 INCREASED LOADING OF WEDGE 60°

After the first three series of testing, the indentation pressure was increased to 3,0 3,4 3,6 and 3,8 times the yield stress of the indented steel, then tested one series with each pressure. For the increased series, the amount of tests was reduced from seven to four tests. The increased loads are given in Table 7 below.

Table 7: Increased loads

C=3,0 Load[kg]	C=3,4 Load[kg]	C=3,6 Load[kg]	C=3,8 Load[kg]
420	476	504	532
841	953	1009	1065
1261	1429	1513	1597
1681	1905	2017	2129

The loads in Table 7 were applied with an accuracy of over 99%.

Average measured values of width and length for the increased loading series can be seen in Table 8.

Table 8: Average measured length and width

Width[mm]				
Series 4	0,474	0,793	1,173	1,535
Series 5	0,532	0,895	1,291	1,721
Series 6	0,570	0,938	1,365	1,804
Series 7	0,645	1,080	1,511	1,898
Length[mm]				
Series 4	3,370	4,271	4,431	4,494
Series 5	3,609	4,353	4,527	4,576
Series 6	3,578	4,374	4,596	4,661
Series 7	3,626	4,479	4,674	4,701

Values of width Table 8 is not plotted graphically because of too many intersecting data points.

Complete set of data for increased loading can be found in Appendix (D.1).

The indenter experienced further deformation in the apex region during testing with increased loads. The deformation did not cause the indenter to fail, although, big dimensional changes occurred in the apex region during the last series of testing, which can be observed in Figure 31.



Figure 31: Wedge 60° indenter after testing with increased loading.[2]

4.5 WEDGE 120°

For the wedge 120° the indentation pressure was initially 2,154 times the yield stress, calculated in chapter 3.7. One series consisted of four tests for this indenter due to its geometric properties. Width, length and peak load was collected and analysed in the same way as it was done for the wedge 60°. The indenter experienced no further deformation during the second and third series of testing. The typical plastic area for wedge 120° can be seen in Figure 32.

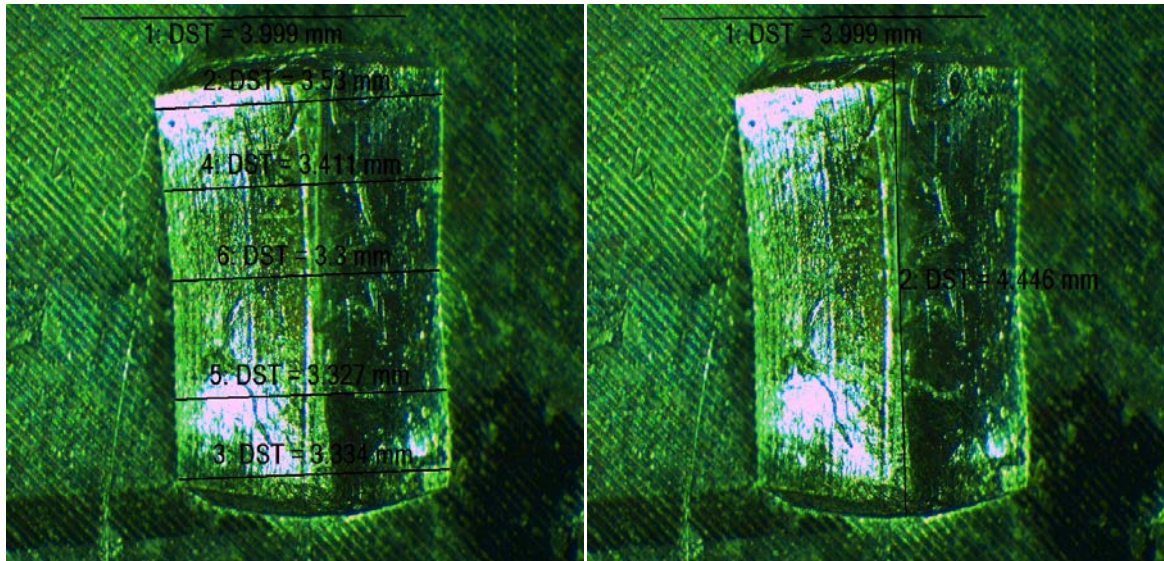


Figure 32: Width and length measurements for wedge 120° indentation.[2]

Average data from the first three series is shown in Table 9 below. The average depths have been calculated from the average width of the impression. Complete set of data can be found in Appendix (D.2)

Table 9: Average data for wedge 120°

Load[kg]				
Theoretical	905	1811	2716	3622
Average	919,6	1829,9	2730,9	3636,1
Width[mm]				
Average	1,036	1,788	2,640	3,416
Standard deviation	0,073	0,037	0,011	0,026
Length[mm]				
Average	3,998	4,305	4,378	4,440
Standard deviation	0,017	0,125	0,105	0,052
Depth[mm]				
Average	0,299	0,516	0,762	0,986

As depicted in Figure 33 the measured average width shows a nearly linear relationship with the load.

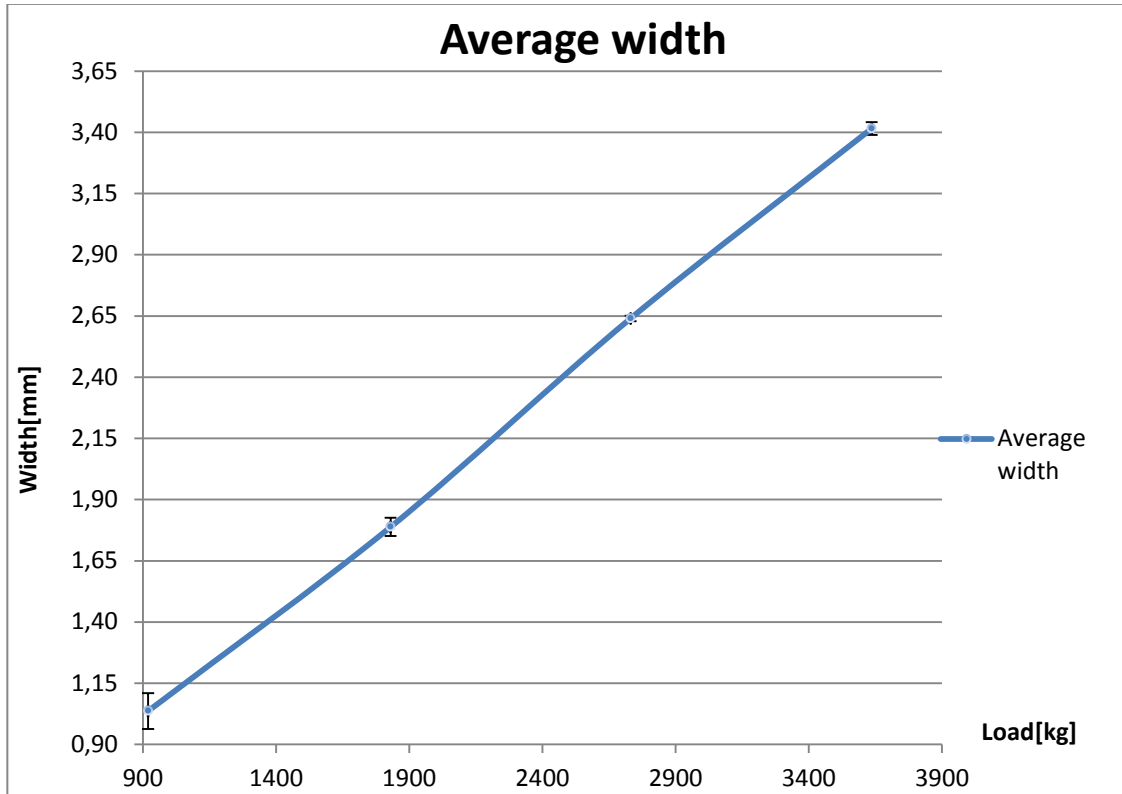


Figure 33: Measured average width and standard deviation.

4.6 INCREASED LOADING WEDGE 120°

After the first three series the indentation pressure was adjusted to 3,0 times the yield stress. One series consisted of four tests. The loads in series 4 were applied with an accuracy of over 99%. Average measured results for wedge 120° increased loading series can be seen in Table 10 below.

Table 10: Average measured data for increased loading series

Load[kg]				
Theoretical	1273	2547	3820	5094
Series 4	1274,9	2560,9	3827,2	5100,5
Width[mm]				
Series 4	1,254	2,390	3,410	4,387
Length[mm]				
Series 4	4,246	4,5	4,581	4,821
Depth[mm]				
Series 4	0,362	0,690	0,984	1,266

Measured average width of the impression plotted against load is shown in Figure 34. The nearly linear relationship with the load is markedly visible for increased loads also.



Figure 34: Measured average width increased loading series.

The indenter deformed considerably during testing with the increased loads. The region along the apex of the indenter became severely compressed, as seen in Figure 35.



Figure 35: Wedge 120° after testing with increased loading.[2]

No further testing was performed with the indenter due to the severe dimensional changes.

4.7 DOUBLE WEDGE 60°

Because the double wedge 60° is dimensionally similar to the single wedge 60° profile it was initially tested with the same indentation pressure, 1,451 times the yield pressure, but with double the load as described in chapter 3.10. Each impression was studied individually in the microscope. This was done to ensure the same level of accuracy in measurement as for the other indentations. The typical plastic impression left by the double wedge pair can be seen in Figure 35 & 36.

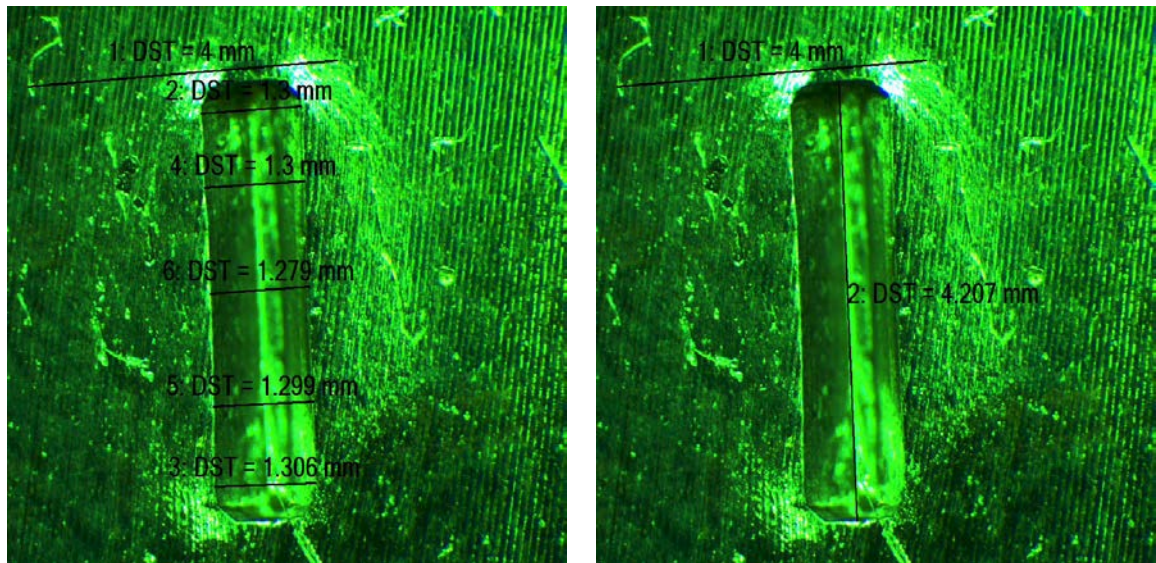


Figure 36: Width and length measurements of the first double wedge profile.[2]

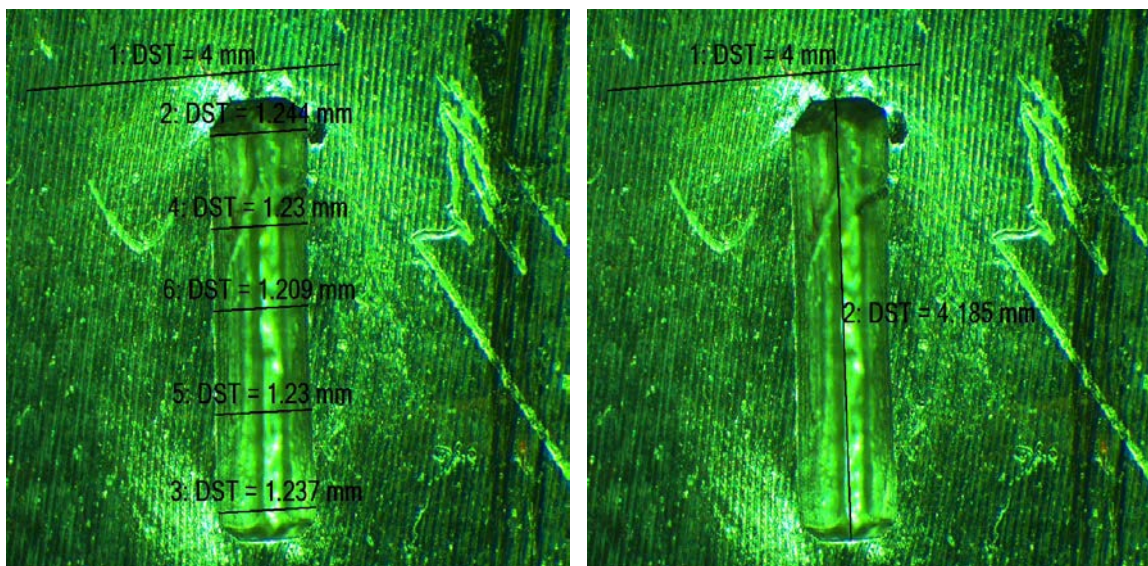


Figure 37: Width and length measurements of the second double wedge profile.[2]

Only minor differences separate the average measured values for the double wedge compared to the single wedge. The average data is shown in Table 11.

Table 11: Average data for double wedge 60°

Load[Kg]							
Theoretical	406	814	1220	1628	2034	2440	2848
Average	411,7	821,3	1228,2	1637,1	2038,2	2451,5	2864,5
Width[mm]							
Average	0,289	0,439	0,605	0,790	0,975	1,156	1,326
Standarddeviation	±0,040	±0,040	±0,038	±0,039	±0,045	±0,052	±0,059
Length[mm]							
Average	3,029	3,853	4,101	4,170	4,193	4,227	4,253
Standarddeviation	±0,374	±0,055	±0,046	±0,080	±0,074	±0,055	±0,045
Depth[mm]							
Average	0,250	0,380	0,524	0,684	0,844	1,001	1,148
Standarddeviation	±0,035	±0,035	±0,033	±0,034	±0,039	±0,045	±0,051

Measured average width and standard deviation is plotted against the load in Figure 38.

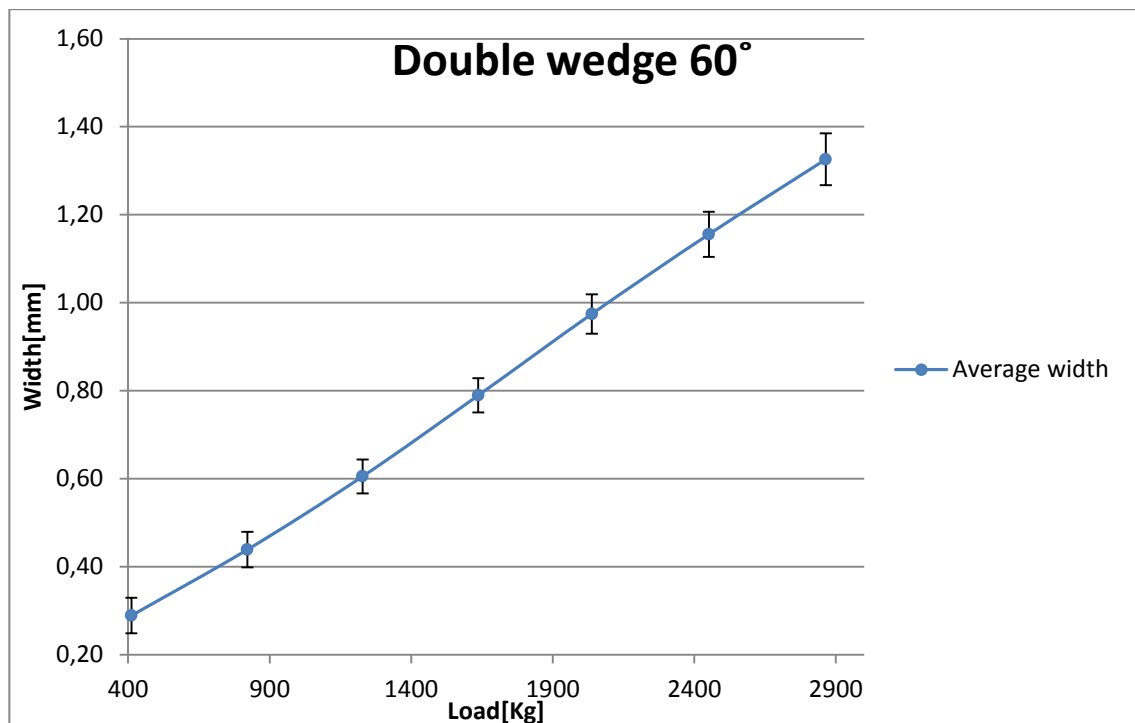


Figure 38: Measured average width and standard deviation for double wedge 60

A general occurring trend for the double wedge seems to be that the width and length of the impression from one profile is somewhat bigger than the other one.

The trend can be seen in Table 12 below. The trend is slightly more marked in terms of width than length. The deviation seems to decline as the load increases. The average deviation between profile 1&2 is 10,71% at the lowest load and decreases to 5,35% at the highest load. The average data is shown in Table 12 below.

Table 12: Difference between average data for profile 1&2

Width[mm]							
Average profile 1	0,305	0,467	0,624	0,814	1,006	1,190	1,362
Average profile 2	0,273	0,411	0,587	0,765	0,944	1,121	1,290
% Average deviation	10,71	12,04	5,96	5,98	6,18	5,78	5,35
Length[mm]							
Average profile 1	3,158	3,893	4,107	4,196	4,215	4,249	4,272
Average profile 2	2,900	3,813	4,095	4,145	4,170	4,205	4,234
% Average deviation	8,18	2,04	0,28	1,22	1,05	1,04	0,91

The difference in width is plotted graphically in Figure 39 below.

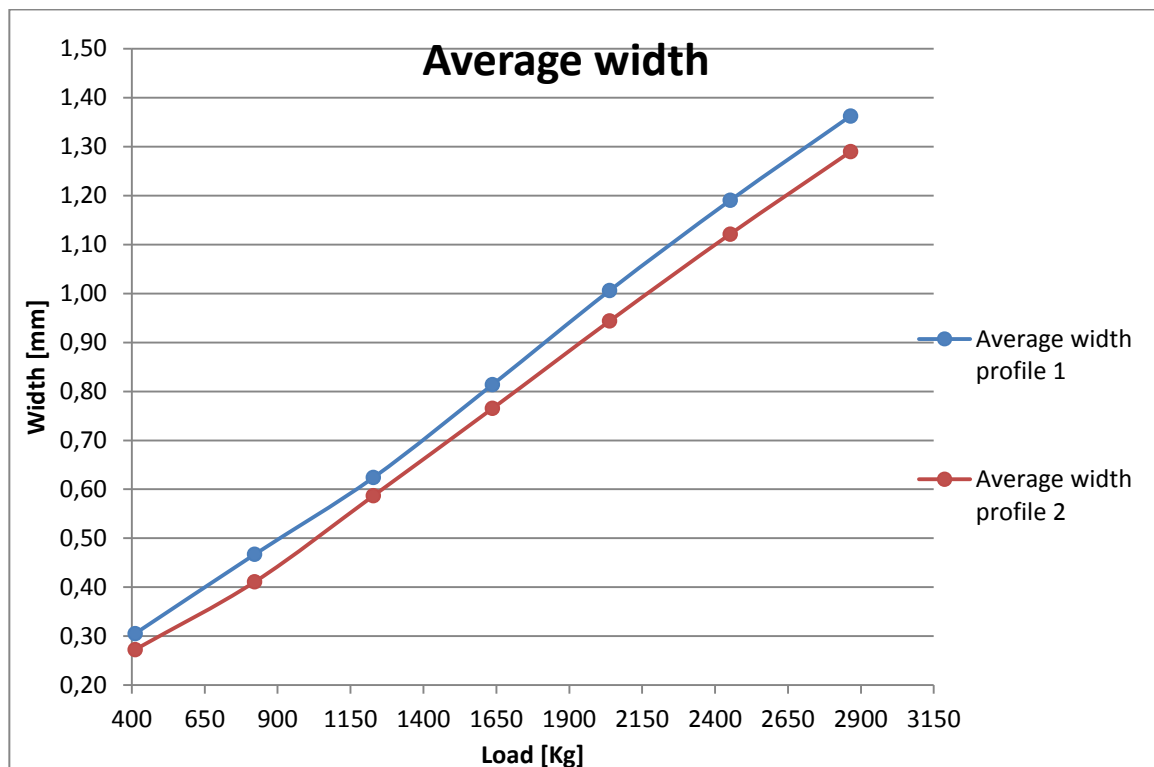


Figure 39: Difference between average width profile 1&2

4.8 INCREASED LOADING DOUBLE WEDGE 60°

The indentation pressure was increased to 3,0 and 3,4 times the yield stress, then tested one series with each pressure. One series consisted of four tests. The results of the increased loading series are shown in Table 13 below.

Table 13: Table of data increased loading series, double wedge 60°

Load[kg]				
Series 4-3,0	851,1	1688,4	2528,7	3376,5
Series 5-3,4	954,9	1943,2	2861	3815,2
Width[mm]				
Average series 4	0,519	0,867	1,248	1,617
Average series 5	0,548	1,008	1,489	1,963
Length[mm]				
Average series 4	3,857	4,246	4,286	4,292
Average series 5	3,994	4,263	4,288	4,320
Depth[mm]				
Average series 4	0,449	0,750	1,081	1,400
Average series 5	0,442	0,814	1,206	1,557

Increased loading for double wedge is plotted graphically in Figure 40 below.

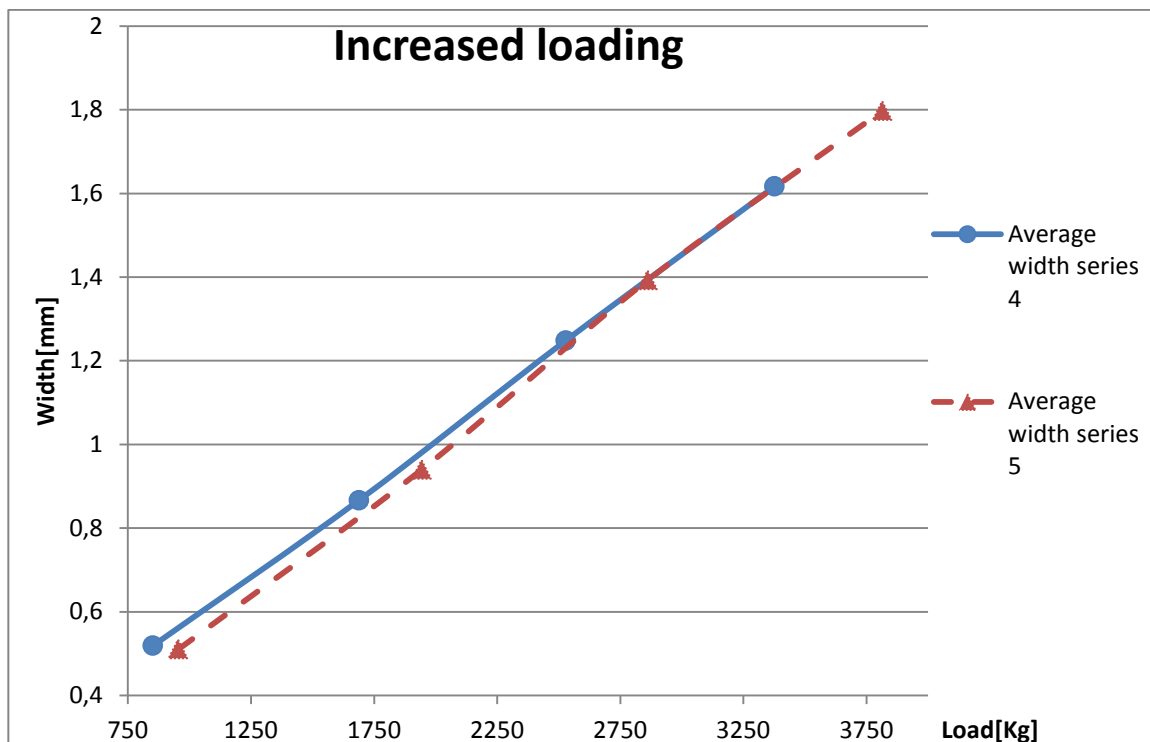


Figure 40: Measured average width, increased loading series

The trend of the width and length of the impression from one profile being somewhat bigger than the other diminished considerably during the increased loads. When comparing the results from the single and double wedge tests performed at 3,0 and 3,4 times the yield stress, it seems that the measured width is bigger for the double wedge. The difference in width is around 7% higher at 3,0 times the yield, and 4,9% at 3,4 times the yield.

The double wedge indenter experienced very little deformation during testing with increased loading. The double wedge indenter can be seen in Figure 41, below.



Figure 41: Double wedge 60° after testing with increased load. [2]

4.9 PYRAMID

Measurements of the width of the pyramid indentations were done by measuring the length of both diagonals across the plastic impression, as shown in Figure 42. The average value of the two diagonals was then used as the effective width called D_{mean} . The depth of penetration was calculated from D_{mean} . Measuring the diagonals is the same way of measuring as in a Vickers hardness test. The reason for measuring this way is because the width and length of the indentation is not uniform. The edges of the impression are slightly bulged because of the work hardening effect that occurs during the indentation. A Typical impression from the pyramid indentation can be seen in Figure 42.

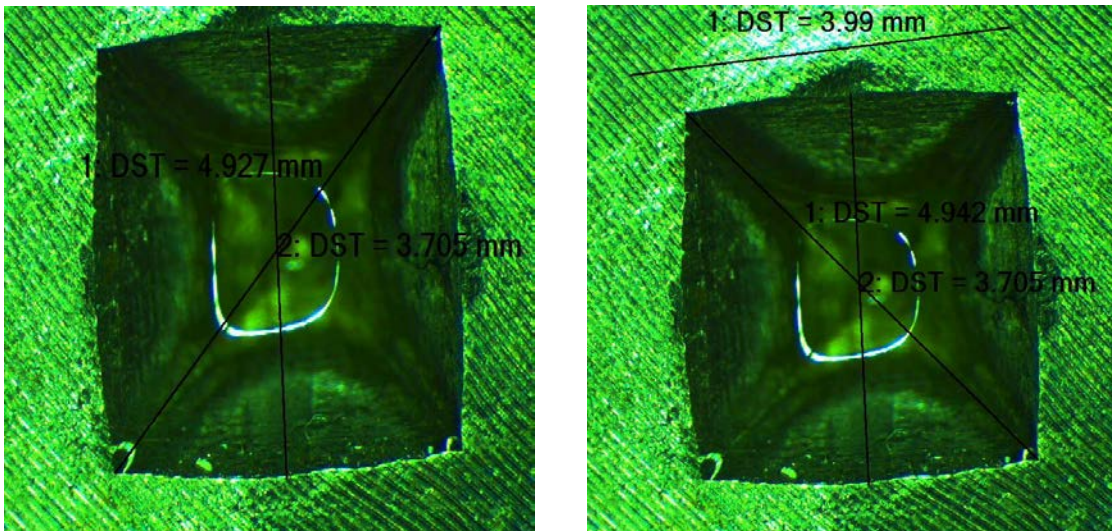


Figure 42: Measurement of diagonals for pyramid indentation.[2]

The Pyramid indenter was tested at 3,4 times the yield stress, as described in chapter 3.8. The pyramid indenter was tested in the same way as the other indenters, i.e. three initial series were tested where one series consisted of four tests. The average results are shown in Table 14 below. Complete tables of data can be found in Appendix (D.4).

Table 14: Average measured data for Pyramid indentations

	Load[Kg]			
Theoretical	206	825	1856	3300
Average	211,8	834	1868,4	3318
	Dmean[mm]			
Average	1,178	2,415	3,638	4,901
Standard-deviation	±0,032	±0,040	±0,041	±0,025
	Depth[mm]			
Average	0,412	0,846	1,274	1,716

Average D_{mean} and standard deviation is plotted against the load in Figure 43.

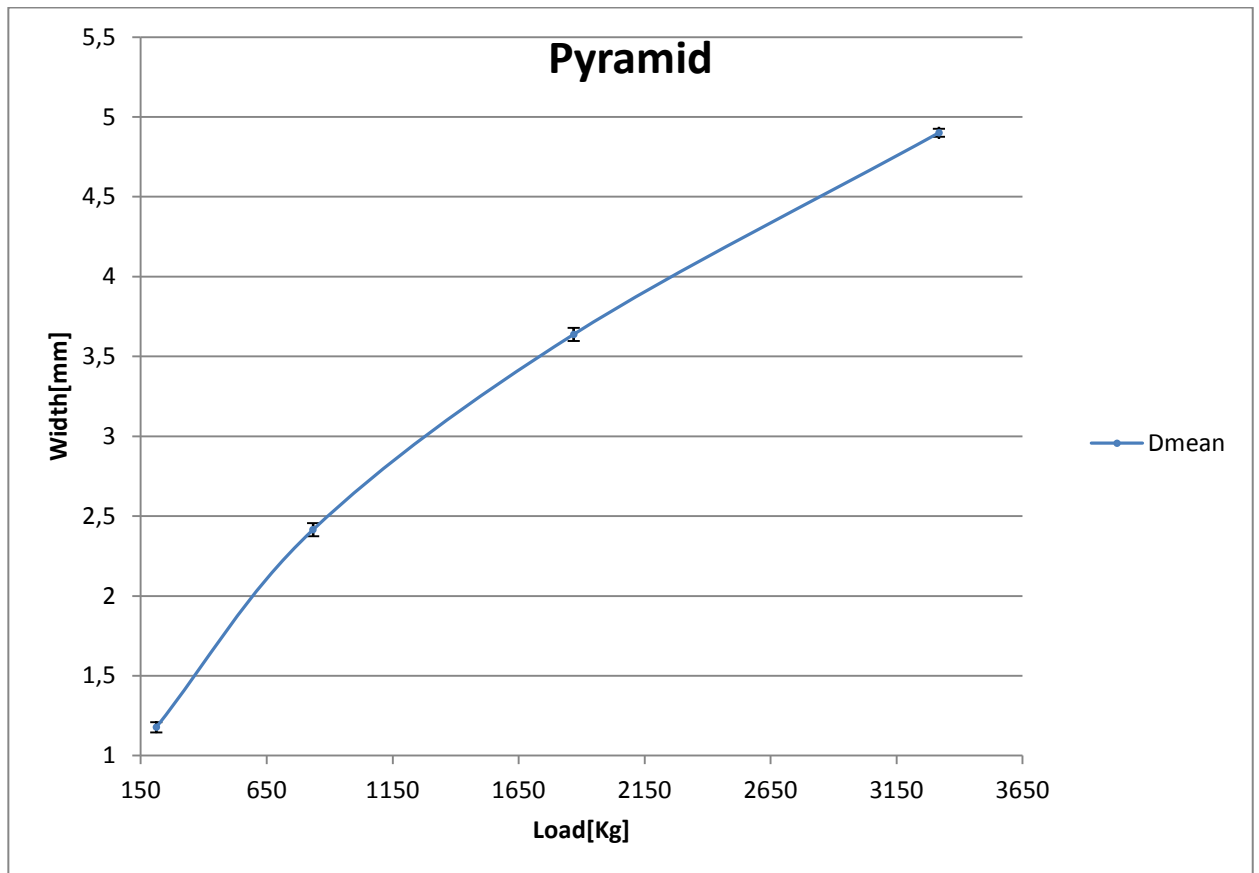


Figure 43: Dmean and standard deviation for pyramid indentations

4.10 INCREASED LOADING PYRAMID

After the first three series of testing the load was increased with 7,5% of the initial load. This was done because measurements done with the calliper at the time indicated that the diagonals were around 7,5% lower than the theoretical value. When the diagonal was measured in the microscope this proved to be wrong. The indenter was tested two series with 7,5% increased loading, one series consisted of four tests. The average results from the 7,5% increased load test can be seen in Table 15.

Table 15: Average measure values 7,5% increased loading

	Load[kg]			
Theoretical	222	887	1995	3547
Average	223,7	889,2	1998,8	3551
	Dmean[mm]			
Average	1,278	2,541	3,831	5,104
Standard deviation	0,006	0,009	0,004	0,002
	Depth [mm]			
Average	0,447	0,890	1,341	1,787

The difference between the first three series and 7,5% increased load is plotted graphically in Figure 44.

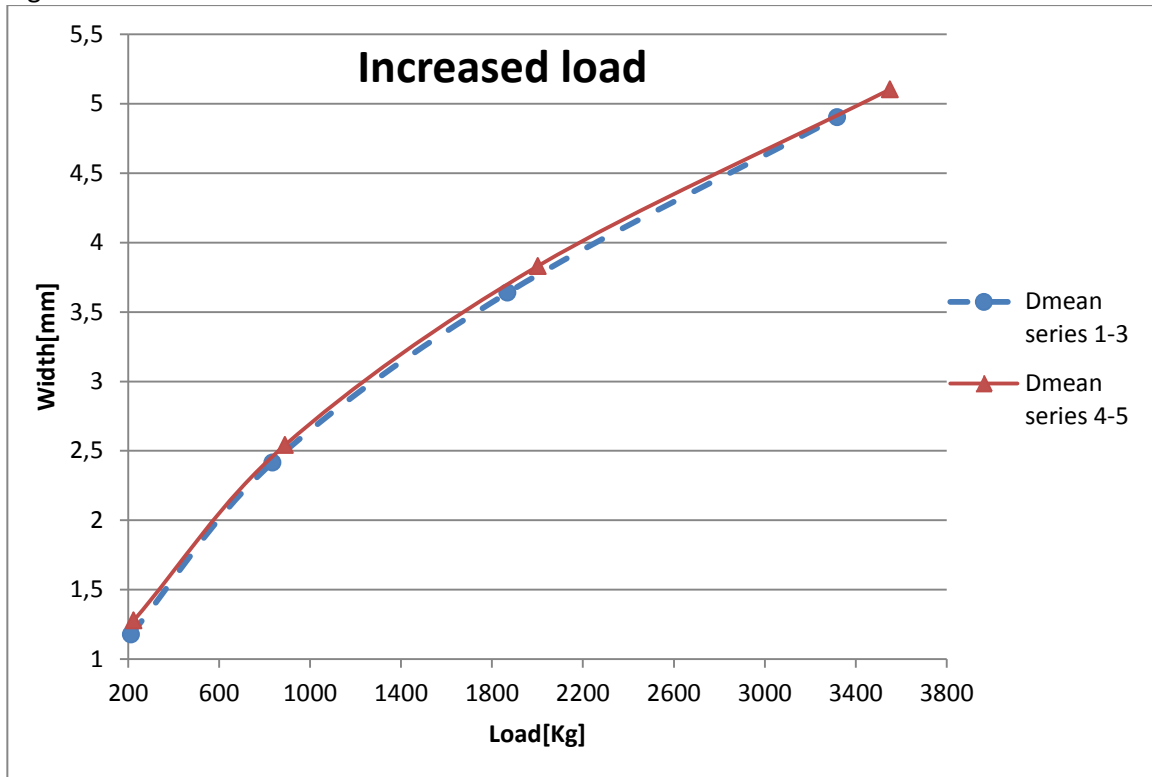


Figure 44: Dmean 7,5% increased load versus Dmean series 1-3

The pyramid indenter experienced no visible deformation during increased loading, as can be seen in Figure 45. The only apparent change in geometry would be that the pyramid tip became slightly blunt.



Figure 45: Pyramid indenter after testing with increased loading.[2]

5 DISCUSSION OF RESULTS

The test results presented in chapter 4 has been analyzed and compared to the theoretically predicted values. An example of a regression curve analysis has been presented for the wedge indenters and the depth of penetration in relation to applied load is discussed. Probable reasons for deviations, deformation, potential sources of errors and design considerations are also discussed. A new model for calculating the indentation pressure, plastic impression analysis and a proposed slips design is presented and discussed.

5.1 DEVIATION BETWEEN THEORETICAL AND MEASURED VALUES

The test results presented in chapter 4 has been compared to the theoretically calculated values of depth, width and length, in addition, a percentage of deviation compared to the theoretical value has been calculated. It is apparent that the slip-line field theory cannot accurately predict the width and depth of penetration for three-dimensional wedge indentations. The discrepancies between measured and theoretically calculated values are very large for the first three test series. For the pyramid indenter, however, the theoretically calculated values were almost identical to the measured values.

5.1.1 Wedge 60°

The measured average width of the impressions versus the theoretical width has been plotted against load in Figure 46 below.

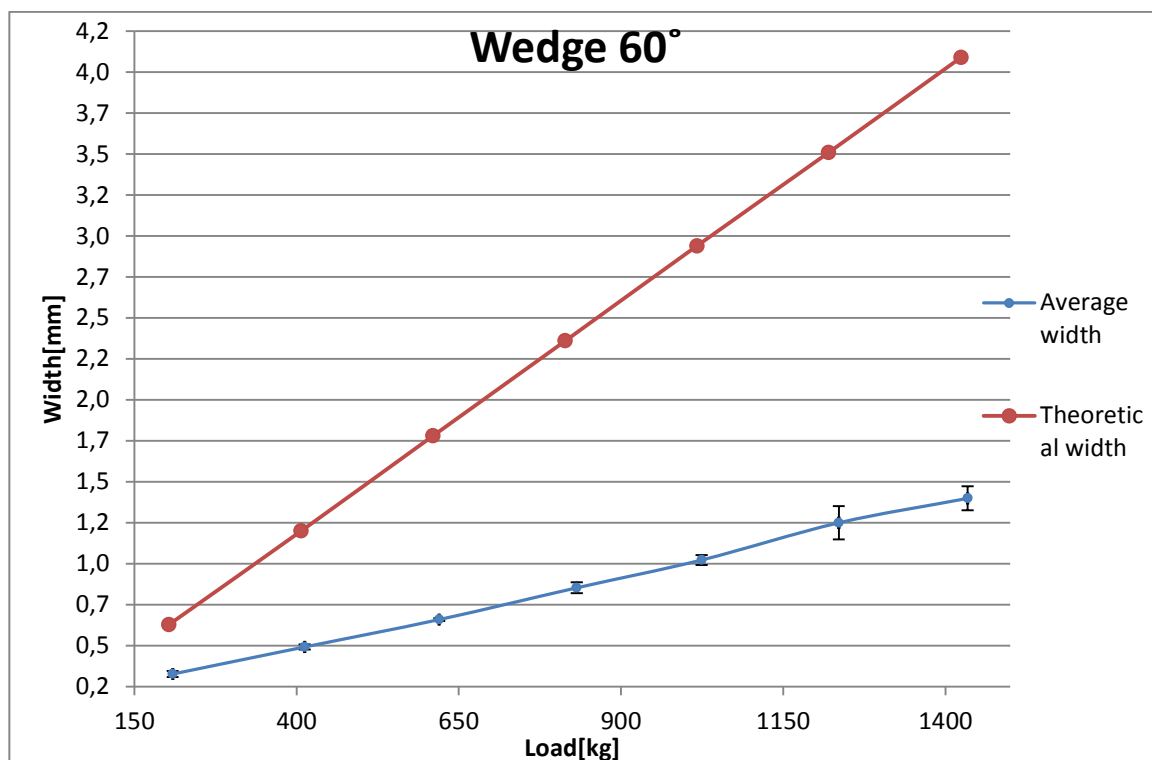


Figure 46: Measured average width compared theoretical average width

For the first three tests series the percentage of deviation in terms of average width ranges from 52,02% at the lowest load to 66,60% on the highest load. The percentage of deviation for depth of penetration is the same as for the width. Depth of the impression is calculated from the measured width.

The variation in the length direction was not accounted for due to the slip-line theory being two-dimensional, therefore the theoretical value was put equal to the length perpendicular to the face of the wedge, 4mm. Variation in average length ranges from 23,97% shorter than 4mm to 8,62% longer. The trend of the plastic impression becoming longer than the actual indenter appears at test number three at an average load of 619,9kg. An example of this can be seen in Figure 29, chapter 3.7.

For the increased loading series the measured width compared to theoretical width can be seen in Table 16 below.

At the lowest loads the deviation is relatively small, but increases as the applied load is increased. The measured results for the increased loading series lie closer to the theoretical values than the initial three test series. The trend of the length of the plastic impression becoming longer than the length of the indenter increased further as the load was increased. The indenter deformed considerably during series 7. The validity of the measured values in series 7 is therefore questionable.

Complete set of compared data for can be found in Appendix (D.1).

Table 16: Measured width compared to the theoretical width increased loading

	Width[mm]			
Theoretical	0,578	1,15	1,73	2,31
Series 4	0,474	0,793	1,173	1,535
% Deviation	18,04	31,05	32,17	33,57
Series 5	0,532	0,895	1,291	1,721
% Deviation	7,97	22,21	25,36	25,51
Series 6	0,570	0,938	1,365	1,804
% Deviation	1,37	18,42	21,08	21,89
Series 7	0,645	1,080	1,511	1,898
% Deviation	-11,55	6,09	12,65	17,85

5.1.2 Wedge 120°

The measured average width of the impressions versus the theoretical width has been plotted against load in Figure 47 below.



Figure 47: Measured width compared to theoretical width wedge 120°

The average percentage of deviation in terms of width for the wedge 120° indenter ranges from 40,1% at the lowest load to 50,71% on the highest load. The deviations from theoretical values are slightly less than for the wedge 60°. Variation in average length varies from 0,05% shorter than the indenter on the lowest load to 11% longer on the highest. The trend of the impression becoming longer than 4mm starts at the second test load of 1830kg.

For the increased loading series the measured width compared to theoretical width can be seen in Table 17 below. The deviation between theoretical and measured values decreased slightly compared to the initial three series, however the indenter was severely deformed during series 4. The validity of the measured values in series 4 is therefore questionable. Complete set of data can be found in Appendix (D.2).

Table 17: Measured width compared to the theoretical width increased loading series

	Width[mm]			
Theoretical	1,73	3,46	5,196	6,93
Series 4	1,254	2,390	3,410	4,387
% Deviation	27,50	30,92	34,38	36,70

5.1.3 Double wedge 60°

The measured average width of the impressions versus the theoretical width has been plotted against load in Figure 48 below.



Figure 48: Measured average width compared to theoretical width for double wedge 60°

Only minor differences separate the average measured values for the double wedge compared to the single wedge. The average percentage of deviation in terms of width ranges from 50,0% at the lowest load to 67,2% on the highest load. In the length direction the deviation is 24,3% shorter than 4mm on the lowest load to 6,3% longer on the highest load. The trend of the impression becoming longer than 4mm starts at the third test load of 1228kg.

Measured width compared to theoretical width for the increased loading series can be seen in Table 18 below. When comparing the width of the impression from the single wedge tests performed at 3,0 and 3,4 times the yield stress, the measured width is bigger for the double wedge. The difference in width is around 7% higher at 3,0 times the yield stress and around 4,9% at 3,4. The trend of the length of the plastic impression becoming longer than the length of the indenter increased further as the load was increased. Complete set of data can be found in appendix

Table 18: Measured width compared to the theoretical width for increased loading series 4&5

	Width[mm]			
Theoretical	0,578	1,15	1,73	2,31
Average series 4	0,519	0,867	1,248	1,617
% Average deviation	10,2 %	24,6 %	27,8 %	30,0 %
Average series 5	0,548	1,008	1,489	1,963
% Average deviation	11,7 %	18,3 %	19,5 %	22,2 %

5.1.4 Pyramid

The measured average diagonal length D_{mean} of the impressions versus the theoretical diagonal length has been plotted against load in Figure 49 below.

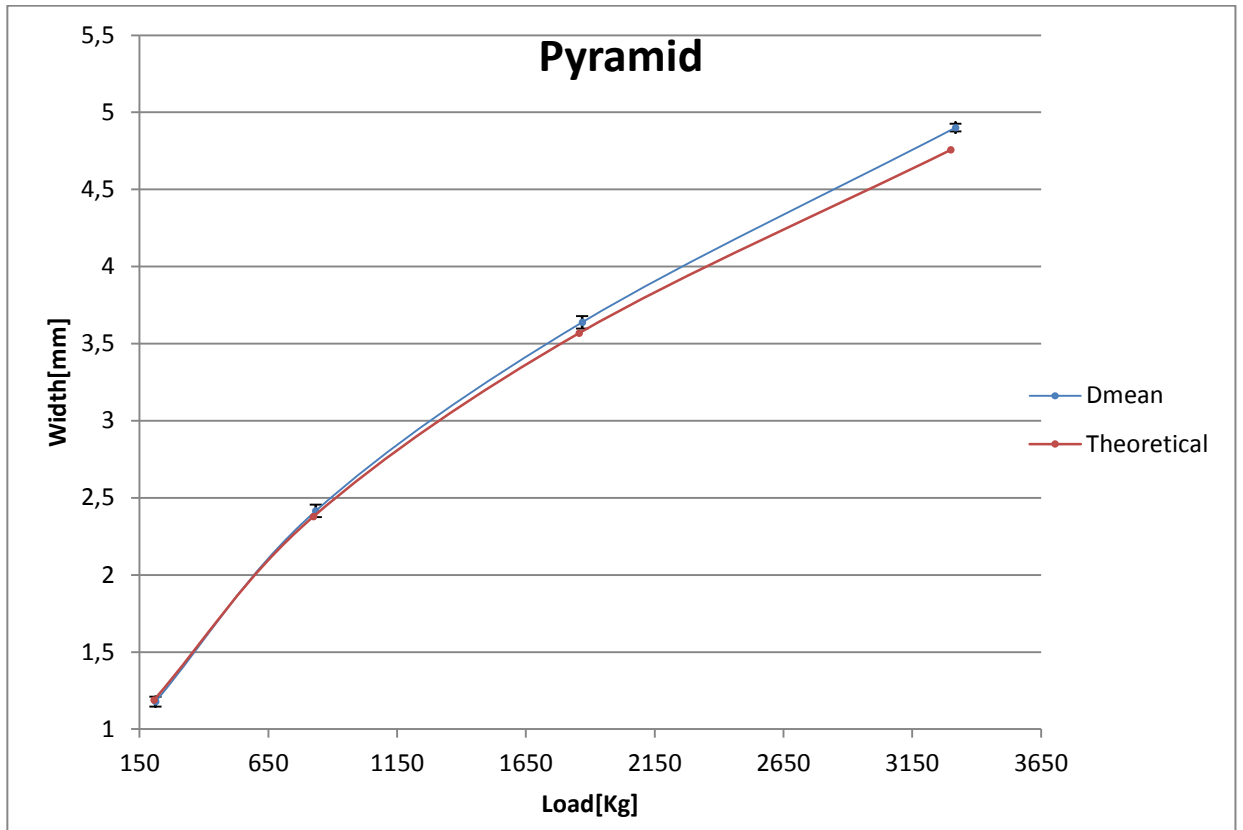


Figure 49: Dmean versus the theoretically calculated values

As seen in Figure 49 above, Table 19 below, the theoretically predicted values and measured values of diagonal length are almost identical for the pyramid indenter. The deviation is 0,96% lower than the theoretical value at the lowest load and 3,03% higher at the highest load. Complete set of data can be found in Appendix (D.4).

Table 19 Dmean compared to theoretically predicted values

	Dmean[mm]			
Theoretical	1,189	2,378	3,568	4,757
Average	1,178	2,415	3,638	4,901
% Average deviation	0,96	-1,54	-1,98	-3,03

5.2 REGRESSION CURVE ANALYSIS

The measured results for the wedge indentations show a nearly linear relationship with the load. A regression curve analysis has therefore been performed on the graphically plotted results by the use of Excel's regression analysis tool. The regression equations are constructed in a simple linear form with two variables, load(x) and width of the impression(y). By combining the regression equations with the load calculation equations described in chapter 3, an iterative expression which approximately gives the measured value of width has been produced. The iterative expressions can only give approximately correct values in relation to the given test series, i.e. the expression for the first three test series does not predict correct values for increased loading series. An example of one of the regression curves for wedge 60° series 4 is shown in Figure 50 below:

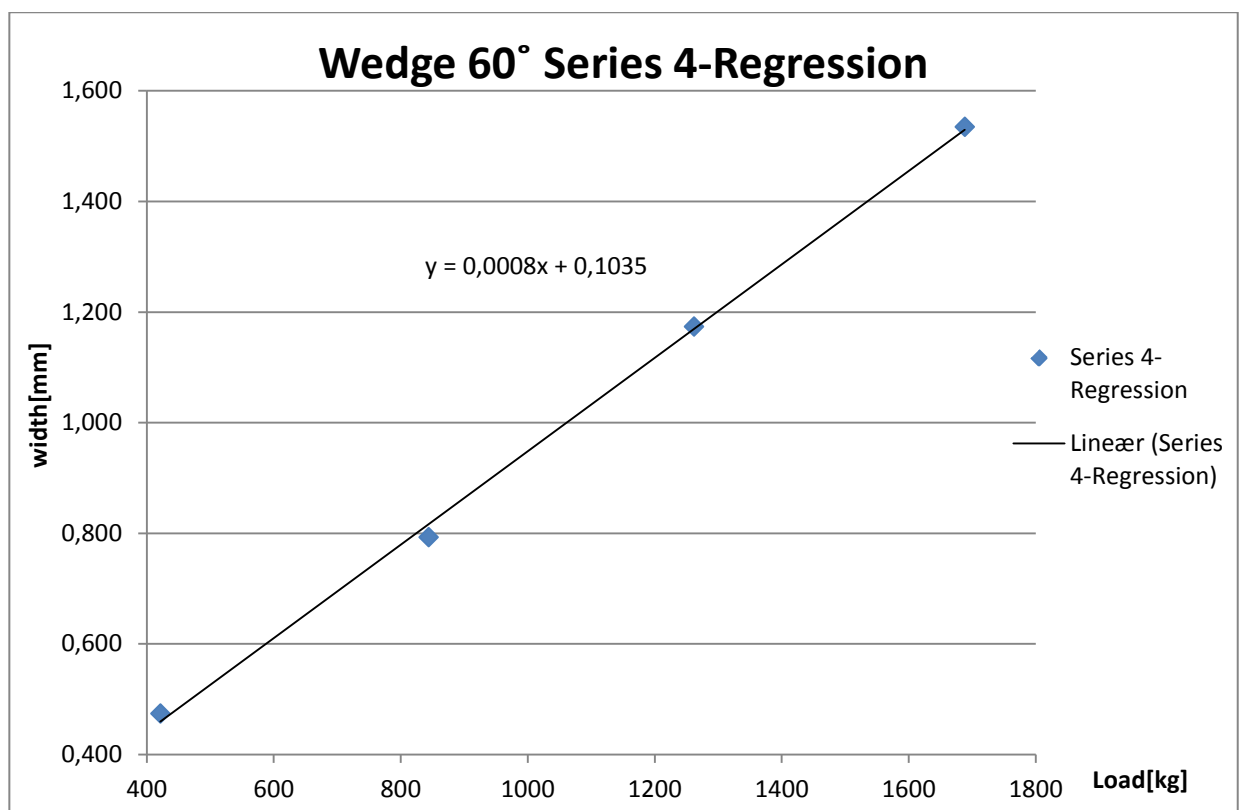


Figure 50: Regression curve analysis

As seen in Figure 50 above the equation for the regression curve for wedge 60° series 4 is as described in Equation (5.1) below:

$$y = 0,0008x + 0,1035 \quad (5.1)$$

Where the y-variable is the width (mm) and the x-variable is the load (kg). The load calculation for a theoretical width of a wedge indenter given in chapter 3 is shown in Equation (3.2):

$$P = \frac{P_w \cdot l}{g} = \frac{(2 \cdot p \cdot h \cdot \sin \alpha) \cdot l}{g} \quad (3.2)$$

The expression for indentation pressure p for series 4 is equal to:

$$p = 3,0 \cdot \text{Yield stress}$$

The correct value for the yield stress $786,3\text{N/mm}^2$ is used from the material certificate, Appendix (C.1). Calculating the theoretical load for a 2mm depth of penetration leads to Equation (3.2) being:

$$P = \frac{(2 \cdot 3,0 \cdot 586,3\text{N/mm}^2 \cdot 2,3\text{mm} \cdot \sin 30) \cdot 4\text{mm}}{9,81} = 1656,7\text{kg} \quad (3.2)$$

By inserting the calculated load from Equation (3.2) into equation (5.1), we get the following iterated value of width:

$$y = 0,0008 \cdot 1656,7 + 0,1035 = 1,429\text{mm} \quad (5.1)$$

The actual measured value of width was 1,535mm. The iterated expression does not give an exact value of width, but a fairly close value. This is because the regression curve does not pass through all of the data points, but very close to them. Regression equations have been produced for all wedge indentation series and can be found in APPENDIX E.

5.3 DEPTH OF PENETRATION IN RELATION TO APPLIED LOAD

The test results have been compared to each other in terms of depth of penetration in relation to the applied load. As seen in figure 51 for the first three test series, the most effective indenters in terms of depth of penetration related to the applied load are the pyramid and wedge 60° .

At a test load of around 200kg the pyramid indenter is clearly the most effective, but as the load is increased, the difference in depth of penetration between the two indenters decreases. At a load of around 1200kg the depth of penetration curves intersect and the wedge 60° seems to become more effective in penetrating the steel. If the depth of penetration curve for the pyramid is compared to the increased loading series curves for the wedge 60° , the lines intersect in a region between 1100kg to 1450kg. This can be seen in Figure 52.

The reason for the wedge 60° becoming more effective than the pyramid in terms of penetration is because the surface area of the pyramid grows exponentially at a given increment of height down to the pyramid base. Equation (3.4) in chapter 3.9 describes this mathematically.

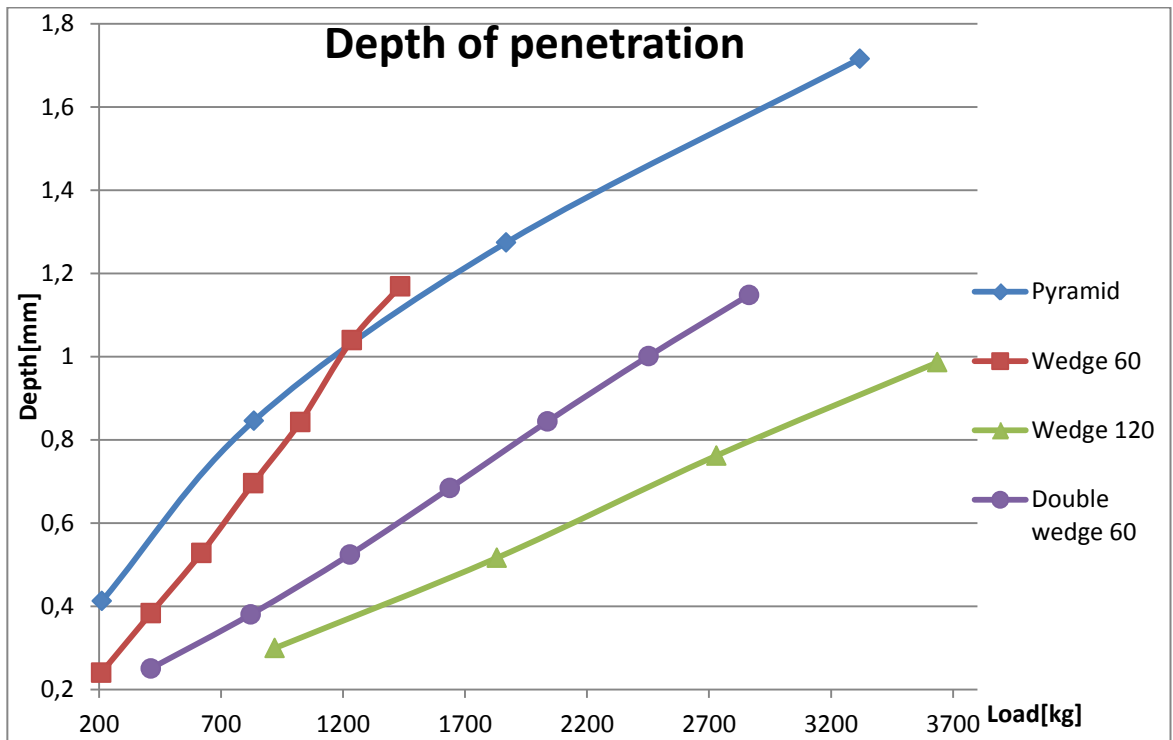


Figure 51: Depth of penetration versus applied load first three test series

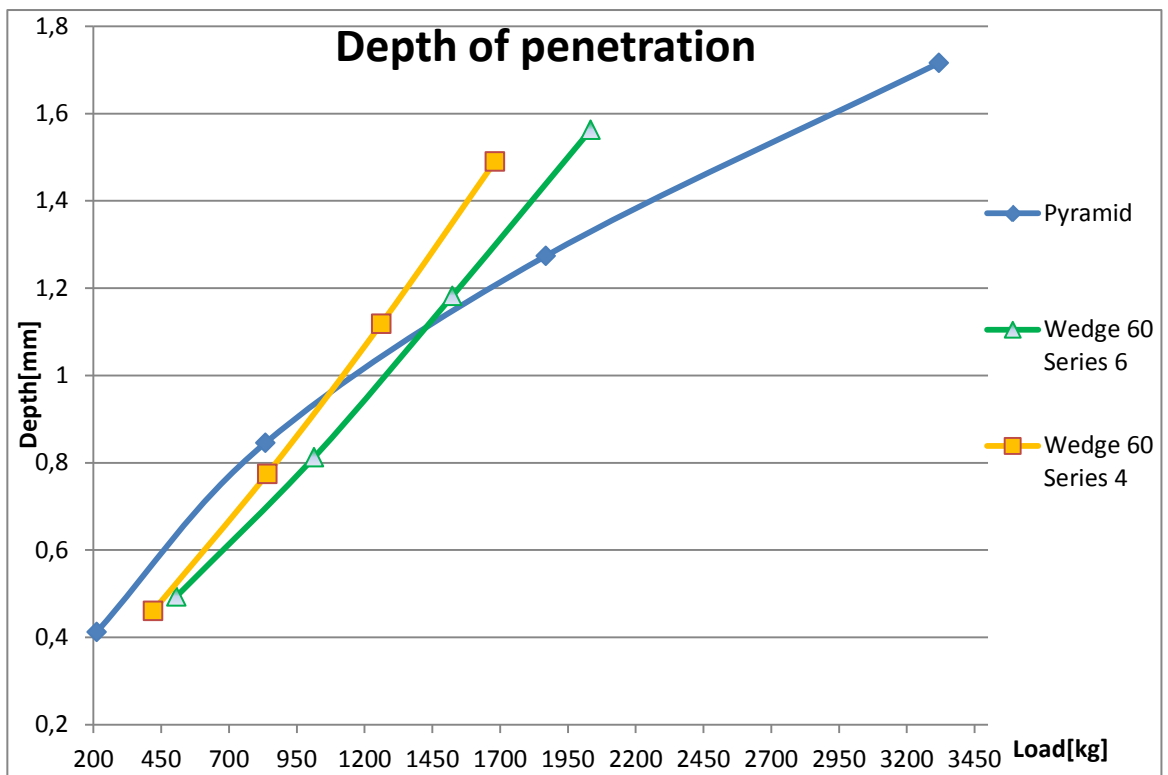


Figure 52: Pyramid and increased loading wedge series compared

5.4 EXPANDING CAVITY MODEL

The model was not known before the indentation testing was already completed. In relevance to the thesis the model has been used to see if it could predict the indentation pressure for the pyramid. The indentation pressure for the pyramid was based on an empirical value and an assumption described in chapter 3.9. As seen previous in chapter 5.1, the indentation pressure proved to be very accurate when comparing theoretical values to the measured results.

The model does not give a good approximation for the wedge indentations since they are not axi-symmetrical.

The expanding cavity model is an elastic-plastic indentation model and was first described by Johnson (1985) [8]. It can be used to describe indentations by axi-symmetrical indenters like cones, pyramids and spheres. It is based on observations that the subsurface displacements produced by the indenter are approximately radial for first point of contact.

The indentation process is idealized by imagining the contact surface between the material and the indenter being encased by a hemispherical hydrostatic core of radius a , as illustrated in Figure 53. Throughout the core the pressure is assumed to be equal in magnitude to the applied pressure p . Outside of the core it is assumed that the stresses and displacements are elastic-perfectly plastic, the boundary between the plastic and elastic regions of deformation is a radius denoted as c .

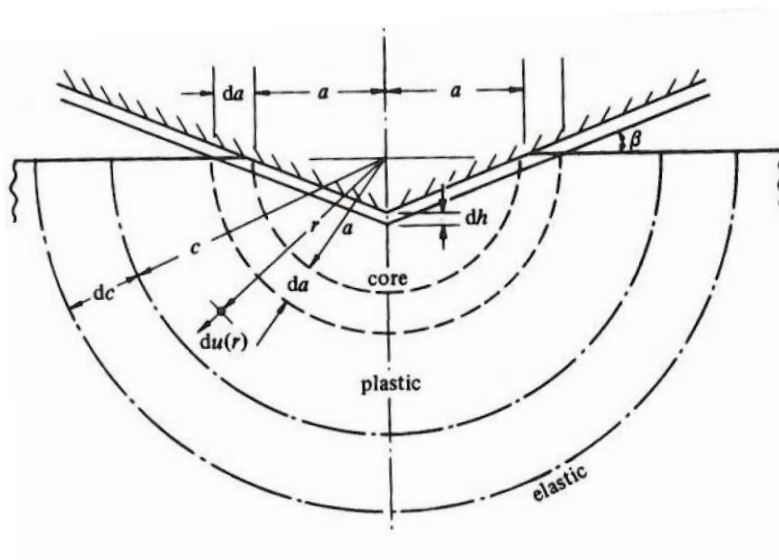


Figure 53: Cavity model of a pyramid/cone indentation.[10]

At the boundary between the core and the plastic zone the stress p is equal to the radial component of stress. The core pressure is then given by Equation (5.2):

$$\frac{p}{Y_f} = -\left(\frac{\sigma_r}{Y_f}\right)_{r=a} = \frac{2}{3} + 2 \ln \frac{c}{a} \quad (5.2)$$

Where a is the radius of contact (the core), σ_r is the radial stress and Y_f is the yield stress, or flow stress representative for the indentation related to work hardening of the material.

The radial displacements of material particles lying on the boundary are given by Equation (5.3):

$$\frac{du(r)}{dc} = \frac{Y_f}{E} 3 \left((1 - \nu) \frac{c^2}{r^2} - 2(1 - 2\nu) \frac{r}{c} \right) \quad (5.3)$$

Where ν is Poisson's ratio, E is the Elastic modulus and r is the distance to a particle lying at the boundary.

Conservation of the volume in the core which gives Equation (5.4) for a pyramid:

$$2a^2 du(a) = a^2 \cdot \tan \beta da \rightarrow \frac{du(a)}{da} = \frac{1}{2} \tan \beta \quad (5.4)$$

Where β is the inclination of the face of the pyramid to the surface, as seen in Figure 53 and is given by Equation (5.5):

$$\beta = \frac{\pi}{2} - \alpha \quad (5.5)$$

α is the semi angle of the pyramid.

By combining Equations (5.3) and (5.4), with Poisson's ratio equal to $\nu = 0,5$ gives Equation (5.6):

$$\frac{c^2}{a^2} = \frac{E}{3 \cdot Y_f} \tan \beta \quad (5.6)$$

Geometric similarity of the strain field with continued penetration requires that the relation between core radius a and boundary radius c is:

$$\frac{dc}{da} = \frac{c}{a} = \text{constant} \quad (5.7)$$

Considering the relation in Equation (5.7) and then inserting Equation (5.6) into Equation (5.2) gives the following relation between core pressure P and yield stress Y_f , shown in Equation (5.8):

$$\frac{p}{Y_f} = \frac{2}{3} \left[1 + \ln \left(\frac{E}{3 \cdot Y_f} \tan \beta \right) \right] \quad (5.8)$$

Equation (5.8) is known as the expanding cavity model equation and can be used to describe indentations by an axi-symmetric indenter with good approximation.

If the material work-hardens the yield stress of the material can be replaced with a representative flow stress measured in a compression test at a given percentage of strain ϵ_R . According to Johnson (1985) [8], ϵ_R is given by Equation (5.9):

$$\epsilon_R = 0,2 \cdot \tan \beta \quad (5.9)$$

As seen in Equation (5.9) the flow stress for a work-hardening material is dependent on the angle β which in turn depends on the angle of the indenter, the relation is given in Equation (5.5).

The elasticity of the indenter can be taken into account by replacing the elastic modulus of the indented material E with a combined elastic modulus E^* in the expanding cavity model Equation (5.8). The combined elastic modulus E^* is described by Equation (5.10):

$$E^* = \left[\frac{1 - \nu_1^2}{E_1} + \frac{1 - \nu_2^2}{E_2} \right]^{-1} \quad (5.10)$$

Where ν_1 and E_1 is poisson's ratio and elastic modulus of the indented material, ν_2 and E_2 is poisson's ratio and elastic modulus of the indenter.

The model has been used for the pyramid indenter to see if it can give a good approximation of the indentation pressure.

Applying the Equations (5.8) and (5.10) for the pyramid indenter described in chapter 3.9 with the following data:

Table 20: Mechanical properties for indenter and indented steel plate

Y_f	$586,3 N/mm^2$
$E_1 = E_2$	$207 \cdot 10^3 N/mm^2$
$\nu_1 = \nu_2$	0,3
β	$\frac{\pi}{4}$

Mechanical properties in Table 20 are taken from material certificate Appendix C.1 and Callister (2007) [9].

By using the elastic modulus and poissions ratio in Table 20, Equation (5.10) becomes:

$$E^* = 113,736 \cdot 10^3 N/mm^2 \quad (5.10)$$

Using the combined elastic modulus and the yield stress given in Table 20 in Equation (5.8):

$$\frac{p}{Y_f} = \frac{2}{3} \left[1 + \ln \left(\frac{113,736 \cdot 10^3 N/mm^2}{3 \cdot 586,3 N/mm^2} \tan \frac{\pi}{4} \right) \right] = 3,446 \quad (5.8)$$

The pressure inside the hydrostatic core is assumed to be equal in magnitude to the applied pressure p , the indentation pressure is therefore equal to p . Equation (5.8) can then be written as:

$$p = 3,446 \cdot Y_f = 3,446 \cdot 586,3 \frac{N}{mm^2} = 2020,4 \frac{N}{mm^2} \quad (5.8)$$

Comparing above results with the empirically based assumption for the indentation pressure described in chapter 3.9 :

$$p = 3,4 \cdot Yield$$

$$p = 3,4 \cdot 551 \frac{N}{mm^2} \cdot 1,08 = 2023,3 \frac{N}{mm^2}$$

Note: 1,48% Higher value than actual, see chapter 3.4

As the results imply, the use of the expanding cavity model gives a very good indication of the indentation pressure for the pyramid indenter. It should be noted that poisson's ratio and the elastic modulus of the indenter has been put equal to the indented steel plate. Modulus of elasticity and poisson's ratio of the indenter might have increased somewhat during heat treatment, which could give a slight difference in combined modulus of elasticity.

Despite giving a very accurate result of the indentation pressure, there are however some problems with the model. In theory, the model should be able to predict the hardness value of the steel plate which indentations were made on. This however proves not to be the case as it predicts a lower hardness value than the one given for the material in the material certificate. This could indicate that the material work hardens to some degree.

Attempts to investigate this problem have been unsuccessful. The original plan was to perform a compression yield test on the indented steel, but due to limitations on the mechanical testing machine at UIS a compression test could not be performed.

More complex expanding cavity models involving work hardening has been presented by X.L Gao(2006) [10].

5.5 PLASTIC IMPRESSION ANALYSIS

An indentation pressure of around 3,4 times the yield stress for the pyramid indenter is also supported by studies of the plastic impression from the pyramid indentations.

The plastic impressions were analyzed by using the same technique as when determining the Vickers hardness value. First a hardness stress called σ_H was found, the hardness stress is described in Equation (5.11):

$$\sigma_H = \frac{\text{Applied force}}{\text{Plastic surface area}} = \frac{F}{A_s} \quad (5.11)$$

Where the plastic surface area is found by using Equation (3.4) from chapter 3.9 and the applied force is simply the load multiplied with g.

$$A_s = \frac{d^2}{2 \sin 45^\circ} \quad (3.4)$$

The hardness stress σ_H , was then divided by the yield stress given in Table 20, previous. Equation (5.12) gives an indentation ratio:

$$I_r = \frac{\sigma_H}{Y_f} \quad (5.12)$$

The ratio I_r is similar to the $\frac{P}{Y_f}$ ratio produced by the expanding cavity model Equation (5.8) presented in section 5.4.

The average value of the I_r ratio from the three first test series is shown in the Table 21 below:

Table 21: I_r ratio for the first three test series

	I_r			
Series 1	3,970	3,604	3,470	3,335
Series 2	3,434	3,293	3,294	3,265
Series 3	3,463	3,266	3,260	3,208
Total Average	3,405			

As seen in Table 20 the total average from the three first test series is 3,405. This further supports the claim of an indentation pressure of about 3,4 times the yield stress is correct for the pyramid indenter. The results for the increased load series shows a bit lower I_r ratio. Complete analysis tables can be found in APPENDIX F.

5.6 PROBABLE REASONS FOR DEVIATIONS

The most likely reason for the large deviation between theoretically predicted and measured values for the wedge indenters is the assumption of plane strain which the slip-line field theory is based on.

As described in the results chapter 4, displacement of metal occurred in the length direction of the wedge indenters on a relatively large scale. This was not accounted for in the calculations of the indentation pressure and depth of penetration due to the slip-line field model being two-dimensional. This probably caused buildup of a complex stress field at the apex ends, resulting in lower rates of penetration by the wedge indenters.

Potentially, this could also have had an effect on the deformation that occurred along the apex. Another reason could be that the wedge geometry causes a higher extent of work-hardening of the steel than the pyramid indenter. The effects of the steel piling up on the sides of the wedge indentations are clearly visible, which is an indication of work-hardening. However, this effect is also visible for the pyramid indentations.

5.7 DEFORMATION

Upon completion of testing a total of five out seven indenters had experienced dimensional changes as a result of deformation. Three of the seven indenters were so severely deformed after the first series of testing that there was no point in further testing with them.

From the theory presented in chapter (2.7), according to Tabor (1950) [2] the indenter should be at least two and a half times as hard as the indented material in order to avoid any permanent deformation. From a material standpoint this requirement is fulfilled as the hardness numbers of the indenters were measured to be 50-51HRc and the hardness number of the indented steel plate 20 HRc (converted from the Brinell hardness number).

Reviewing which of the indenters that severely deformed the common denominator is that the indenters having the largest volume (square, rectangular and wedge 120°) were the ones which deformed the most. Judging by the information in the heat treatment procedure it seems that every indenter has been hardened and tempered for the same amount of time.

Based on this information the logic reason for the square, rectangular and wedge 120° indenters severely deforming is due to the heat treatment not providing sufficient hardness throughout the whole volume of the indenters. Heat treatment procedure can be found in Appendix (C.3).

Another reason for the deformation could be due to inaccuracies in placement of the indenters causing a skewed angle during application of the loads. This could have led to an uneven pressure distribution between indenter and plate. This is probably the reason why the single wedge 60° indenter deformed while the double wedge 60° did not.

Each of the indenter profiles on the double wedge was subjected to the same loads as the single wedge 60° indenter. A slight un-evenness in loading between the double wedge 60° profiles is probably the reason for the small differences in the measured dimensions.

As mentioned in the section 5.6 above another potential reason for the wedge indenters deforming along the apex could be from high stress concentrations at the apex ends.

5.8 POTENTIAL SOURCES OF ERROR IN RESULTS

As stated in chapter 3.4 the most obvious error was discovered shortly after test completion. The applied loads were 1,48% higher than what they theoretically should have been, this has affected the results by giving fractionally higher measured geometric values than what they probably would have been. The error is however so small it is considered negligible.

There is some possibility that the execution of the indentation process i.e. inaccuracies in placement of the indenters may have caused some deviation in measured results.

Another potential source of error in the measured results could have arisen due to the slight deformation the wedge 60° & 120° indenters experienced during the first series of testing. The measured results for the first three series of testing for the single wedge 60° are practically equal to the double wedge which did not experience any deformation. It therefore seems that the deformation had no major effect on the measured results at lower loads.

Looking at the tests performed with higher loads i.e. the last series of the adjusted loading one should be aware that the indenters deformed quite a bit, the measured results for these series therefore have questionable validity.

Equipment used for testing like the load measurement cell is not considered as a source which could have accumulated much error. The calibration certificate provided from the supplier shows a 0% variance in load error up to 3750kg. The calibration certificate can be found in Appendix (C.4).

5.9 DESIGN CONSIDERATIONS

Based on the study and analysis of the test results many important considerations can be made in regards design for slips teeth profiles.

The fact that many of the indenters failed due to excessive deformation, a phenomena which seems to be a result of incomplete heat treatment has led to the following conclusion. The teeth profiles chosen for use on slips should have approximately the same volume in order to achieve equal hardness from heat treatment procedures. The profiles should have a hardness value of at least two and a half times that of the indented material, preferably the hardness ratio should be even higher than that if possible.

On the basis of the test results and the expanding cavity model presented in chapter 5.4, it seems very favorable to use an axi-symmetric indenter geometry like the pyramid compared to the other tested geometries. Because of the axial symmetry of the pyramid indenter, the force distribution along the four 45° inclined pyramid faces is equal in magnitude, force distribution along the four 55° ridge angles is also equal in magnitude. This leads to an effective dispersion of the applied force onto the steel plate in a cutting manner. The material is displaced equally in all principal directions while maintaining a low stress concentration on the indenter itself. This is reflected in both the test results and the fact that the pyramid was the only single indenter which did not experience any deformation. By use of the expanding cavity model the indentation pressure for different angled pyramids can be calculated.

One possible downside in using the pyramid geometry as teeth profiles is due to excessive tubing deformation. If a lot of force is applied to the pyramid indenter the plastic impression becomes very big compared to the actual depth of penetration. As mention in chapter 5.3 the surface area increases almost exponentially at an increment of penetration. The amount of force applied to each pyramid indenter should therefore not exceed 1100kg. At loads above 1100kg the test results indicate that the wedge 60° proved to be more effective in terms of penetration. The amount of force each teeth profile is subjected to can be controlled by adjusting the number of teeth profiles placed on the surface.

If a wedge teeth profile is to be used on a slips element the wedge 60° indenter would be the obvious choice based on the test results. There are however some concerns in regards to deformation and the mathematical difficulties in accurately predicting the depth of penetration. The single indenter experienced quite a bit of deformation during the tests, however, the double wedge 60° experienced very little. If applied as teeth profiles on a slips element, the teeth profiles should be designed in the same way as the double wedge 60° indenter, 2mm distance between profiles. If the distance between the teeth profiles is bigger, the geometry should be changed so it becomes less susceptible to a skewed angle and deformation.

An alternative design for the wedge 60° indenter can be found in APPENDIX G.

5.10 PROPOSED SLIPS DESIGN

A proposed slips element designed with pyramid teeth profiles can be seen in Figure 54, below. The pyramid geometry has been selected since it has proved to be the most effective based on test results and the indentation process the easiest to mathematically approximate.

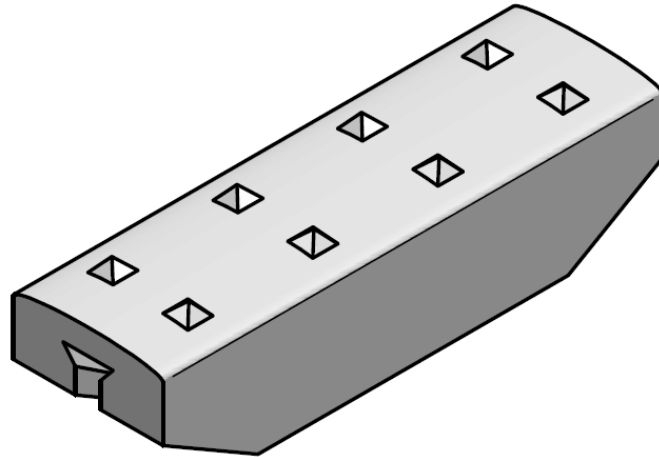


Figure 54: Slips element seen from isometric view with pyramid profiles on the top surface.[2]

The dimensions of the slips element is based on a slips element that was borrowed from E-Plug. The original teeth profiles on the top surface have been replaced with eight four sided pyramid teeth profiles with similar face angles of 90° and ridge angles of 110° , same as the pyramid indenter.

Dimensions like height and base area of the pyramids has however been modified. The height has been adjusted to 2,5mm and the base area has been reduced to 5x5mm. Eight pyramids have been symmetrically distributed along the top surface. As seen in Figure 54 the top surface where the pyramid are placed is rounded with a radius in order to match the inside radius of the tubing wall. This is to ensure that the indentations made on the tubing ID is approximately level with the tubing wall.

Based on several tests with the TorcPlug[®], E-Plug has found the ideal number of teeth profiles to be eight, the number of pyramids placed on the surface has therefore been chosen to eight.

As can be seen in Figure 55&56, the underside of the slip is formed as ramp with a tail shaped groove running from the middle of the front side to the underside of the slips element. This is to allow the element to be expanded outwards by the upper and lower slips-cone. The details surrounding this feature is E-Plugs intellectual property, the feature shown in the drawings have been replicated from the borrowed slips element.

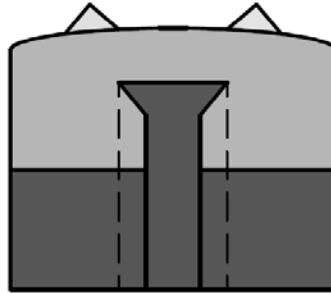


Figure 55: Slip element seen in front view with pyramid profiles and tail groove clearly visible.[2]

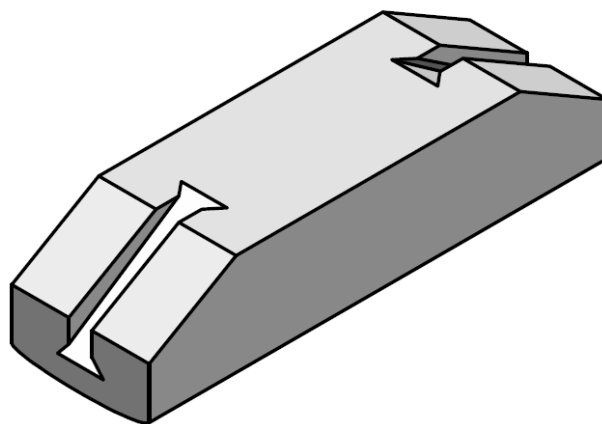


Figure 56: Ramp formed underside of the slip element with tail groove.[2]

Based on the theory and the results presented throughout the thesis, calculations of indentation pressure, surface area and depth of penetration can be formulated for the proposed slips element. A simplified example of the calculations is described below.

The force created when setting force is applied to the plug is calculated to be 40 metric tons, frictional effects neglected. The expansion force is distributed equally on five slips which accounts to 8tons per slips element. By dividing 8tons of force per element on 8 pyramid teeth profiles gives an indentation load of 1000kg per pyramid. Using the indentation pressure found with the expanding cavity model in chapter 5.4

$$p = 3,446 \cdot Y_f = 3,446 \cdot 586,3 \frac{N}{mm^2} = 2020,4 \frac{N}{mm^2}$$

By applying equations found in chapter 3.9 leads to a penetration depth of 0,9173mm. Diagonal length of the impression 2,62mm and plastic surface area of 4,885mm² for each of the 8 pyramid profiles.

The above example is simplified in terms of the expansion force, frictional effects and yield stress. An exact value of the expansion force per slip element is unknown. Tubing yield stress is in this example is taken as the same as for AISI 4140 steel. Complete design drawing of the slip and detailed calculations can be found in APPENDIX G.

5.11 RELEVANCE OF THE TESTST RESULTS AND STUDY

Since the TorcPlug's area of operation is in an oil well where the pressure and temperature is completely different compared to the environment where the tests were performed, there is a degree of uncertainty in whether the tests results would be reproducible in such an environment. However, the physical trends related to indentation pressure, surface area and angles discovered in the study would likely follow the same pattern. The study should be considered a guideline in terms of design considerations related to indentation and of how the indenters can be applied as teeth profiles on slips. If results found in the thesis are applied on a slips element, one should consider how the tests were performed.

6 CONCLUSIONS

A theoretical and physical study on the subject of indentation related to slips profile design has been conducted. Seven indenters with different geometries have been tested for the purpose of finding a correlation between indentation pressure, surface area, indenter angle and depth of penetration.

The use of the slip-line field theory in calculations of indentation pressure for the indentation of three dimensional wedge formed indenters resulted in large deviations between measured and theoretically predicted values. The accuracy of the theory only seems reliable if the criteria's of plane strain indentation is fulfilled. The actual value of the indentation pressure lies closer to three times the yield stress of the indented steel. However, even at this pressure there are still some discrepancies between theoretical and measured values in terms of predicted geometry of the indentation.

Regression curve analysis has been performed on the measured data, an example of how an iterated equation based on the regression curve can produce approximately correct values of width and depth has been demonstrated.

A successful method of calculating indentation pressure, plastic surface area and depth of penetration at a given load, has been discovered for a pyramid indenter with a 90° face angle. The theoretical calculations matched the test results by a margin of less than one percent on the lowest load to three percent on the highest load. A mathematical model for calculating the indentation pressure for axi-symmetric pyramid shaped indenters has been presented. The model is called the expanding cavity model. The indentation pressure calculated by using the model is supported by physical data from the indentation tests that were performed. Analysis of the plastic impressions from the pyramid indentations indicates the same value of indentation pressure as the other results. It can be concluded with high certainty that the indentation pressure for the pyramid indenter is about 3,4 times the yield stress of the indented steel.

The two most effective indenters in terms of penetration in relation to applied load are the pyramid and the 60° wedge. At loads up to around 1100kg the pyramid is the most effective in terms of penetration. Between 1100-1450kg there seems to be a transition area where the 60° wedge indenter becomes more effective in terms of penetration. This is due to the surface area of the pyramid exponentially growing at a given increment of depth.

The effect of two neighboring wedge indenter profiles 2mm apart showed to have no effect on the measured results. Doubling the load for the double wedge 60° indenter gave nearly identical results as the single wedge 60° indenter. However, the double wedge 60° displayed more stability during loading and little signs of deformation, whereas the single wedge 60° gradually deformed when the test loads were increased.

The indenters that were tested for the purpose of demonstrating the relation between surface area and indentation pressure, the square and rectangular indenters, failed as a result of excessive deformation during testing. The relation has therefore not been physically documented, but according to the theory presented in the thesis, the relation is about 3 times the yield stress of the indented material. I.e. the applied force needed to cause an indentation is directly proportional to the surface area necessary to produce a stress 3 times the yield stress between indenter and the indented material.

Several of the indenters that were tested failed as a result of excessive deformation. The indenters which deformed the most were the ones having the largest volume. The reason for the deformation looks to be a result of incomplete heat treatment throughout the volume of the indenters, leading to lower total hardness value. This conclusion is supported by reviewing the heat treatment procedure which states that all indenters have been subjected to heat treatment for the same amount of time.

For design considerations in relation to slips for the TorcPlug®, the profiles chosen for slips application should have a hardness value of at least two and a half times that of the indented metal (tubing). Preferably the hardness ratio should be even higher if possible. The profiles should have the same volume in order to achieve equal hardness from heat treatment procedures.

A slips element designed with pyramid shaped teeth profiles on the top surface has been proposed. The pyramid indenter has been found to be the most suited indenter profile for slips application.

7 SUGGESTIONS FOR FURTHER WORK

- Perform a compression yield test to determine the extent of work hardening involved in indentations of AISI 4140 indented steel.
- Perform an axial-load test with the indenters that proved to be the most effective to see how much axial load they can withstand before sliding. The test should be performed with an actual piece of tubing.
- Develop a realistic finite element slips model in order to see if the results presented in the thesis and the axial load test can be verified by the model. The FEM program used would likely have to be a fully licensed version.
- Develop a realistic finite element model that can simulate the slips mechanism in a realistic oil well scenario. The FEM program used would likely have to be a fully licensed version.

8 REFERENCES

LITERATURE LIST

- [1] E Plugs homepage: *TorcPlug® technical data and animation*:
<http://www.eplug.no/home/>
- [2] D.Tabor (1951): *"The hardness of metals"*, Oxford University Press
- [3] R.S. Fries(1975): *Estimation of yield stress from Hardness values*, NTIS:
<http://www.dtic.mil/cgi-bin/GetTRDoc?AD=ADA016166>
- [4] Online Hardness conversion calculator according to ASTM E 140-97:
<http://www.tribology-abc.com/calculators/hardness.htm>
- [5] ASTM E 103 - 84: *"The standard test method for rapid indentation hardness testing for metallic materials"*. <http://www.astm.org/Standards/E103.htm>
- [6] Sverdrup steels homepage: *Mechanical properties AISI4140*:
<http://www.sverdrupsteel.com/no/aisi-4140/>
- [7] W.F. Hosford, R.M Caddell(1983): *"Metal forming, Mechanics and Metallurgy"*, Prentice-Hall International, Inc. pp.168-201.
- [8] K.Johnson (1985): *"Contact mechanics"*, Cambridge University Press, pp.153-179.
- [9] D.Callister(2007): *"Material Science and engineering, an introduction"*, 7th ed. John Wiley & Sons. Inc. Appendix B: Properties of selected Engineering materials.
- [10] X.L. Gao, X.N. Jing, G.Subhash (2006): *Two new expanding cavity models for indentation deformations of elastic strain hardening solids*. International Journal of Solids and Structures. Vol 43. Issues 7-8, April 2006, pp.2193-2208.
<http://www.sciencedirect.com/science/article/pii/S0020768305001836>
- [11]R. Hill(1950) : *"The mathematical theory of plasticity"*, Oxford University Press, pp.213-254.
- [12]A. Olsen (2002): *Hardhetsprøving av metalliske materialer*, kompendium Høgskolen i Vestfold.
<http://www-bib.hive.no/tekster/hveskrift/kompendium/2002-01/komp1-2002.pdf>
- [13]J.Odland(2012): *"Offshore field development"*, OFF500 lecture notes, PDF
- [14]Heriott Watt-Institute of petroleum engineering (2005): *"Field Development compendium"*, Flame development, PDF
- [15] Univeristy of cambridge: *Analysis of the deformation process, Henckys relation*:
http://www.doitpoms.ac.uk/tlplib/metal-forming-3/hencky_derivation.php
- [16]C.J.Studman, M.A. Moore, S.E Jones (1976): *On the correlation of indentation experiments*. Journal of physics D: Appl.Phys, Vol10, 1977. pp.949-956.

<http://iopscience.iop.org/0022-3727/10/6/019>

[17] Tubing mechanical properties and size data:

http://www.vamservices.com/technical_information/connection_ds.aspx

[18] American Petroleum Institute (API) tubing grades:

http://petrowiki.org/File%3ADevol2_1102final_Page_290_Image_0001.png

FIGURE REFERANCES

[1] TorcPlug illustrations: <http://www.eplug.no/home/>

[2] Photos, illustrations and drawings taken or produced self

[3] Slips model illustration provided by E Plug

[4] Rigid Perfectly plastic solid stress-strain curve:

http://homepages.engineering.auckland.ac.nz/~pkel015/SolidMechanicsBooks/Part_II/08_Plasticity/08_Plasticity_01_Introduction.pdf

[5] W.F. Hosford, R.M Caddell(1983): *"Metal forming, Mechanics and Metallurgy"*, Prentice-Hall International, Inc. pp.-172.

[6] Illustrations of the stress components, slip lines and Mohr circle:

http://www.doitpoms.ac.uk/tlplib/metal-forming-3/hencky_derivation.php

[7] R. Hill(1950) : *"The mathematical theory of plasticity"*, Oxford University Press, pp.-256

[8] D.Tabor (1951): *"The hardness of metals"*, Oxford University Press, pp.-103

[9] API grade table: http://petrowiki.org/File%3ADevol2_1102final_Page_290_Image_0001.png

[10] K.Johnson (1985): *"Contact mechanics"*, Cambridge University Press, pp.174.

[11]W.F. Hosford, R.M Caddell(1983): *"Metal forming, Mechanics and Metallurgy"*, Prentice-Hall International, Inc. pp. 202-203.

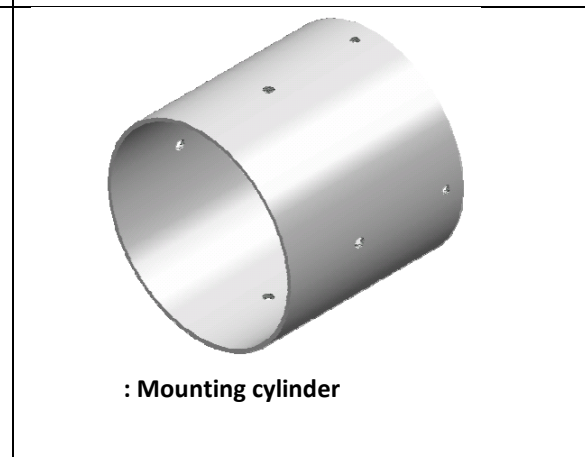
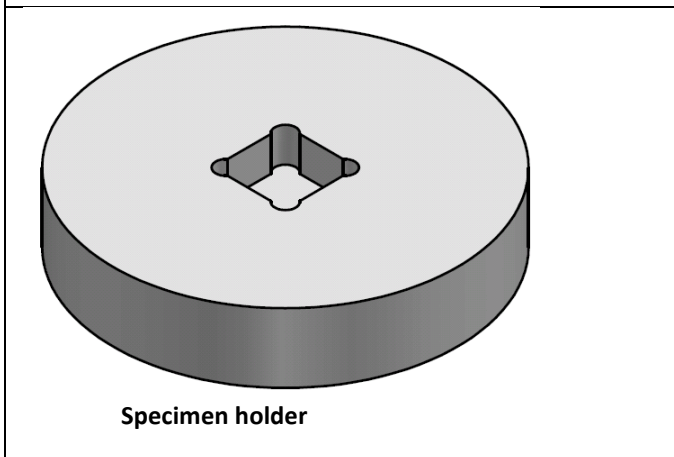
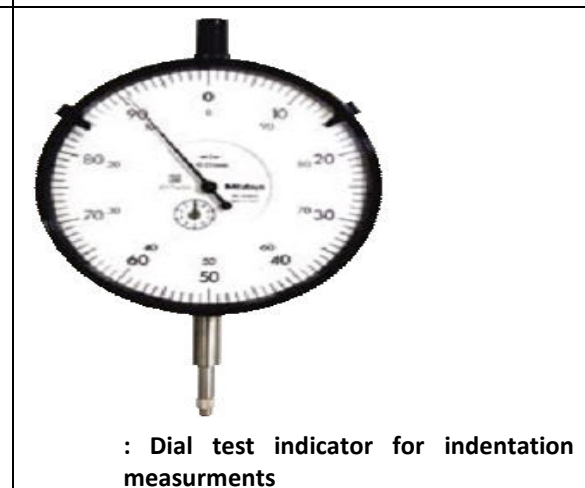
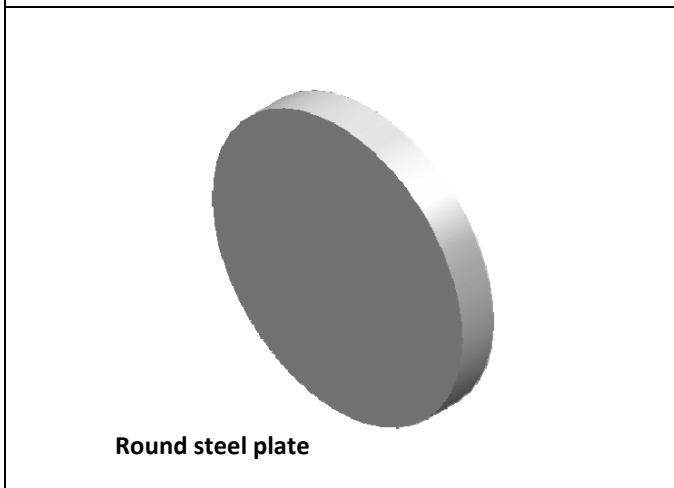
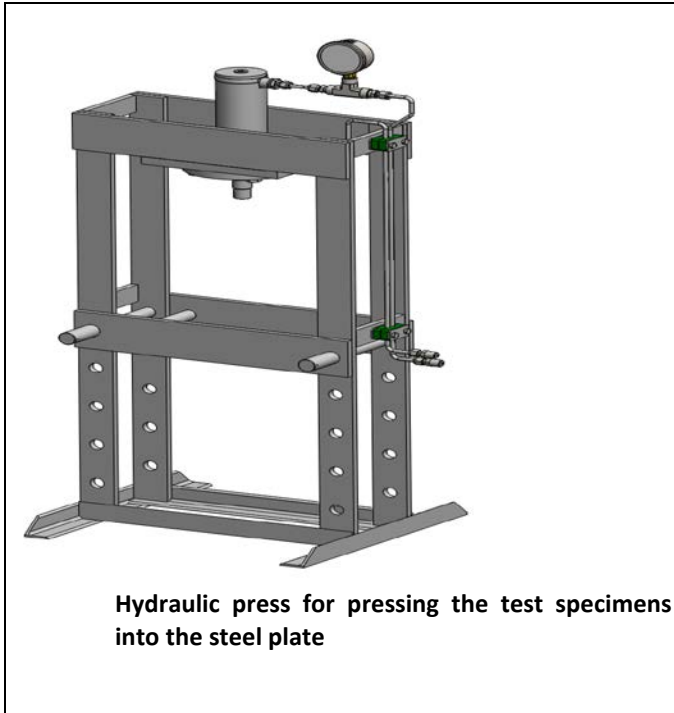
APPENDIX A. INDENTATION TEST PROCEDURE

A series of indentation tests are to be performed with five steel specimens of different geometric properties. The specimens are to be indented into a steel plate with a hydraulic press. The goal of the tests is to observe how the geometries effectively cause yielding, plastic flow and indentation from predetermined pressure criterions. A hypothesis for load and indentation pressure for each of the geometries has been formulated from the literature studied. The tests will be performed with these loads to check if the theory is correct. Specimen geometries have been chosen from theory of indentation, plasticity and geometries which may be applicable for use as slips teeth. A sixth specimen with two similar geometries besides each other will also be tested to observe the metal pile up effect which occurs between two slips teeth. For physical similarity the steel specimens are made in the same scale as teeth used on slips. The specimens are made of AISI 4140 steel with Rockwell C hardness over 50. The steel plate is also made of AISI 4140 with Rockwell C hardness between 18 and 22. Location of the testing will be at E-Plug's workshop which has a 30tonn hydraulic press at their disposal.

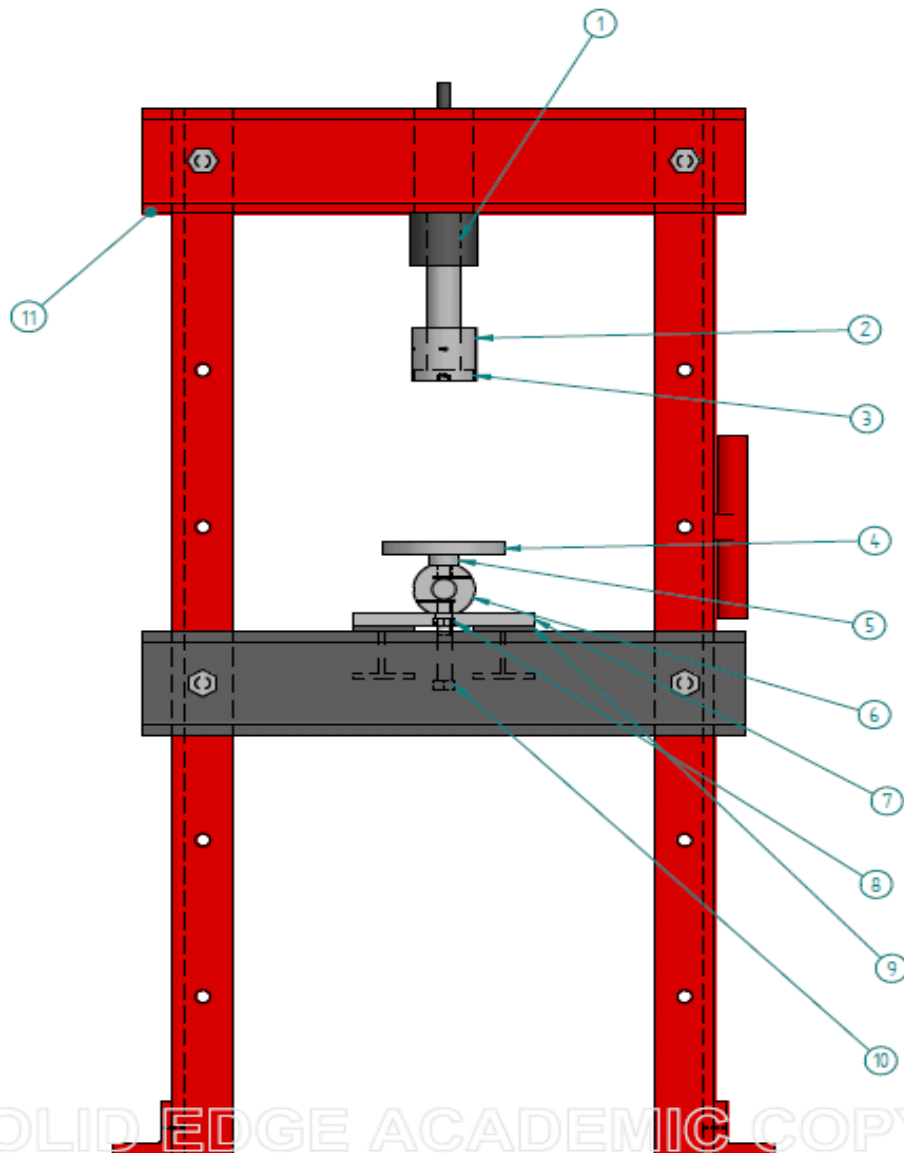
A.1. EQUIPMENT LIST

- Hydraulic press, 30tonn
- Six AISI 4140 test specimens, 50HRC
- Two AISI 4140 round steel plates, 18-22HRC- 25mm thickness
- Specimen holder AISI 4140
- AEP-TS, 7,5tonn load measurement cell with logger program
- Anvil
- Dial test indicator, $1\mu m$ accuracy with needle point and setup rig
- Forming putty
- Video and photo camera
- Additional tools, plates and bolts for rig up of load measurement cell.

Title	Master Thesis Spring 2013 Johannes Ohnstad	Page 76
-------	---	---------



A.2. EQUIPMENT SETUP



Equipment setup

1. Piston-Hydraulic press	7. Mounting plate with 25mm hole
2. Mounting cylinder	8. Support beams (H-profile)
3. Specimen holder	9. Threaded Bolt-M24x2
4. Steel plate, round	10. Fastening nut-M24x2
5. End piece	11. Hydraulic press-30t
6. TS-7,5t load cell (compression)	

A.3. GUIDELINES

- The distance from the centre of the indentation to the edge of the specimen or edge of another indentation, shall be at least two and a half times the diameter of the indentation.
- The test force shall be applied to the specimen without shock or vibration.
- The angle between the load line and the normal to the specimen shall not exceed 2°.
- The surface on which the indentation is to be made shall be filed, ground, machined or polished with an abrasive material. The surface in contact with the test support shall be clean, dry and free of any conditions which may affect the test results.
- The depth measurement device shall be verified over the working range by the use of an accurate reference scale, or other means, and shall correctly indicate the depth of penetration to an accuracy of $\pm 0,005\text{mm}$.
- At least five indentations shall be made for each of the geometries.

Guidelines are taken from "*The standard test method for rapid indentation hardness testing for metallic materials*" ASTM E 103 - 84.

A.4. LOAD CALCULATIONS

The load calculations for plastic flow and indentation for the geometries is based on the slip-line field theory. The slip-line field theory can predict more or less exact solutions depending on the geometry of the indenter. When using the theory certain assumptions are made:

- Plain strain deformation(2-dimensional)
- The metal is considered as rigid-perfectly plastic after yield
- Temperature effects, strain rate, and time are not considered
- Constant shear stress at the interface boundary. Usually, either a frictionless condition or sticking friction is assumed.

Slip-line fields are known for five of the six geometries. For square and rectangular geometries the depth of penetration related to contact pressure is hard to predict theoretically. Measurements for depth of penetration versus applied load will be plotted graphically.

Mechanical properties for AISI 4140 round steel plate:

Title	Master Thesis Spring 2013 Johannes Ohnstad	Page 79
-------	---	---------

Hardness: 18-22HRC
Ultimate tensile strength: 689 N/mm²
Yield stress (0,2% proof): 551N/mm²
Elongation: 20%min
Red. of area: 40%
Ref,[4]

Plate geometry:

Thickness: 25,4mm
Original diameter of plate: 410mm

The plate will be cut to into smaller pieces better suited for testing

The effect of work-hardening as a result of the indentation itself is dependent on the heat treatment technique which the steel has been subjected to. The effect of work hardening in relation to the indentation load can be accounted for by adding 8-10 percent to the indentation load. From D.Tabor Ref,[2] an addition of 8 percent seems to be valid for a wide range of indentations on heat treated steel. The theoretical indentation loads has been multiplied with an additional 8% to account for work-hardening.

Multiple test runs will be performed for calibration purposes. The load application will be logged on a computer for each test load. Penetration depth of the indentation will be checked with a dial test indicator.

Indentation loads marked with yellow will likely not be tested since desired depth of penetration is a little less then 2mm.

Title	Master Thesis Spring 2013 Johannes Ohnstad	Page 80
-------	---	---------

A.5. SQUARE

The square geometry has a surface area of 4x4mm and a maximum penetration depth of 3,5mm. The relation between the thickness of the plate H, and width of the indenter L is $\frac{H}{L} = 6,35$.

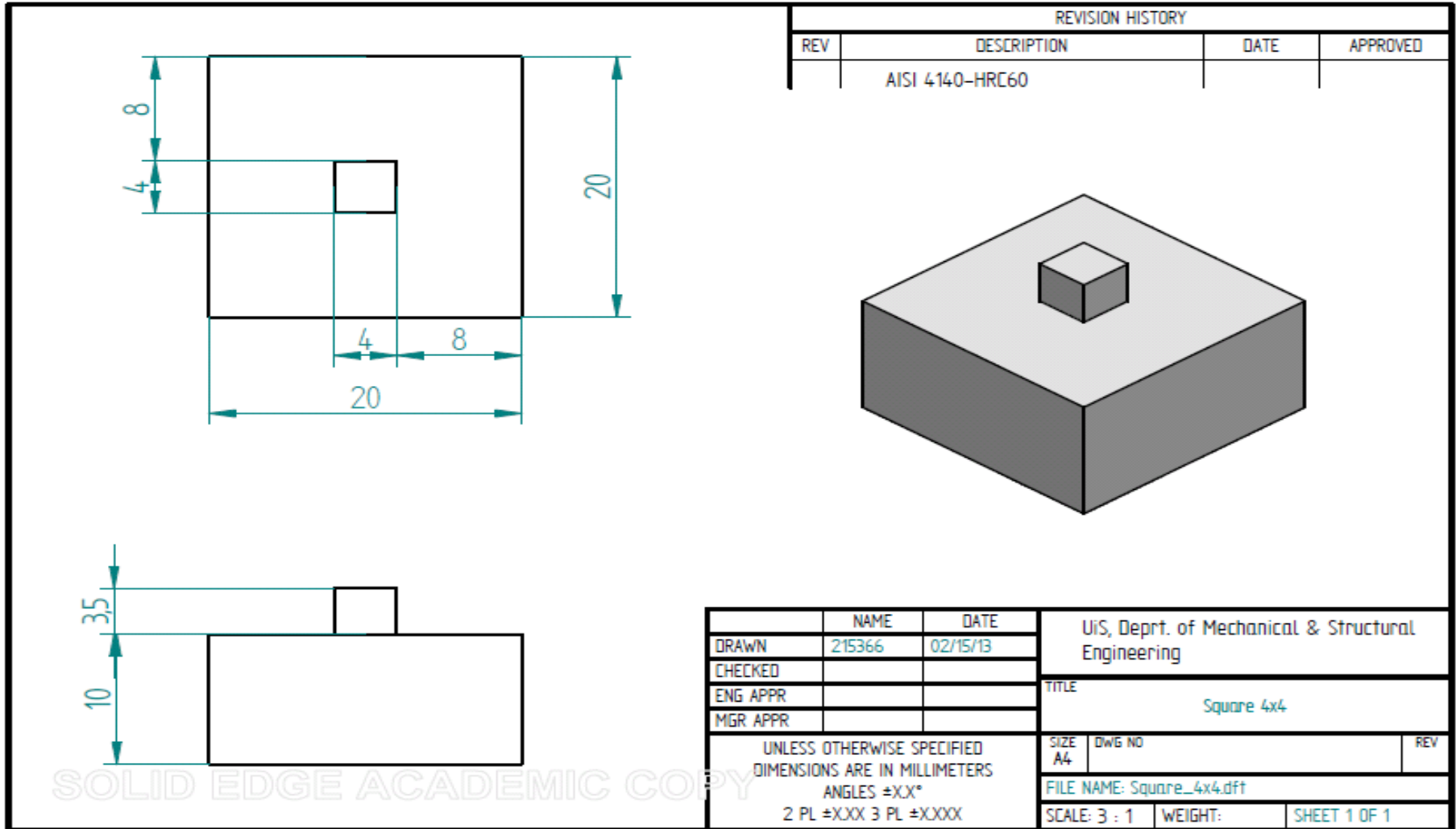
The indentation pressure is then given by:

$$p = 2k \left(1 + \frac{\pi}{2} \right) = 2,96 \cdot Yield$$

$$p = 2,96 \cdot 551 \frac{N}{mm^2} = 1631 \frac{N}{mm^2}$$

Yield point load	899Kg
Verification load	2500Kg
Indentation load (theoretical)	2660Kg
Verification load	2700Kg
Indentation load with work hardening	2873Kg
If full penetration is not achieved:	
Min upper load	2900Kg
Intermediate load	2950Kg
Max load	3000Kg

In order to check the accuracy of the hypothesis a series of indentation tests will be done with verification loads. From theory plastic flow and penetration of the metal will happen at the indentation load. If sufficient penetration depth is not achieved at the indentation load (with work hardening), three upper loads will be applied.



SOLID EDGE ACADEMIC COPY

A.6. RECTANGLE

The rectangular geometry has a surface area of 6x4mm and a maximum penetration depth of 3,5mm. The relation between the thickness of the plate H, and width of the indenter L is $\frac{H}{L} = 4,23$ which is just below the limit of 4,37, which gives a penetrating slip-line field.

The indentation pressure is then given by:

$$p = 2k(1 + 2\Delta\varphi)$$

Where $\Delta\varphi = 40^\circ = \frac{2}{9}\pi$

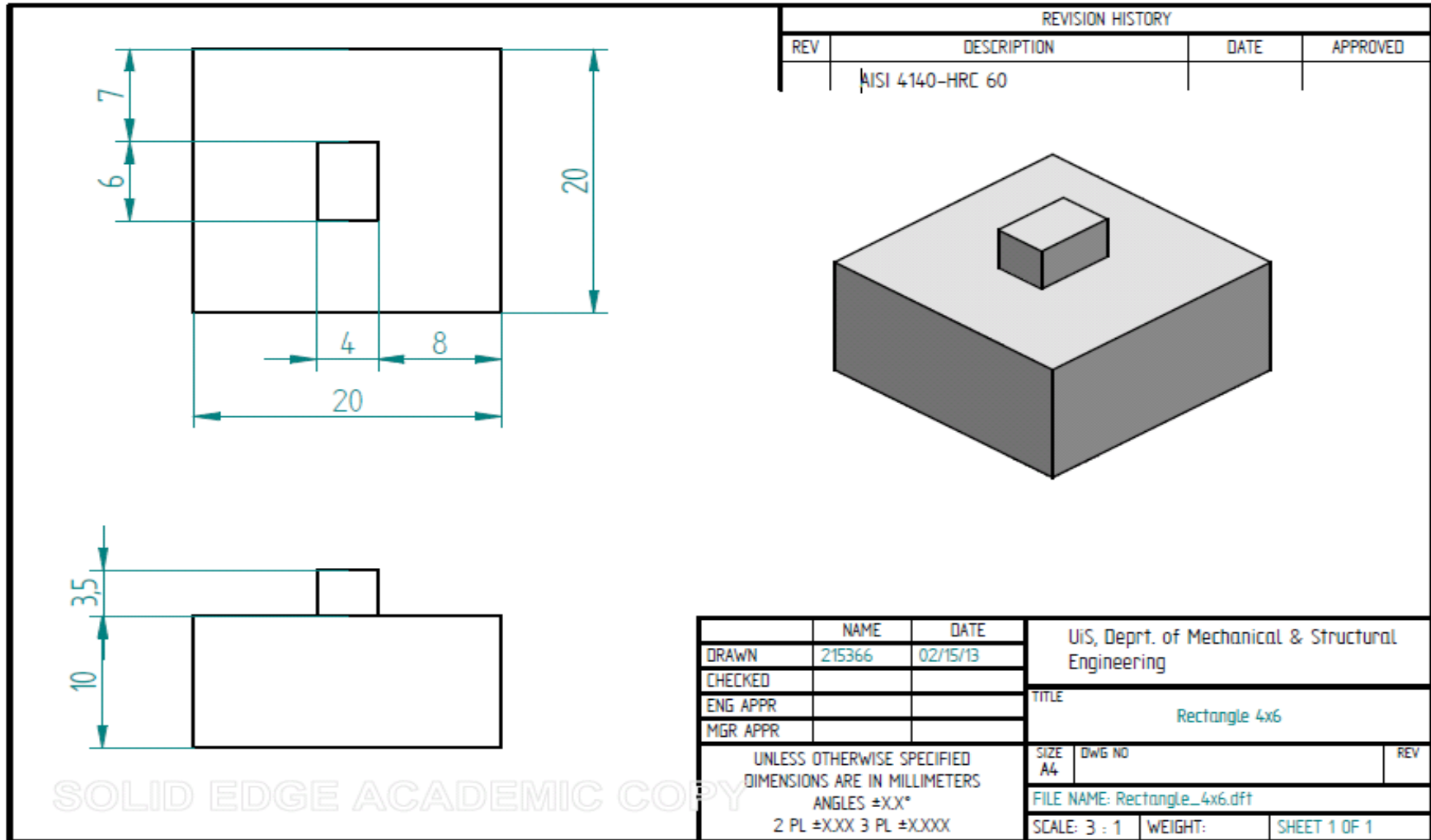
Angle taken from appendix chap.9. Ref,[3].

$$p = 2k \left(1 + 2 \cdot \frac{2}{9} \pi \right) = 2,756 \cdot Yield$$

$$p = 2,756 \cdot 551 \frac{N}{mm^2} = 1519 \frac{N}{mm^2}$$

Yield point load	1348Kg
Verification load	3500Kg
Indentation load (theoretical)	3716Kg
Verification load	3750Kg
Indentation load with work hardening	4014Kg
If full penetration is not achieved:	
Min upper load	4050Kg
Intermediate load	4100Kg
Max load	4150Kg

In order to check the accuracy of the hypothesis a series of indentation tests will be done with verification loads. From theory plastic flow and penetration of the metal will happen at the indentation load. If sufficient penetration depth is not achieved at the indentation load (with work hardening), three upper loads will be applied.



SOLID EDGE ACADEMIC COPY

Title	Master Thesis Spring 2013 Johannes Ohnstad	Page 84
-------	---	---------

A.7. WEDGE 60°

The wedge has an angle of 60° and a 30° semi angle. The base of the wedge is 4,04x4mm and the maximum penetration depth of the wedge is 3,5mm. The slip line field for a wedge is found to be valid for a plate of finite thickness, Ref[6], the $\frac{H}{L}$ relation is not considered. For indentation by a wedge the indentation pressure is given by:

$$p = 2k(1 + \psi)$$

Where $\psi = 15^\circ = \frac{\pi}{12}$

Angle taken from Fig.52,Ref[2]

The indentation pressure is then:

$$p = 2k \left(1 + \frac{\pi}{12} \right) = 1,451 \cdot Yield$$

$$p = 1,451 \cdot 551 \frac{N}{mm^2} = 800 \frac{N}{mm^2}$$

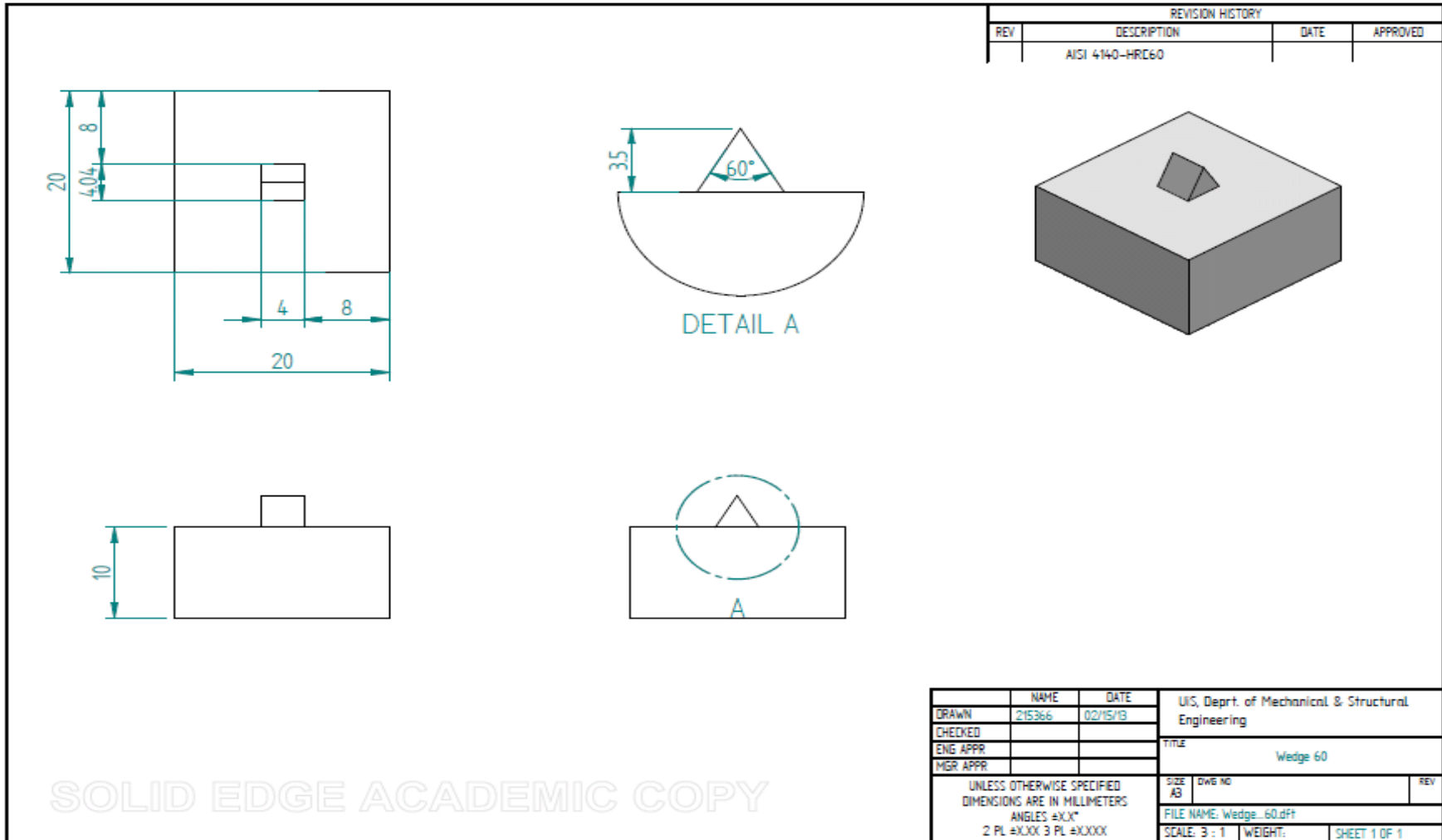
The pressure on the apex of the wedge is in theory considered infinite. For load calculations we consider the surface area at a height of 3,0mm of the wedge and go from there down to the base. The length of the wedge is constant (4mm)

Surface area of the wedge:

Height		Width		Area	
H ₀	3,0	W ₆	0,578	A ₆	2,31
H ₁	2,5	W ₅	1,15	A ₅	4,62
H ₂	2,0	W ₄	1,73	A ₄	6,93
H ₃	1,5	W ₃	2,31	A ₃	9,24
H ₄	1,0	W ₂	2,89	A ₂	11,55
H ₅	0,5	W ₁	3,46	A ₁	13,86
H ₆	0	W ₀	4,04	A ₀	16,6

Load calculations:

	Indentation pressure	Indentation with work hardening
H ₀	188Kg	203Kg
H ₁	377Kg	407Kg
H ₂	565Kg	610Kg
H ₃	753Kg	814Kg
H ₄	942Kg	1017Kg
H ₅	1130Kg	1220Kg
H ₆	1318Kg	1424Kg



A.8. WEDGE 120°

The wedge has an angle of 120° and a 60° semi angle. The base of the wedge is 6,93x4mm and the maximum penetration depth of the wedge is 2mm. The height of the whole profile is 3,5mm. The slip line field for a wedge is found to be valid for a plate of finite thickness, Ref[6], the $\frac{H}{L}$ relation is not considered. For indentation by a wedge the indentation pressure is given by:

$$p = 2k(1 + \psi)$$

Where $\psi = 50^\circ = \frac{5\pi}{18}$

Angle taken from Fig.52,Ref[2]

$$p = 2k \left(1 + \frac{5\pi}{18} \right) = 2,154 \cdot \text{Yield}$$

$$p = 2,154 \cdot 551 \frac{\text{N}}{\text{mm}^2} = 1187 \frac{\text{N}}{\text{mm}^2}$$

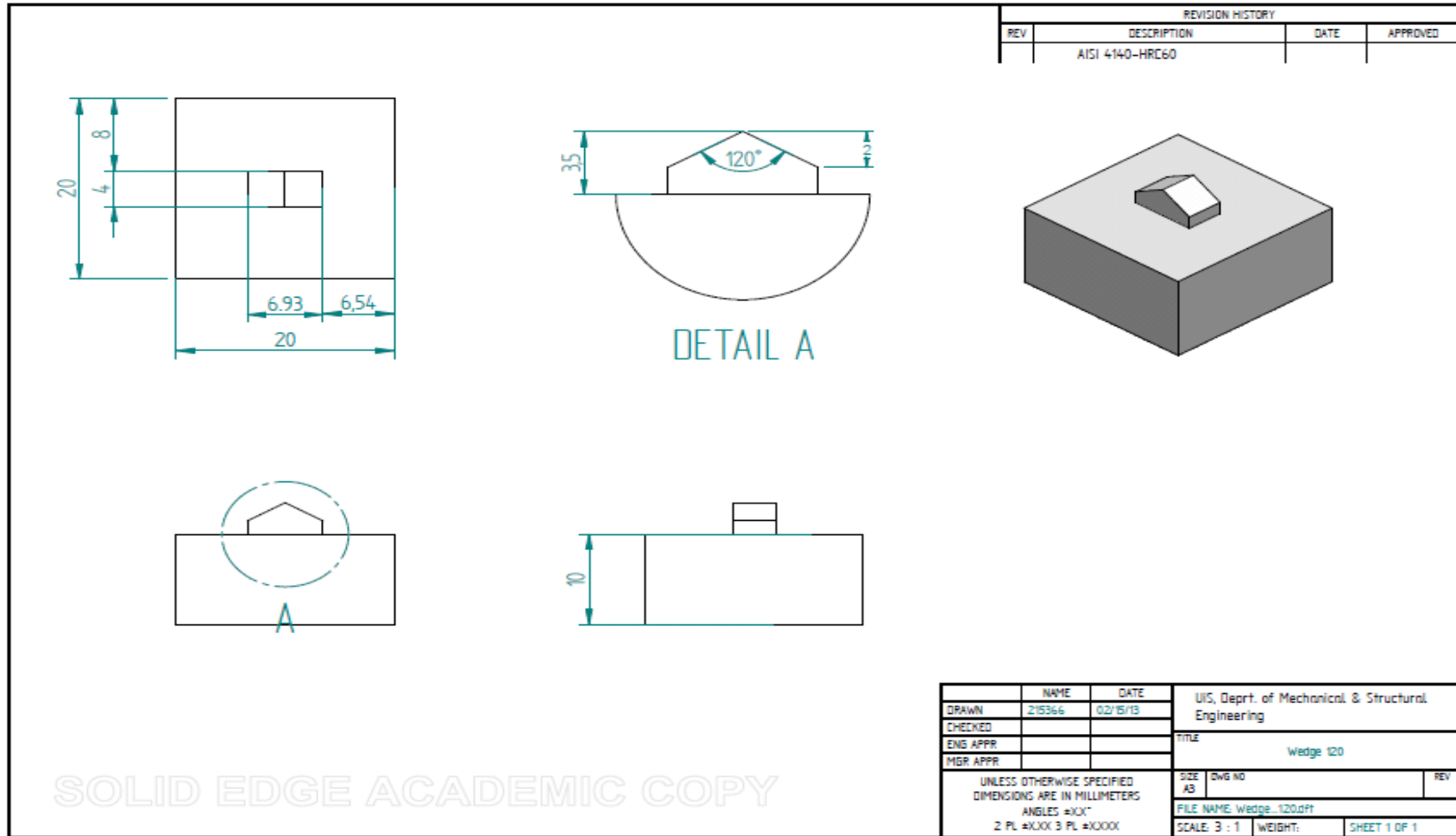
The pressure on the apex of the wedge is in theory considered infinite. For load calculations we consider the surface area at a height of 3,0mm of the wedge and go from there down to the base at 1,5mm. The length of the wedge is constant (4mm).

Surface area of the wedge:

	Height		Width		Area
H ₀	3,0	W ₀	1,73	A ₀	6,928
H ₁	2,5	W ₁	3,46	A ₁	13,86
H ₂	2,0	W ₂	5,196	A ₂	20,78
H ₃	1,5	W ₃	6,93	A ₃	27,72
H ₄	1,0	W ₄	6,93	A ₄	27,72
H ₅	0,5	W ₅	6,93	A ₅	27,72
H ₆	0	W ₆	6,93	A ₆	27,72

Load calculations:

	Indentation load	Indentation with work hardening
H ₀	838Kg	905Kg
H ₁	1677Kg	1811Kg
H ₂	2515Kg	2716Kg
H ₃	3354Kg	3622Kg
H ₄	3354Kg	3622Kg
H ₅	3354Kg	3622Kg
H ₆	3354Kg	3622Kg



Title	Master Thesis Spring 2013 Johannes Ohnstad	Page 88
-------	---	---------

A.9. PYRAMID

The load calculations for the pyramid are hard to accurately predict with slip-line field theory. The plastic flow pattern is three dimensional where as for the wedge the deformation is two dimensional. Experiments done with a Vickers pyramid indicates that the value of the indentation pressure is around $3,3 \cdot Yield$, Ref[2]. The Vickers pyramid has a semi-angle of 68° while the one chosen for testing is 45° . In theory the indentation pressure decreases with a smaller semi-angle, however experiments have shown that for a pyramid the indentation pressure increases with a smaller angle, Ref[2]. A conservative approach to the load calculations is therefore taken with predicted indentation pressure set to:

$$p = 3,4 \cdot Yield$$

$$p = 3,4 \cdot 551 \frac{N}{mm^2} = 1873,4 \frac{N}{mm^2}$$

The tip of the pyramid is considered in the same way as the apex of the wedge, the pressure is in theory infinite and causes yielding at the smallest loads. The base of the pyramid is 7x7mm with the maximum penetration depth being 3,5mm. For load calculations we consider the surface area at a height of 3,0mm of the pyramid and go from there down to the base. Because of the geometry increase in width and length is equal.

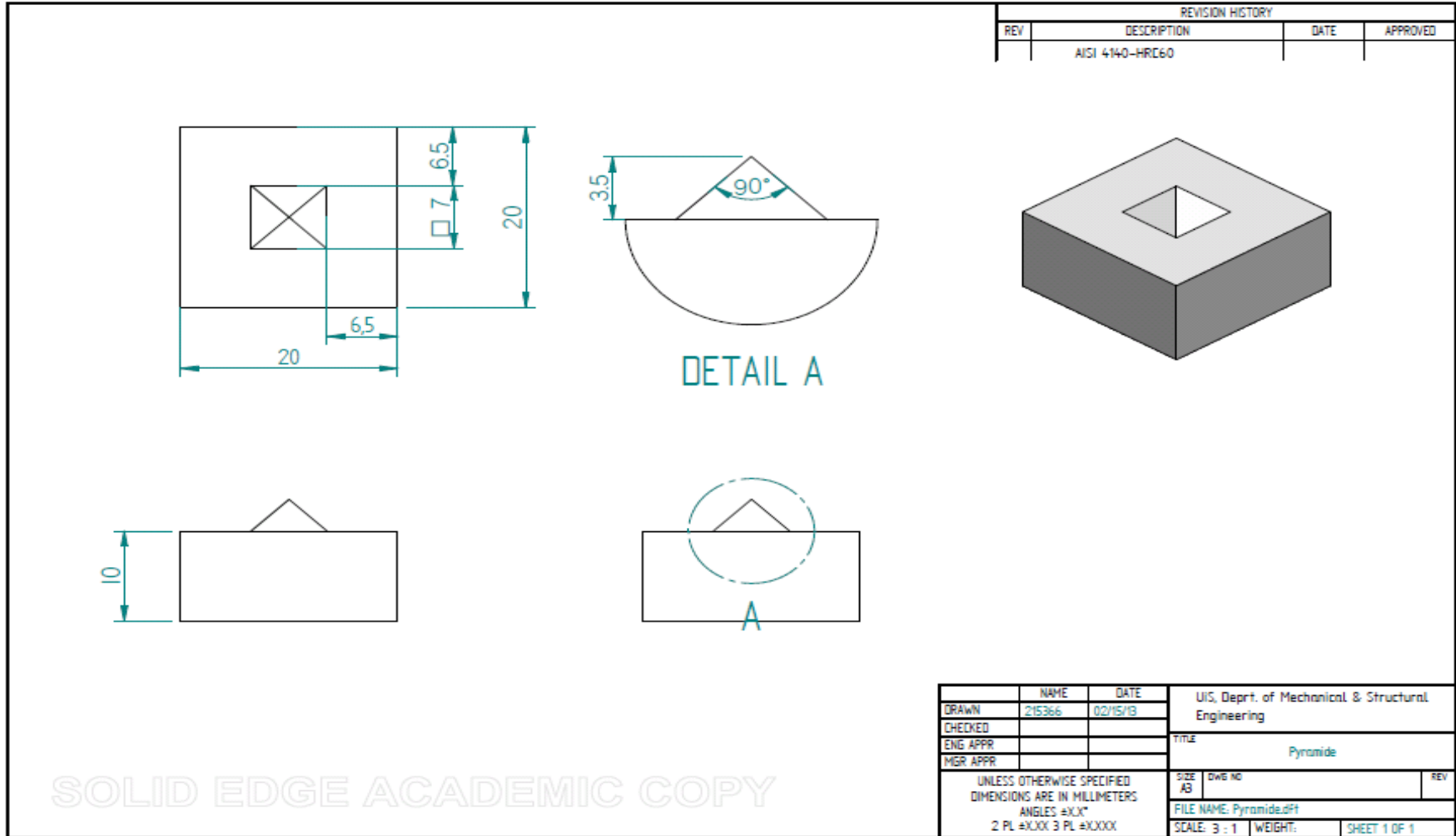
Surface area of Pyramid:

	Height		Width		Area
H ₀	3,0	W ₀	1	A ₀	1
H ₁	2,5	W ₁	2	A ₁	4
H ₂	2,0	W ₂	3	A ₂	9
H ₃	1,5	W ₃	4	A ₃	16
H ₄	1,0	W ₄	5	A ₄	25
H ₅	0,5	W ₅	6	A ₅	36
H ₆	0	W ₆	7	A ₆	49

Load calculations:

	Indentation load	Indentation with work hardening
H ₀	191Kg	206Kg
H ₁	764Kg	825Kg
H ₂	1719Kg	1856Kg
H ₃	3055Kg	3300Kg
H ₄	4774Kg	5156Kg
H ₅	6875Kg	7425Kg
H ₆	9357Kg	10106Kg

Testing over 7500kg is not possible.



A.10. DOUBEL WEDGE 60 °

The double wedge specimen will be tested to observe the pile up effect between a pair of 60° wedges and how two indentations close to each other affect the indentation pressure. The wedges have the same dimensions as the single 60° wedge described earlier. The distance between the two wedges is 2mm. Theory predicts that the volume displaced by a wedge is equal to the volume of penetration; this volume is distributed equally to each side of the wedge. The gap between the two wedges will therefore be filled with the same volume as the penetrating depth of one wedge. How this effect the indentation pressure related to penetrating depth is not yet clear.

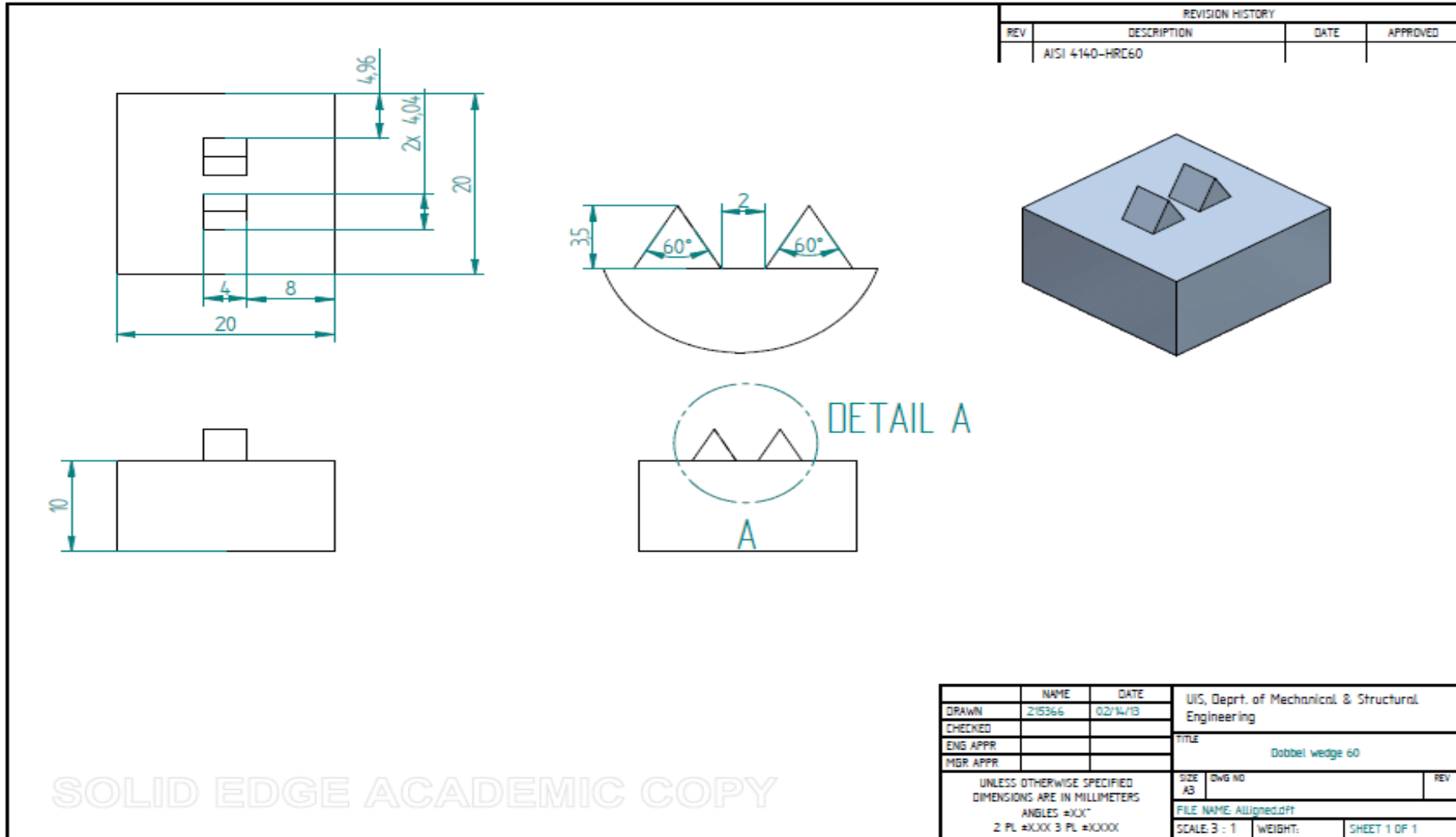
The planned testing load is double the load of the single wedge.

Surface area of the wedge:

	Height		Width		Area
H ₀	3,0	W ₆	0,578	A ₆	2,31
H ₁	2,5	W ₅	1,15	A ₅	4,62
H ₂	2,0	W ₄	1,73	A ₄	6,93
H ₃	1,5	W ₃	2,31	A ₃	9,24
H ₄	1,0	W ₂	2,89	A ₂	11,55
H ₅	0,5	W ₁	3,46	A ₁	13,86
H ₆	0	W ₀	4,04	A ₀	16,6

Load calculations:

	Indentation pressure	Indentation with work hardening
H ₀	376Kg	406Kg
H ₁	754Kg	814Kg
H ₂	1130Kg	1220Kg
H ₃	1506Kg	1628Kg
H ₄	1884Kg	2034Kg
H ₅	2260Kg	2440Kg
H ₆	2636Kg	2848Kg



Title	Master Thesis Spring 2013 Johannes Ohnstad	Page 88
-------	---	---------

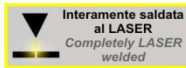
A.11. LOAD CELL TECHNICAL SHEET

Data Sheet: TS.116.R6 Cella di carico

www.aep.it
TS - TSA
Load cell

Accessori Accessories

Teste a snodo sferico
Knuckle joints



Dimensioni Dimensions

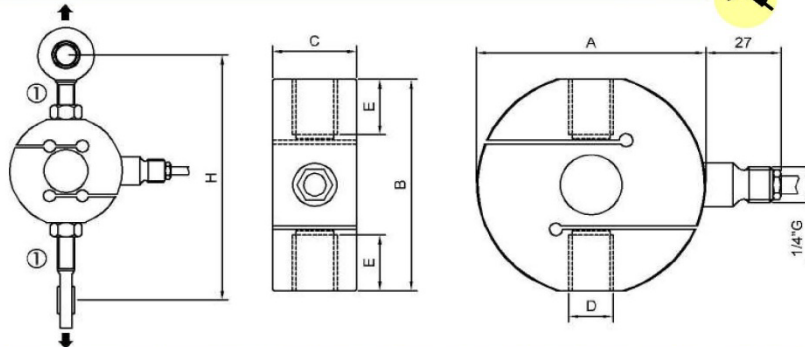
[mm]



① ACCESSORI
Teste a snodo sferico

ACCESSORIES
Knuckle joints

LOAD	CODE
25 + 500 kg	CACCEM12
500 kg + 2t	CACCEM16
2.5 t	CACCEM20
5, 7.5 t	CACCEM25



TS
IN ACCORDANCE

CODE (C2)	CODE (C3)	LOAD	A	B	C	D	E	H
CTS6310KC25	CTS6310KC35	10 kg	63.5	59.5	22	M12X1.75	12	~ 134
CTS6325KC25	CTS6325KC35	25 kg						
CTS6350KC25	CTS6350KC35	50 kg						
CTS63100KC25	CTS63100KC35	100 kg						
CTS63200KC25	CTS63200KC35	200 kg						
CTS63300KC25	CTS63300KC35	300 kg						
CTS63500KC25	CTS63500KC35	500 kg	82	78	30	M16X2	20	~ 170
CTS82500KC25	CTS82500KC35	500 kg						
CTS821TC25	CTS821TC35	1 t						
CTS822TC25	CTS822TC35	2 t						
CTS822T5C25	CTS822T5C35	2.5t						
CTS822TC25	CTS822TC35	2 t						
CTS1025TC25	CTS1025TC35	5 t	102	90	45	M24X2	21.5	~ 235
CTS1027T5C25	CTS1027T5C35	7.5t						

TSA
APPROVED

CODE (C2)	CODE (C3)	CODE (C4)	LOAD	A	B	C	D	E	H
CTSA63100KC25	CTSA63100KC35	/	100 kg	63.5	59.5	22	M12X1.75	12	~ 134
CTSA63200KC25	CTSA63200KC35	/	200 kg						
CTSA63300KC25	CTSA63300KC35	/	300 kg						
CTSA63500KC25	CTSA63500KC35	/	500 kg						
CTSA82500KC25	CTSA82500KC35	CTSA82500KC45	500 kg	82	78	30	M16X2	20	~ 170
CTSA821TC25	CTSA821TC35	CTSA821TC45	1 t						
CTSA822TC25	CTSA822TC35	CTSA822TC45	2 t						
CTSA822T5C25	CTSA822T5C35	CTSA822T5C45	2.5t						
CTSA1025TC25	CTSA1025TC35	/	5 t	102	90	45	M24X2	21.5	~ 235
CTSA1027T5C25	CTSA1027T5C35	/	7.5t						

APPENDIX B. $\Delta\phi_{PRQ}$ -VALUES

TABLE 9-1 Coordinates of a 5° Net for the Slip-Line Field Determined by Two Centered Fans

$\Delta\phi_u$	n	$m=n$	$m=n+1$	$m=n+2$	$m=n+3$	$m=n+4$	$m=n+5$	$m=n+6$	$m=n+7$	$m=n+8$
0°	0	$y = 1.000$ $x = 0.0$	1.0833	1.1584	1.2247	1.2817	1.3288	1.3660	1.3926	1.4087
5°	1	1.1826	1.2741	1.3572	1.4312	1.4951	1.5484	1.5907	1.6214	1.6399
10°	2	0.0	1.000	.2083	.3243	.4472	.5762	.7101	.8484	.9897
15°	3	1.3831	1.4845	1.5770	1.6597	1.7320	1.7925	1.8407	1.8760	1.8975
20°	4	0.0	.1106	.2312	.3613	.4999	.6463	.7995	.9583	1.1218
25°	5	1.6050	1.7177	1.8214	1.9146	1.9963	2.0653	2.1206	2.1611	2.1861
30°	6	0.0	.1232	.2582	.4046	.5617	.7285	.9038	1.0868	1.2760
35°	7	1.8519	1.9781	2.0946	2.2001	2.2929	2.3718	2.4351	2.4820	2.5108
40°	8	0.0	.1377	.2898	.4554	.6339	.8243	1.0257	1.2307	1.4562
45°	9	2.1283	2.2701	2.4018	2.5215	2.6272	2.7176	2.7905	2.8446	2.8781
50°	10	0.0	.1550	.3267	.5146	.7181	.9364	1.1680	1.4118	1.6665
55°	11	2.4390	2.5991	2.7484	2.8846	3.0056	3.1093	3.1934	3.2560	3.2948
60°	12	0.0	.1749	.3698	.5839	.8166	1.0610	1.3340	1.6162	1.9119
65°	13	2.7897	2.9713	3.1413	3.2968	3.4356	3.5549	3.6519	3.7245	3.7696
70°	14	0.0	.1984	.4200	.6647	.9314	1.2196	1.5278	1.8547	2.1985
75°	15	3.1874	3.3940	3.5879	3.7662	3.9257	4.0632	4.1755	4.2595	4.3121
80°	16	0.0	.2257	.4787	.7589	1.0655	1.3977	1.7540	2.1332	2.5331
85°	17	3.6394	3.8755	4.0976	4.3023	4.4859	4.6447	4.7747	4.8723	4.9335
90°	18	0.0	.2575	.5472	.8688	1.2219	1.6054	2.0182	2.4586	2.9243
			.2947	.6272	.9973	1.4046	1.8482	2.3269	2.8389	3.3828
			.3380	.7205	1.1472	1.6179	2.1318	2.6873	3.2831	
			.3886	.8296	1.3223	1.8670	2.4631	3.1091		
			.4982	.9573	1.5269	2.1584	2.8505			
			.5758	1.0267	1.5269	2.1584	2.8505			
			.5172	1.1055	1.7658	2.4986				
			8.1290	8.6864	9.2085	9.6961				
			0.0	.5981	1.2794	2.0455				
			9.3375	9.9715	10.5771					
			0.0	.6925	1.4827					
			10.7255	11.4605						
			0.0	.8031						
			12.3341							
			0.0							



From [11].

n	$n+9$	$n+10$	$n+11$	$n+12$	$n+13$	$n+14$	$n+15$	$n+16$	$n+17$	$n+18$
0	1.4141 1.0000	1.4087 1.1233	1.3926 1.2456	1.3659 1.3660	1.3288 1.4837	1.2816 1.5977	1.2246 1.7071	1.1584 1.8112	1.0833 1.9090	1.0000 2.0000
1	1.6463 1.1334	1.6399 1.2718	1.6068 1.4222	1.5892 1.5653	1.5449 1.7061	1.4879 1.8434	1.4189 1.9765	1.3379 2.1036	1.2455 2.2240	
2	1.9048 1.2891	1.8975 1.4582	1.8751 1.6282	1.8375 1.7979	1.7846 1.9658	1.7163 2.1305	1.6330 2.2909	1.5347 2.4452		
3	2.1946 1.4708	2.1860 1.6686	2.1595 1.8688	2.1151 2.0694	2.0522 2.2690	1.9707 2.4658	1.8707 2.6583			
4	2.5207 1.6828	2.5107 1.9141	2.4797 2.1497	2.4272 2.3865	2.3527 2.6233	2.2555 2.8574				
5	2.8895 1.9304	2.8778 2.2014	2.8414 2.4777	2.7795 2.7580	2.6913 3.0372					
6	3.3083 2.2196	3.2944 2.5366	3.2519 2.8610	3.1789 3.1901						
7	3.7853 2.5573	3.7692 2.9281	3.7191 3.3089							
8	4.3303 2.9518	4.3114 3.3859								
9	4.9548 3.4129									

From [11].

APPENDIX C. MATERIAL CERTIFICATES

C.1. MECHANICAL PROPERTIES INDENTED STEEL

energyalloys							Test Certificate			
Sverdrup Steel AS Strandsvingen 2 N 4032 STAVANGER, NORWAY Norway							Cert Number 463051-16 Test Reference 1415879		26/10/2012	
Sold To: Sverdrup Steel AS, Strandsvingen 2, N 4032 STAVANGER, NORWAY, Norway Ship To: Sverdrup Steel AS, Strandsvingen 2, N 4032 STAVANGER, NORWAY, Norway							Issued from Energy Alloys UK Limited Advantage House Poplar Way Cardiff ROTHERHAM S60 5TR			
Customer 13582/0 Our Order 225510-1-1			Your Order Packing List		Reference 805070 (24/10/2012) 463051-1 (26/10/2012)		Product Information Heat 65270 Lot FA940 Pcs 1 M 5.938			
Round Turned Bar Forged - AISI 4140 Modified Quench & Temper to 18 - 22 HRC 16" Diameter x 5938mm										
Chem Composition										
C	Mn	Si	P	S	Cu	Cr	Ni	Mo	As	
0.42	1.03	0.28	0.008	0.001	0.09	1.06	0.22	0.27	0.005	
Al	Sn	Al	V	Nb	Ti	B	As	Sb	Co	
0.035	0.006	0.035	0.004	0.003	0.008	0.0002	0.005	0.0022	0.009	
		H	N							
		1.0 PPM	40 PPM							
Physical Tests										
Rm (L)		Rp0.2 (L)		Rp0.5 (L)		A % (L)				
109.06 KSI		85.02 KSI		85.11 KSI		23 %				
Z % (L)		HB								
65 %		225, 222								
Heat Treatment					Impact Tests					
Heat Trmt	Temp	Time	Cool Mthd	Impc	UM	Temp	D	Rsit 1	Rsit 2	Rsit 3
QUENCH	1616 F	12:45 HRS	WATER 0 C	KCV	FP	-32 C	L	57.0	54.0	44.0
TEMPER	1202 F	17:00 HRS	AIR 0 C	KCV	FP	-51 F	L	34.0	32.0	39.0
				KCV	FP	-32 C	L	59.0	57.0	46.0
				KCV	FP	-51 F	L	45.0	33.0	41.0
BATCH NO: FA940 MECHANICAL RESULTS REPORTED AT MID-RADIUS, ADDITIONAL TESTS AT 1" BELOW FOR INFORMATION. ELECTRIC VDG GRAIN SIZE ASTM E112:- 7 REDUCTION RATIO:- 4.2:1 SURFACE HARDNESS:- 223 BHN CONFORMS TO NACE MR0175/ISO 15156 LATEST EDITION ULTRASONIC SATISFACTORY TO ASTM A388 API 6A PSL 3 LATERAL EXPANSIONS @ -32C 0.44 0.44 0.43 MM SHEAR% 0.52 0.54 0.52(MID-RAD) LATERAL EXPANSIONS @ -51F 0.42 0.43 0.40 MM SHEAR% 0.47 0.51 0.48(MID-RAD) LATERAL EXPANSIONS @ -32C 0.47 0.49 0.46 MM SHEAR% 0.55 0.57 0.54(1" BELOW) LATERAL EXPANSIONS @ -51F 0.43 0.45 0.44 MM SHEAR% 0.50 0.54 0.51(1" BELOW) DI VALUE:- 7.66" EAGL-011 REV 5 SUP 1,3,4										
 										

C.2. MECHANICAL PROPERTIES INDENTER STEEL BEFORE HEAT TREATMENT

ASCOMETAL



Département Métallurgie Qualité
 Usine des Dunes - Boite postale 41
 59941 Dunkerque Cedex 2
 Téléphone : 03 28 29 60 00
 Télécopie : 03 28 29 60 03

DOCUMENT DE CONTROLE
 Inspection Documents / Prüfbescheinigungen

Certificat de réception 3.1
 NFEN 10204 DIN EN 10204 ISO R 404
 2004 2004 2004

Livraison 80185893 / 000003
 N° Contrôle 030000229091

Date 16.10.2012
 Date d'édition 16.10.2012

ORDRE DE FABRICATION <small>WORKS ORDER NUMBER / WERKBESTELLUNG</small> AFFAIRE SUIVIE PAR <small>YOUR CONTACT IS / BEARBEITER</small> N/REFERENCE <small>ASCOMETAL ORDER / WERKBESTELLUNG</small> V/REFERENCE <small>YOUR ORDER / IHRE ZEICHNUNG</small> QUANTITE <small>QUANTITY / MENGE</small> PRODUIT <small>PRODUCT DESCRIPTION / BESCHREIBUNG</small> SPECIFICATION CLIENT <small>SPECIFICATION / SPEZIFIKATION</small> IND <small>REV / ENTWURF</small> SPECIFICATIONS SUPP.	H7559AA CHADEYRON 227110901 / 000010 (70060562) EUR-913855 20.06.2012 5.320 TO AISI4140 ROL. ROUNDS CLESS TURN HOWCO HG4140 BAR HT36 4 EXC CVN-20C 20 FL (RD-5)	COULEE H7559 <small>CAST / SCHMELZE</small> NUANCE AISI4140 <small>GRAD. / WERKSTOFF</small>	DESTINATAIRE DOCUMENT <small>DOCUMENT FOR / EMPFANGER</small> Société HOWCO WHITHAM 3 BLAIRLINN ROAD BLAIRLINN INDUSTRIAL ESTATE CUMBERNAULD G67-2TF Grande Bretagne MARQUE		
IND	4	DATE	23.08.2010	CCU	D000006727

Analyse chimique de coulée / Ladle analysis / Schmelzeanalyse

Elément	Element	Teil	C	Mn	Si	Cr	Ni	Mo	Cu	P	S	Al
Mini	Spec min	Min	0.380	0.750	0.150	0.800	0.150	0.150	0.093	0.007	0.014	0.015
Valeur	Actual	Werte	0.417	0.943	0.312	1.045	0.210	0.223	0.250	0.025	0.025	0.028
Maxi	Spec max	Max	0.430	1.000	0.350	1.100	0.250	0.250	0.250	0.025	0.025	0.035
Elément	Element	Teil	Sn	V	Cb	Ti	B	H2				
Mini	Spec min	Min										
Valeur	Actual	Werte	0.005	0.007	0.0000	0.0020	0.0004	0.000134				
Maxi	Spec max	Max	0.100	0.030				0.000200				
Calcul												
Elément	Element	Teil	DI									
Mini	Spec min	Min	6.00									
Valeur	Actual	Werte	6.72									
Maxi	Spec max	Max										

Dureté éprouvette / Test coupon hardness / Probestück Härte

Nappe / Batch number / Loss number : 000000000000001653
 Surface tested

Elément	Element	Teil	HRc
Mini	Spec min	Min	30.0
Valeur	Actual	Werte	30.3
Maxi	Spec max	Max	36.0

Nappe / Batch number / Loss number : 000000000000001653
 Surface tested

Elément	Element	Teil	HRc
Mini	Spec min	Min	30.0
Valeur	Actual	Werte	30.3
Maxi	Spec max	Max	36.0

HOWCO METALS MANAGEMENT
 CERTIFIED TRUE COPY Page 2 of 4
 COC-CERT No. 6852
 SIGNED *homme*



Caractéristiques mécaniques / Mechanical properties / Mechanische Kennwerte

Traction / tensile test / Zugversuch
 Nappe / Batch number / Loss number : 000000000000001653
 Diameter of test specimen (in) 0.50
 mid radius tested
 Longitudinal test
 Tensile test temperature (°F) 70

ASCOMETAL



Département Métallurgie Qualité
 Usine des Dunes - Boite postale 41
 59941 Dunkerque Cedex 2
 Téléphone : 03 28 29 60 00
 Télécopie : 03 28 29 60 03

DOCUMENT DE CONTROLE

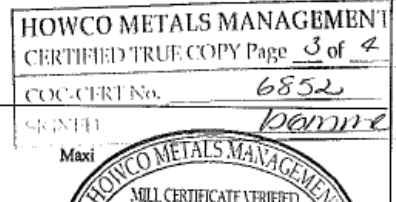
Inspection Documents / Prüfbescheinigungen

Certificat de réception 3.1
 NFEN 10204 2004 DIN EN 10204 2004 ISO R 404 2004

Livraison 80185893 / 000003
 N° Contrôle 030000229091

Date 16.10.2012
 Date d'édition 16.10.2012

ORDRE DE FABRICATION H7559AA <small>WORKS ORDER NUMBER / WERKBESTELLUNG</small>		COULEE H7559 <small>CAST / SCHMELZE</small>		DESTINATAIRE DOCUMENT <small>DOCUMENT FOR / EMPFANGER</small>				
AFFAIRE SUIVIE PAR <small>YOUR CONTACT IS / BEARBEITER</small> CHADEYRON		N/REFERENCE <small>ASCOMETAL ORDER / WERKBESTELLUNG</small> 227110901 / 000010 (70060562)		Société HOWCO WHITHAM 3 BLAIRLINN ROAD BLAIRLINN INDUSTRIAL ESTATE CUMBERNAULD G67-2TF Grande Bretagne MARQUE				
V/REFERENCE <small>YOUR ORDER / IHRE ZEICHE</small> EUR-913855 20.06.2012		QUANTITE <small>QUANTITY / MENGE</small> 5.320 TO		NUANCE AISI4140 <small>GRAD / WERKSTOFF</small>				
PRODUIT <small>PRODUCT DESCRIPTION / BESCHREIBUNG</small> AISI4140 ROL.ROUNDS CLESS TURN 3,000 EN HAR.TEMP		SPECIFICATION CLIENT <small>SPECIFICATION / SPEZIFIKATION</small> HOWCO HG4140 BAR HT36						
IND <small>REV / ENTWURF</small> 4		DATE <small>DATE / DATUM</small> 23.08.2010		CCU		D000006727		
SPECIFICATIONS SUPP. EXC CVN-20C 20 FL (RD>5)								
Elément Unité Mini Valeur Maxi	Element Unit Spec min Actual Spec max	Teil Meinheit Min Werte Max	Ys.2% PSI 110000 113289 140000	UTS PSI 130000 131820 160000	E (2in) % 13.0 21.9	RA % 40 63		
Résilience / Impact test / Kerbschlagproben Nappe / Batch number / Los nummer : 00000000000001653 notch test 10 x 10 Mid radius testing Charpy V notch Longitudinal test Impact test temperature (°C)								
-32								
Elément Unité Mini Valeur Maxi	Element Unit Spec min Actual Spec max	Teil Meinheit Min Werte Max	Joules J 20.0 88.0	Joules J 20.0 89.6	Joules J 20.0 90.9	Average J 27.0 89.5	% shear % 80.0 80.0 80.0	% shear % 0.30 0.30 0.30 0.91 0.93 0.95
Traitement thermique / Heat treatment / Warmbehandlung Starting and ending water quench temperatures do not exceed 100 deg F								
Traitement Aust. temp. Revenu/Tempering/Anlass	T Min 860 °C 538 °C	T 875 °C 645 °C	T Max 885 °C 650 °C	Durée 2.50 hrs 3.00 hrs	Refroidissement Austenitized water quenched Tempered air cooled			
Dureté de surface sur barres / Bars surface hardness / Stöße Randhärte								
Elément Mini Valeur Maxi	Element Spec min Actual Spec max	Teil Min Werte Max	BHN top 285 287 341					
Autres résultats / Other results / Andere Prüfergebnisse								
Elément Grain size per ASTM E112 = Reduction ratio	Mini 5 4.00	Valeur 7 16.50						



Nous certifions que les produits ci-dessus sont conformes aux prescriptions de la commande, respectent la directive européenne 2000/53/CE du 18 septembre 2000 et présentent un niveau de radioactivité au plus égal à la radioactivité ambiante.

We hereby certify the above mentioned products are complying with the order requirements, are respectful of the September, 18th 2000 - 2000/53/CE - european directive, and have a radioactivity level which does not exceed that present in the environment.

Wir bestätigen hiermit dass die oben genannten Ergebnisse den Bestellevorschriften, die EU-Richtlinie 2000/53/CE von 18 September 2000 entsprechen und die gefertigten Produkte keine Radioaktivität, die Höher ist als natürliche Strahlung der Umwelt, aufweisen.

ASCOMETAL SAS
 su capital de 65 285 430 EUR

Siège social : Immeuble le Confiscé - 8, avenue de l'Arche, Faubourg de l'Arche, 92419 COURBEVOIS Cedex

C.3. HEAT TREATMENT PROCEDURE FOR INDENTERS

 <p>kverneland group Kverneland Klepp AS Met. lab N-4355 Kverneland</p>	<h2>RAPPORT</h2>	<p>Rapport nr: 75</p>
<p>Dato: 23.04.2013</p>	<p>Saksbehandler: S.Voll</p>	<p>Antall blad: 1</p>
<p>Varmebehandling og hardhetsmåling av deler i.h.t.ordre nr. 100209.</p>		
<p>Hensikt: QA</p>	<p>Målgruppe Ålgård CNC</p>	

Sammendrag.

Div deler er varmebehandlet i.h.t. ordre nr. 100209 og hardhetsmålt med HRc metode i.h.t.NS—EN 10109.

Hardhetsmålingen er foretatt på overflate slipt på abrasivt slipepapir korning 80 og 220.

Varmebehandlingsprosedyre:

Herde temp.: 860°C

Herdemedie: 180°C salt +0,5% vann

Deler pakket i stålfolie ved oppvarming.

Anløping temp.: 240°C, 2t på temperatur.

Måleresultat:

50-51HRc.

C.4. LOAD MEASUREMENT CELL CERTIFICATE



Proof report

Instrument Calibrated		Calibration Normals	
TYPE:	TS 7,5t	ID No.:	M 861503
Description:	Compression load cell	Description:	5103-C3 20K 30NT
Manufacture:	AEP	Manufacture:	Revera
Serie No:	811468	Last Calibrated:	2012.11.19
Range:	0-7500 kg	Proof No:	MTmPX26067-K02
Accuracy:		Traceability	Sveriges Provnings-ock Forskningsinstitut

Calibrationresults at 20° C

Real Weight	Read Weight			Average deviation	Variance	Variance	variance of max. load
	test 1	test 2	test 3				
kg	kg	kg	kg	kg	kg	%	%
1250	1250	1250	1250	1250	0	0,00	0,00
2500	2500	2500	2500	2500	0	0,00	0,00
3750	3747	3748	3748	3748	-2	-0,05	-0,03
5000	4995	4997	4997	4996	-4	-0,08	-0,05
6250	6248	6249	6248	6248	-2	-0,03	-0,03
7500	7500	7498	7499	7499	-1	-0,01	-0,01

Calibrated: 05.04.2013
Arvid Stokkeland
Terje Obrestad
Even Obrestad Hægstad
Age Obrestad



Postadresse: 4365 NÆRBØ Besøksadresse: Haavegen 196 Telefon: 51 79 84 00 Telefax: 51 79 84 01 E-post: teo@teo.no Internett: www.teo.no Foretaksregisteret: NO 936 940 218 MVA

Title	Master Thesis Spring 2013 Johannes Ohnstad	Page 96
-------	---	---------

APPENDIX D. MEASURED VALUES

D.1. WEDGE 60°

Series 1-3							
Load(kg)							
Theoretical	203	407	610	814	1017	1220	1424
Series 1	209,8	416,6	633,5	856	1028,3	1254,6	1441,2
Series 2	212	410,6	613,3	821,2	1023,5	1227,3	1431,8
Series 3	205,7	410,2	612,9	818,2	1021,2	1225	1429,9
Average	209,1667	412,4667	619,9	831,8	1024,333	1235,633	1434,3
Standard deviation	4,040111	4,004997	10,81708	19,32692	4,71098	15,5515	7,136467
Width(mm)							
Theoretical	0,578	1,15	1,73	2,31	2,89	3,46	4,04
Series 1	0,253	0,441	0,614	0,841	1,015	1,338	1,432
Series 2	0,283	0,425	0,597	0,809	0,954	1,096	1,254
Series 3	0,296	0,462	0,618	0,760	0,950	1,167	1,362
Average	0,277	0,442	0,610	0,803	0,973	1,200	1,349
Average deviation	52,02 %	61,52 %	64,76 %	65,22 %	66,32 %	65,31 %	66,60 %
Standard deviation	0,018	0,015	0,009	0,033	0,030	0,102	0,073
Length(mm)							
Theoretical	4	4	4	4	4	4	4
Series 1	3,288	3,894	4,113	4,162	4,143	4,235	4,256
Series 2	3,138	3,663	4,045	4,200	4,260	4,317	4,368
Series 3	2,698	3,594	4,034	4,221	4,387	4,383	4,411
Average	3,041	3,717	4,064	4,194	4,263	4,312	4,345
Average deviation	23,97 %	7,08 %	-1,60 %	-4,86 %	-6,58 %	-7,79 %	-8,62 %
Standard deviation	0,250	0,128	0,035	0,024	0,100	0,061	0,065
Depth(mm)							
Theoretical	0,5	1	1,5	2	2,5	3	3,5
Series 1	0,219	0,382	0,532	0,729	0,879	1,158	1,240
Series 2	0,245	0,368	0,517	0,701	0,826	0,949	1,086
Series 3	0,256	0,400	0,535	0,658	0,823	1,011	1,180
Average	0,240	0,383	0,528	0,696	0,843	1,039	1,169
Average deviation	51,97 %	61,68 %	64,80 %	65,21 %	66,29 %	65,36 %	66,61 %
Standard deviation	0,016	0,013	0,008	0,029	0,026	0,088	0,063

Series 4-7-Adjusted-c=3,0-3,8				
Load(kg)				
Theoretical 4	420	841	1261	1681
Series 4	421,5	844	1262,1	1688,4
Deviation	-0,36 %	-0,36 %	-0,09 %	-0,44 %
Theoretical 5	476	953	1429	1905
Series 5	478	954,2	1428,8	1906,5
Deviation	-0,42 %	-0,13 %	0,01 %	-0,08 %
Theoretical 6	504	1009	1513	2017
Series 6	505,7	1013,7	1524	2033,8
Deviation	-0,34 %	-0,47 %	-0,73 %	-0,83 %
Theoretical 7	532	1064	1597	2129
Series 7	536,1	1066,2	1601,9	2144,4
Deviation	-0,77 %	-0,21 %	-0,31 %	-0,72 %
Width(mm)				
Theoretical	0,578	1,15	1,73	2,31
Series 4	0,474	0,793	1,173	1,535
Deviation	18,04 %	31,05 %	32,17 %	33,57 %
Series 5	0,532	0,895	1,291	1,721
Deviation	7,97 %	22,21 %	25,36 %	25,51 %
Series 6	0,570	0,938	1,365	1,804
Deviation	1,37 %	18,42 %	21,08 %	21,89 %
Series 7	0,645	1,080	1,511	1,898
Deviation	-11,55 %	6,09 %	12,65 %	17,85 %
Length(mm)				
Theoretical	4	4	4	4
Series 4	3,37	4,271	4,431	4,494
Deviation	15,75 %	-6,78 %	-10,78 %	-12,35 %
Series 5	3,609	4,353	4,527	4,576
Deviation	9,78 %	-8,82 %	-13,18 %	-14,40 %
Series 6	3,578	4,374	4,596	4,661
Deviation	10,55 %	-9,35 %	-14,90 %	-16,53 %
Series 7	3,626	4,479	4,674	4,701
Deviation	9,35 %	-11,98 %	-16,85 %	-17,53 %
Depth(mm)				
Series 4	0,410	0,687	1,016	1,329
Series 5	0,461	0,775	1,118	1,490
Series 6	0,494	0,812	1,182	1,563
Series 7	0,558	0,935	1,309	1,643

D.2. WEDGE 120°

Series 1-3				
Load(kg)				
Theoretical	905	1811	2716	3622
Series 1	933,6	1852,1	2748,6	3650
Series 2	913	1814,3	2721,3	3628,6
Series 3	912,2	1823,3	2722,8	3629,7
Average	919,6	1829,9	2730,9	3636,1
Standard deviation	9,904881	16,12203	12,53076	9,839038
Width(mm)				
Theoretical	1,73	3,46	5,196	6,93
Series 1	0,93344	1,7358	2,6254	3,4438
Series 2	1,077	1,819833	2,6534	3,3804
Series 3	1,098617	1,808714	2,641333	3,423
Average	1,0	1,8	2,6	3,4
Average deviation	40,10 %	48,32 %	49,19 %	50,71 %
Standard deviation	0,073	0,037	0,011	0,026
Length(mm)				
Theoretical	4	4	4	4
Series 1	3,975	4,13	4,232	4,374
Series 2	4,002	4,367	4,425	4,446
Series 3	4,017	4,418	4,476	4,5
Average	3,998	4,305	4,378	4,440
Average deviation	0,05 %	-7,62 %	-9,44 %	-11,00 %
Standard deviation	0,017	0,125	0,105	0,052
Depth(mm)				
Theoretical	0,499409	0,998817	1,499958	2,000521
Series 1	0,269461	0,501083	0,757889	0,994141
Series 2	0,310904	0,525341	0,765972	0,975839
Series 3	0,317144	0,522132	0,762488	0,988136
Average	0,299	0,516	0,762	0,986
Average deviation	40,10 %	48,32 %	49,19 %	50,71 %
Standard deviation	0,021	0,011	0,003	0,008

Series 4-adjusted-c=3,0				
Load(kg)				
Theoretical	1273	2547	3820	5094
Series 4	1274,9	2560,9	3827,2	5100,5
Deviation	-0,15 %	-0,55 %	-0,19 %	-0,13 %
Width(mm)				
Theoretical	1,73	3,46	5,196	6,93
Series 4	1,25	2,39	3,41	4,39
Deviation	27,50 %	30,92 %	34,38 %	36,70 %
Lengde				
Theoretical	4	4	4	4
Series 4	4,246	4,500	4,581	4,821
Deviation	-6,15 %	-12,50 %	-14,53 %	-20,53 %
Dybde				
Theoretical	0,499409	0,998817	1,499958	2,000521
Series 4	0,362	0,690	0,984	1,266
Deviation	27,50 %	30,92 %	34,38 %	36,70 %

D.3. DOUBLE WEDGE 60 °

Series 1-3							
Load(kg)							
Theoretical	406	814	1220	1628	2034	2440	2848
Series 1	418,8	826	1236,6	1640,5	2041,3	2457,5	2885,4
Series 2	408	815,9	1222	1633	2036,5	2442,9	2853,1
Series 3	408,3	821,9	1226,1	1637,9	2036,8	2454,2	2855
Average	411,7	821,2667	1228,233	1637,133	2038,2	2451,533333	2864,5
Standard deviation	5,7742965	5,513922	7,399268	5,524793	3,038092	8,505096511	16,94312

Width(mm)							
Theoretical	0,578	1,15	1,73	2,31	2,89	3,46	4,04
Series 1_profile_1	0,2728	0,44274	0,61654	0,79152	0,96228	1,1334	1,2968
Series 1_profile_2	0,2307	0,37674	0,55392	0,72902	0,90952	1,0714	1,23
Series 2_profile_1	0,33882	0,51196	0,59478	0,84094	1,046	1,2112	1,3786
Series 2_profile_2	0,33446	0,43988	0,64164	0,81664	0,98252	1,1558	1,3048
Series 3_profile_1	0,30468	0,44652	0,66032	0,80944	1,0091	1,2254	1,4118
Series 3_profile_2	0,253	0,41585	0,56454	0,750283	0,93886	1,136333333	1,3338
Average profile_1	0,31	0,47	0,62	0,81	1,01	1,19	1,36
Average profile_2	0,27	0,41	0,59	0,77	0,94	1,12	1,29
Deviation between 1-2	10,71 %	12,04 %	5,96 %	5,98 %	6,18 %	5,78 %	5,35 %
Average	0,29	0,44	0,61	0,79	0,97	1,16	1,33
Standard deviation	0,040	0,040	0,038	0,039	0,045	0,052	0,059
Average Deviation theory	49,99 %	61,83 %	65,01 %	65,82 %	66,27 %	66,60 %	67,18 %

Length							
Theoretical	4	4	4	4	4	4	4
Series 1_profile_1	3,605	3,927	4,041	4,076	4,117	4,173	4,207
Series 1_profile_2	3,393	3,86	4,043	4,055	4,07	4,14	4,185
Series 2_profile_1	3,113	3,917	4,111	4,233	4,254	4,275	4,31
Series 2_profile_2	2,725	3,793	4,137	4,19	4,212	4,237	4,266
Series 3_profile_1	2,757	3,834	4,168	4,278	4,273	4,298	4,3
Series 3_profile_2	2,582	3,787	4,106	4,189	4,229	4,237	4,25
Average profile 1	3,158	3,893	4,107	4,196	4,215	4,249	4,272
Average profile 2	2,900	3,813	4,095	4,145	4,170	4,205	4,234
Deviation between 1-2	8,18 %	2,04 %	0,28 %	1,22 %	1,05 %	1,04 %	0,91 %
Average	3,029	3,853	4,101	4,170	4,193	4,227	4,253
Standard deviation	0,374	0,055	0,046	0,080	0,074	0,055	0,045
Average Deviation theory	24,27 %	3,68 %	-2,53 %	-4,25 %	-4,81 %	-5,67 %	-6,32 %

Depth(mm)							
Theoretical	0,5	1	1,5	2	2,5	3	3,5
Series 1_profile_1	0,2362511	0,383423	0,533938	0,685474	0,833357	0,981550417	1,123059
Serie 1_profile_2	0,1997915	0,326265	0,479707	0,631348	0,787665	0,927856994	1,065208
Serie 2_profile_1	0,2934259	0,443369	0,515093	0,728273	0,90586	1,048927003	1,193899
Serie 2_profile_2	0,28965	0,380946	0,555675	0,707229	0,850885	1,000949331	1,129987
Serie 3_profile_1	0,264	0,387	0,572	0,701	0,874	1,061	1,223
Serie 3_profile_2	0,219	0,360	0,489	0,650	0,813	0,984	1,155
Average profile 1	0,265	0,404	0,540	0,705	0,871	1,031	1,180
Average profile 2	0,236	0,356	0,508	0,663	0,817	0,971	1,117
Deviation between 1-2	10,71 %	12,04 %	5,96 %	5,98 %	6,18 %	5,78 %	5,35 %
Average	0,250	0,380	0,524	0,684	0,844	1,001	1,148
Standard deviation	0,035	0,035	0,033	0,034	0,039	0,045	0,051
Average Deviation theory	49,93 %	61,99 %	65,05 %	65,81 %	66,24 %	66,64 %	67,19 %

Serie 4-5-Adjusted-c=3,0-3,4				
Last				
Theoretical 4	841	1681	2522	3362
Series 4	851,1	1688,4	2528,7	3376,5
Deviation	-1,20 %	-0,44 %	-0,27 %	-0,43 %
Standard deviation	7,14177849	5,232590181	4,737615434	10,25304833
Theoretical 5	953	1905	2858	3810
Series 5	954,9	1943,2	2861	3815,2
Deviation	-0,20 %	-2,01 %	-0,10 %	-0,14 %
Standard deviation	1,343502884	27,01147904	2,121320344	3,676955262

Width(mm)				
Theoretical 4	0,578	1,15	1,73	2,31
Series 4_profile_1	0,479167	0,839283	1,22	1,6005
Series 4_profile_2	0,558486	0,8939	1,276833	1,632833
Average	0,518826	0,866592	1,248417	1,616667
Deviation between 1-2	14,20 %	6,11 %	4,45 %	1,98 %
Average Deviation theory	10,24 %	24,64 %	27,84 %	30,01 %
Theoretical 5	0,578	1,15	1,73	2,31
Series 5_profile_1	0,497383	0,937833	1,391167	1,7798
Series 5_profile_2	0,523367	0,941717	1,393857	1,815667
Average	0,510375	0,939775	1,392512	1,797733
Deviation between 1-2	4,96 %	0,41 %	0,19 %	1,98 %
Average Deviation theory	11,70 %	18,28 %	19,51 %	22,18 %

Length(mm)				
Theoretical 4	4	4	4	4
Series 4_profile_1	3,877	4,222	4,27	4,257
Series 4_profile_2	3,837	4,27	4,301	4,326
Average	3,857	4,246	4,2855	4,2915
Deviation between 1-2	-1,04 %	1,12 %	0,72 %	1,60 %
Average Deviation theory	3,57 %	-6,15 %	-7,14 %	-7,29 %
Theoretical 5	4	4	4	4
Series 5_profile_1	4,047	4,23	4,257	4,288
Series 5_profile_2	3,941	4,296	4,318	4,352
Average	3,994	4,263	4,2875	4,32
Deviation between 1-2	-2,69 %	1,54 %	1,41 %	1,47 %
Average Deviation theory	0,15 %	-6,58 %	-7,19 %	-8,00 %

Depth(mm)				
Theoretical 4	0,5	1	1,5	2
Series 4_profile_1	0,414969	0,726839	1,056548	1,38607
Series 4_profile_2	0,483661	0,774138	1,105767	1,414071
Average	0,449315	0,750488	1,081157	1,40007
Deviation between 1-2	14,20 %	6,11 %	4,45 %	1,98 %
Average Deviation theory	10,14 %	24,95 %	27,92 %	30,00 %
Theoretical 5	0,5	1	1,5	2
Series 5_profile_1	0,430745	0,812185	1,204782	1,541348
Series 5_profile_2	0,453248	0,815548	1,207112	1,572409
Average	0,441996	0,813867	1,205947	1,556878
Deviation between 1-2	4,96 %	0,41 %	0,19 %	1,98 %
Average Deviation theory	11,60 %	18,61 %	19,60 %	22,16 %

D.4. PYRAMID

Series 1-3				
Load(kg)				
Theoretical	206	825	1856	3300
Series 1	215	847	1880,2	3348,4
Series 2	209	828,7	1866,8	3304,6
Series 3	211,3	826,4	1858,1	3301,2
Average	211,767	834,033	1868,367	3318,067
Standard deviation	2,472	9,217	9,090	21,494
Dmean(mm)				
Theoretical	1,189	2,378	3,568	4,757
Series 1	1,132	2,358	3,581	4,874
Series 2	1,200	2,440	3,662	4,894
Series 3	1,202	2,447	3,673	4,935
Average	1,178	2,415	3,638	4,901
Average Deviation	0,96%	-1,54%	-1,98%	-3,03%
Standard deviation	0,032	0,040	0,041	0,025

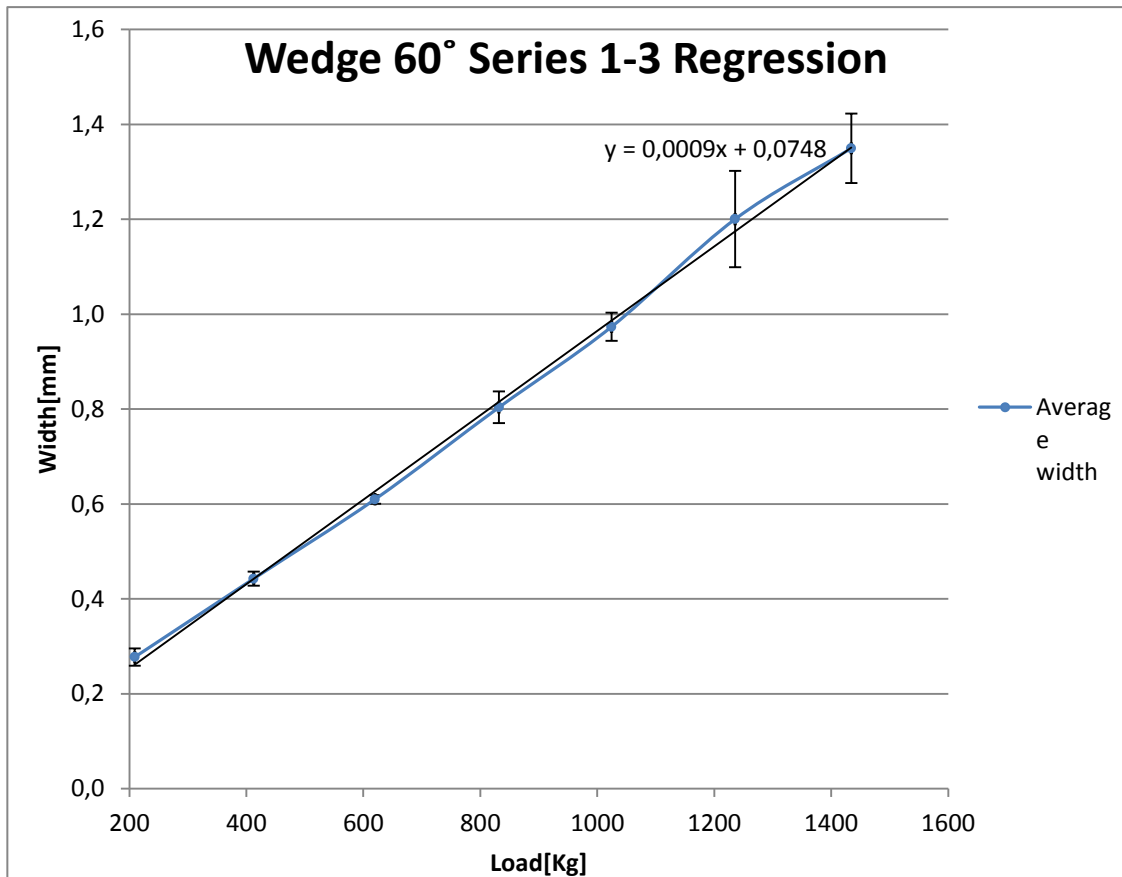
Surface area(mm ²)				
Theoretical surface area	1,000	4,000	9,000	16,000
Series 1	0,906	3,932	9,065	16,798
Series 2	1,018	4,210	9,482	16,936
Series 3	1,021	4,234	9,537	17,218
Average	0,986	4,094	9,271	16,738
Average deviation	1,37 %	-2,35 %	-3,01 %	-4,61 %
Depth(mm)				
Theoretical	0,416	0,833	1,249	1,665
Series 1	0,396	0,826	1,254	1,706
Series 2	0,420	0,854	1,282	1,713
Series 3	0,421	0,857	1,286	1,728
Average	0,412	0,846	1,274	1,716
Average deviation	0,96 %	-1,54 %	-1,98 %	-3,03 %

Series 4-5				
Load(kg)				
Theoretical	222	887	1995	3547
Series 4	223,7	889,4	2001,2	3550,7
Series 5	223,7	889	1996,4	3551,4
Average	223,7	889,2	1998,8	3551,05
Standard deviation	-	0,2	2,4	0,35
Dmean(mm)				
Teoretisk	1,189	2,378	3,568	4,757
Serie 4	1,272	2,532	3,834	5,106
Serie 5	1,284	2,551	3,827	5,101
Gjennomsnitt	1,278	2,541	3,831	5,104
Gjen prosent avik	-7,45 %	-6,85 %	-7,37 %	-7,29 %
Standard avik	0,006	0,009	0,004	0,002
Surface area(mm ²)				
Series 4	1,143	4,533	10,394	18,435
Series 5	1,166	4,600	10,356	18,399
Average	1,154	4,567	10,375	18,417

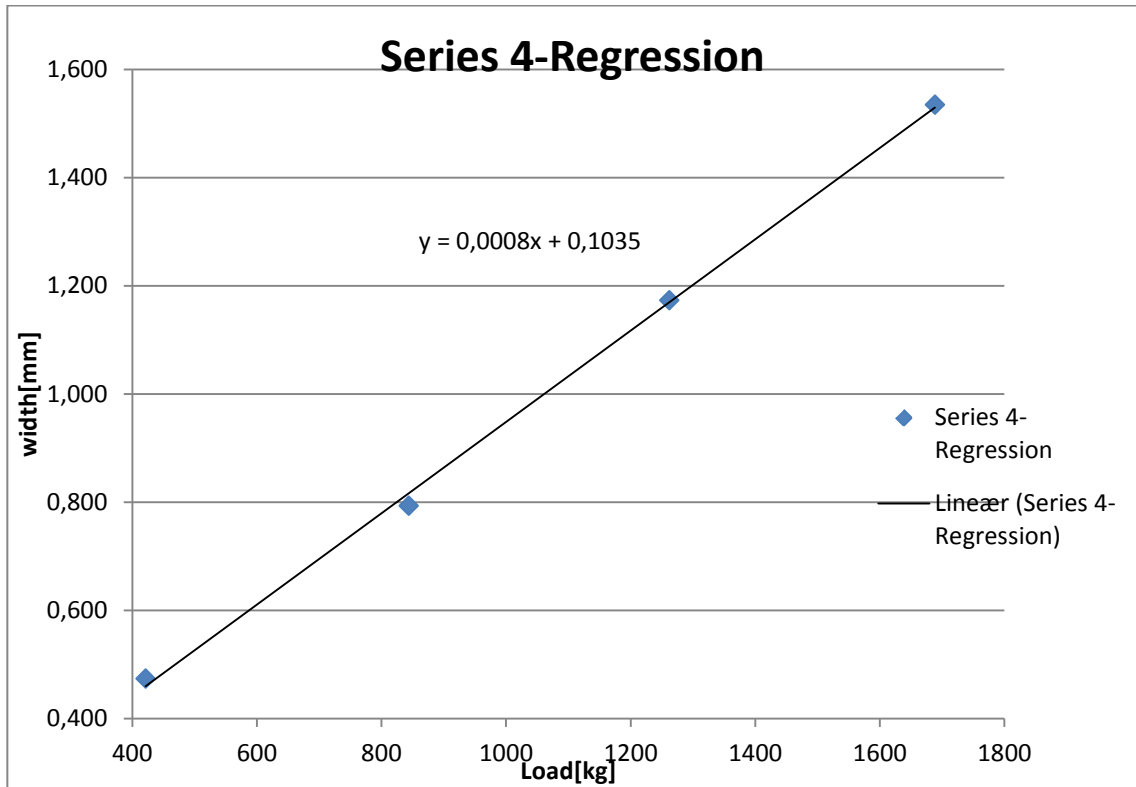
	Depth(mm)			
Series 4	0,445	0,886	1,342	1,788
Series 5	0,450	0,893	1,340	1,786
Average	0,447	0,890	1,341	1,787

APPENDIX E. REGRESSION CURVES

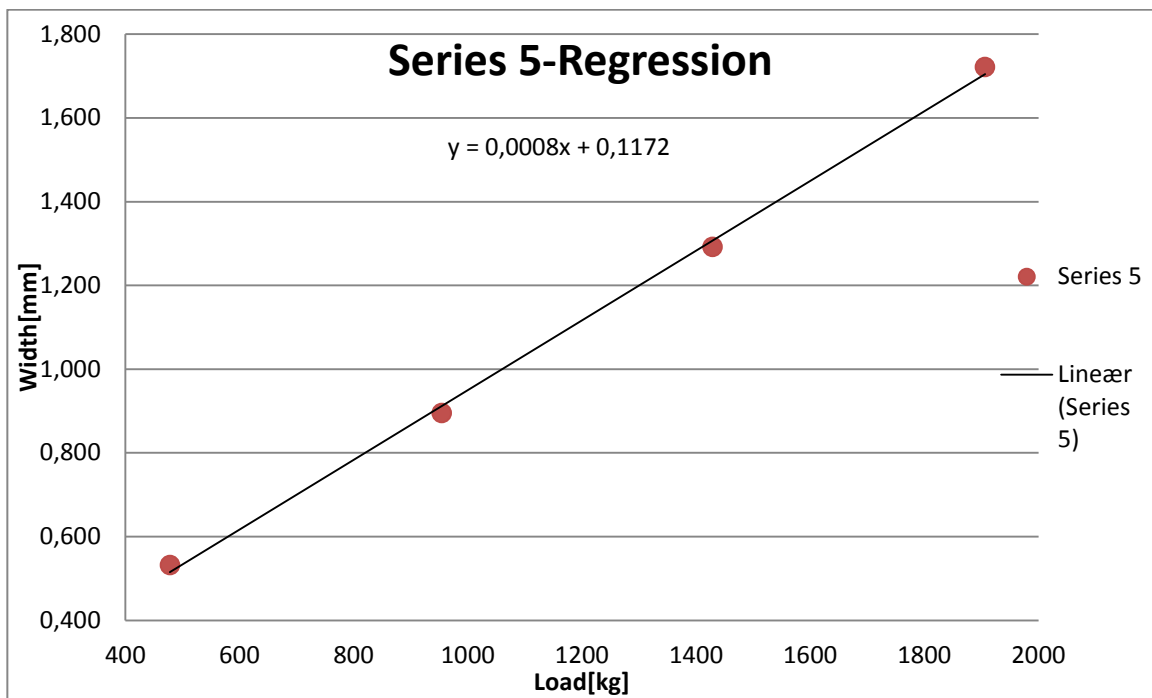
E.1.WEDGE 60°



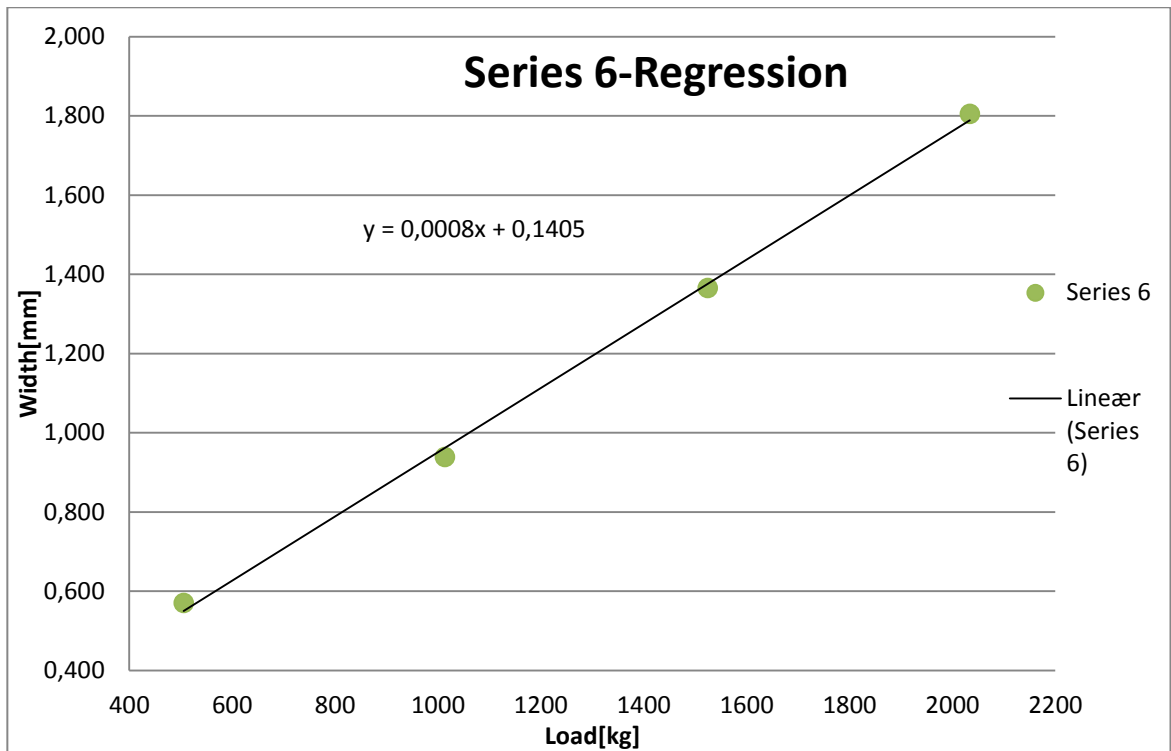
$$p = 1,451 \cdot \text{Yield}$$



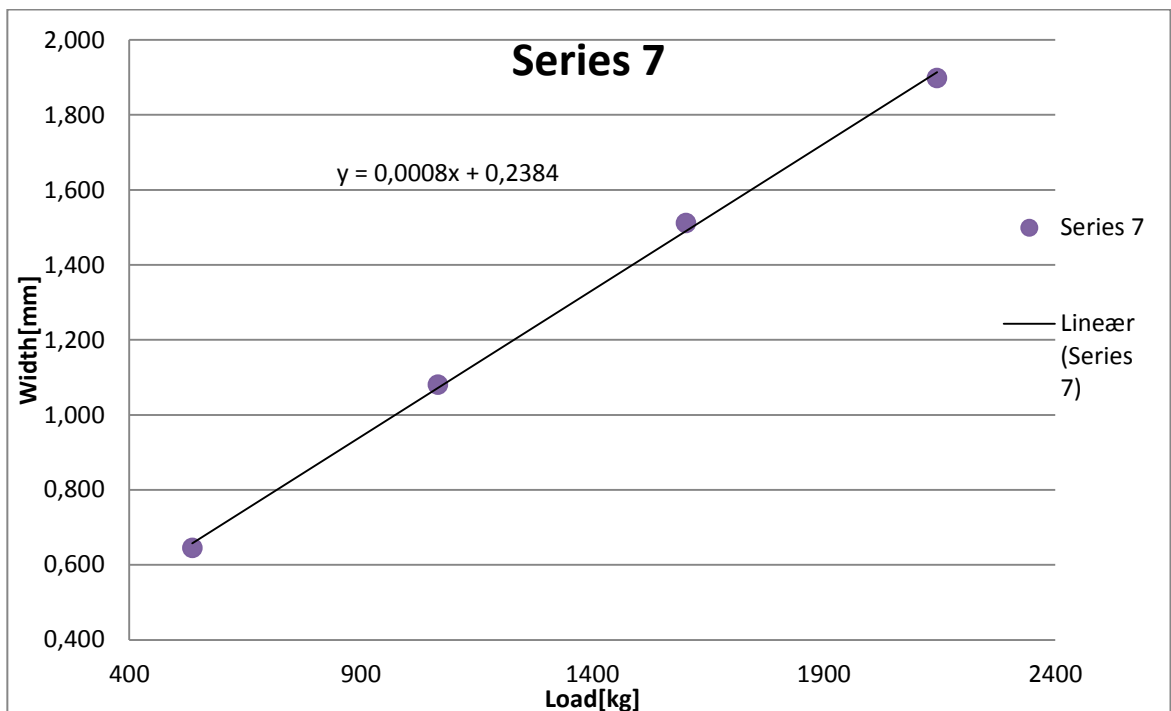
$p = 3,0 \cdot \text{Yield}$



$p = 3,4 \cdot \text{Yield}$

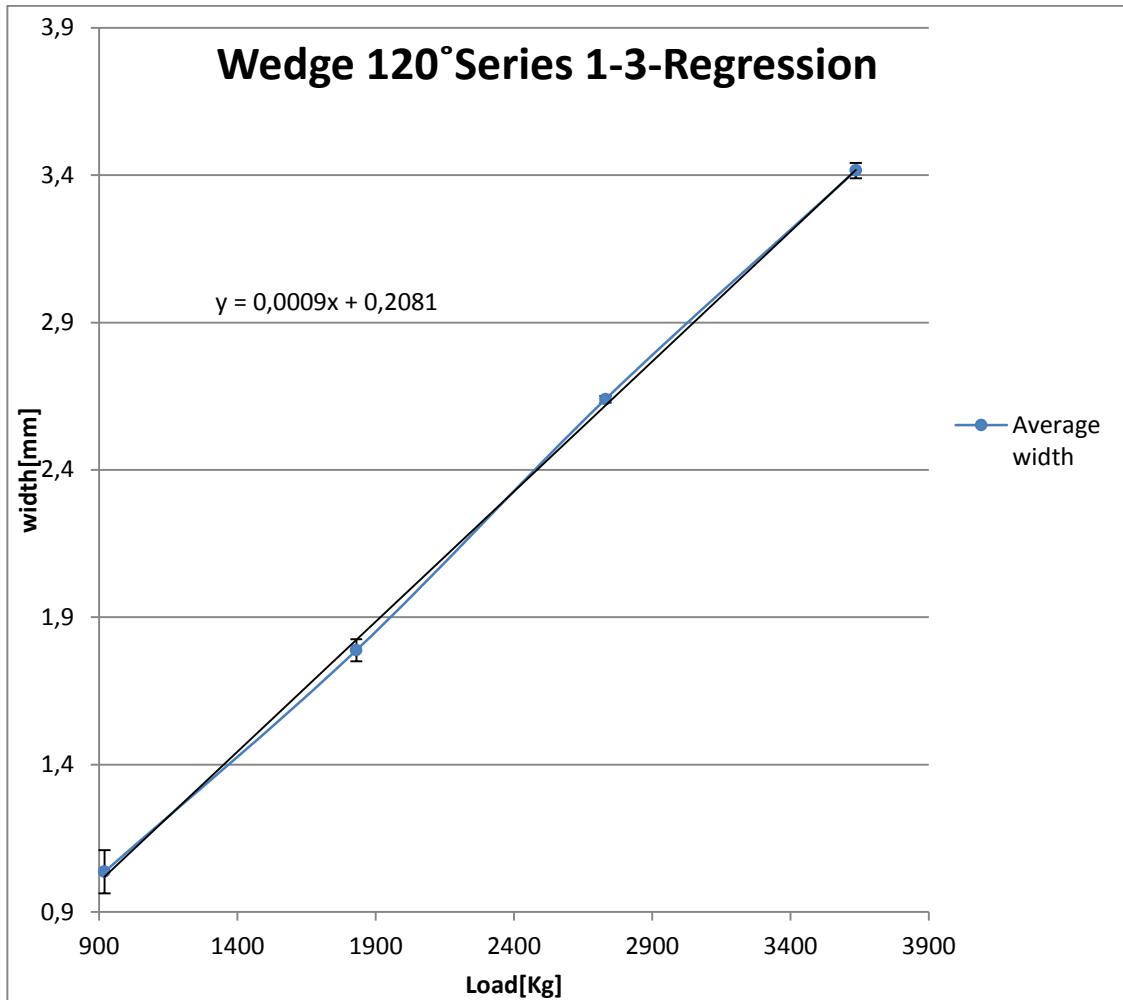


$p = 3,6 \cdot Yield$

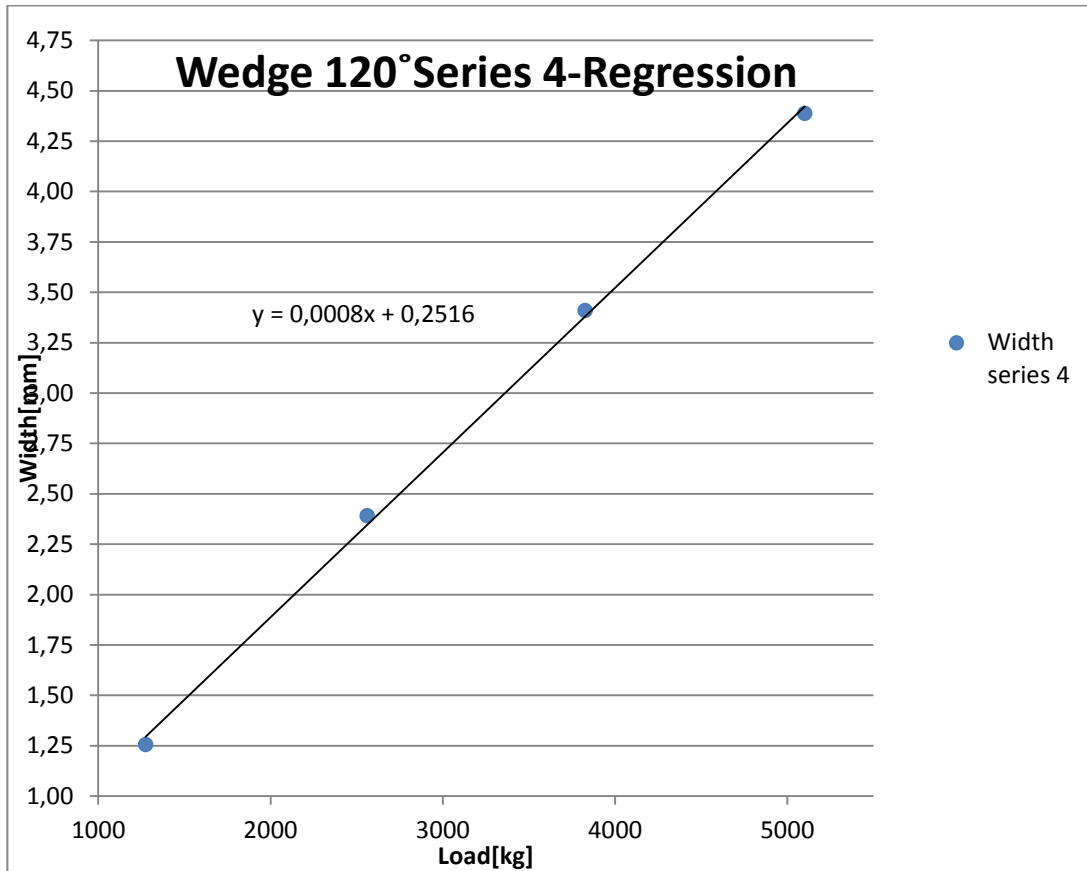


$p = 3,8 \cdot Yield$

E.2.WEDGE 120°



$p = 2,154 \cdot Yield$

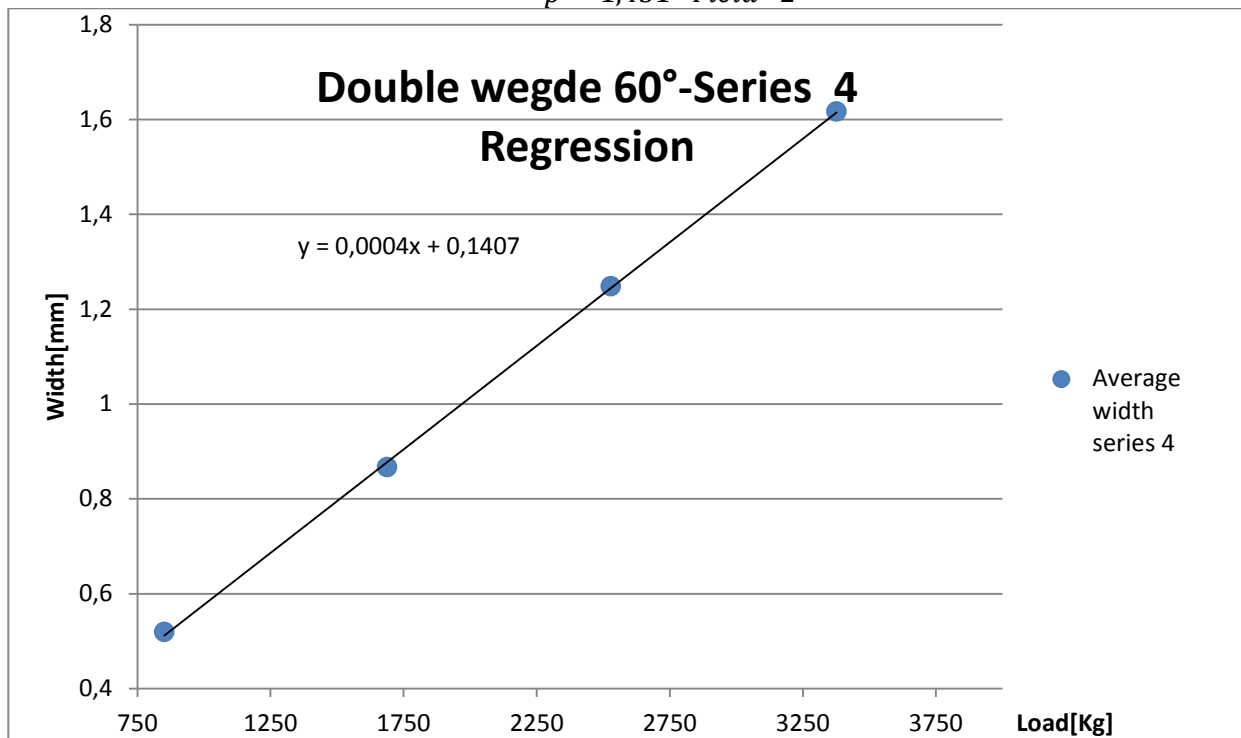


$p = 3,0 \cdot Yield$

E.3.DOUBLE WEDGE 60°



$p = 1,451 \cdot Yield \cdot 2$



$p = 3,0 \cdot Yield \cdot 2$



$$p = 3,4 \cdot Yield \cdot 2$$

APPENDIX F. PLASTIC IMPRESSION ANALYSIS

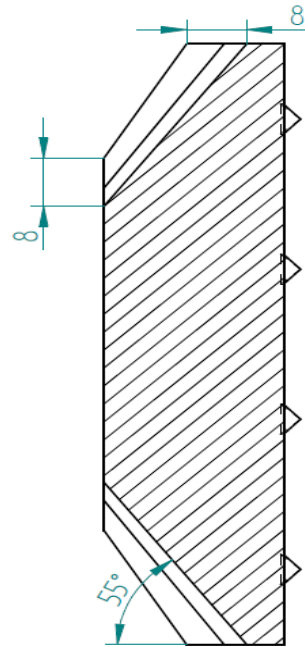
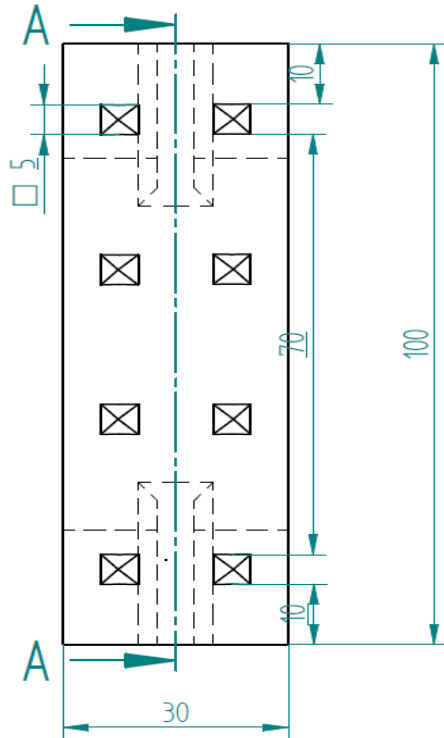
Sigma H				
Series 1	2327,714	2113,391	2034,701	1955,466
Series 2	2013,575	1931,086	1931,279	1914,146
Series 3	2030,654	1914,725	1911,303	1880,917
Series 4-adjusted	1919,629	1924,659	1888,732	1889,454
Serie 5-adjusted	1882,435	1895,986	1891,101	1893,533

Ir Ratio				
Series 1	3,970	3,604	3,470	3,335
Series 2	3,434	3,293	3,294	3,265
Series 3	3,463	3,266	3,260	3,208
Average	3,622409	3,387769	3,341199	3,269139
Total Average	3,405			

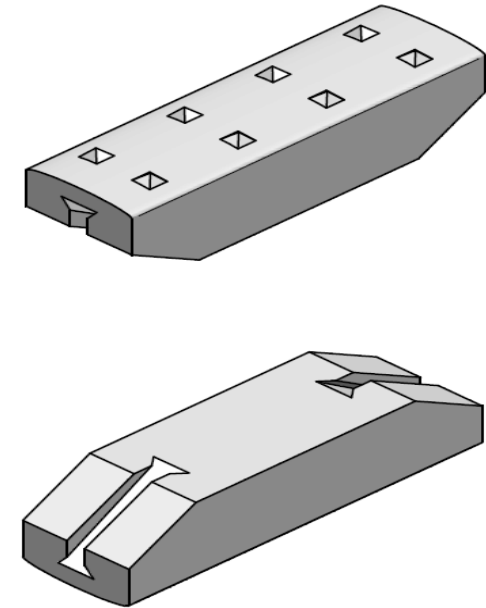
Ir Ratio				
Series 4-adjusted	3,274	3,282	3,221	3,222
Series 5-adjusted	3,210	3,234	3,225	3,229
Average	3,242174	3,258019	3,223216	3,225907
Total Average	3,237			

APPENDIX G. PROPOSED SLIPS ELEMENT DESIGN DRAWINGS & WEDGE ADJUSTMENT

REVISION HISTORY			
REV	DESCRIPTION	DATE	APPROVED
	AISI 4140-steel slips element-pyramid profiles heat treated to 50-51Hrc		



SECTION A-A



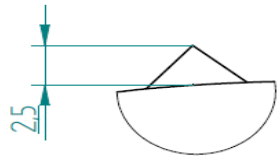
Unspecified tolerances are according to ISO 2768-m

DRAWN	NAME	DATE	UiS, Dept. of Mechanical & Structural Engineering	
CHECKED	Z15366	06/06/13	TITLE	
ENG APPR			Pyramid slips element	
MGR APPR			SIZE	DWG NO
UNLESS OTHERWISE SPECIFIED DIMENSIONS ARE IN MILLIMETERS ANGLES ±XX° 2 PL ±X.XX 3 PL ±X.XXX			A3	REV
			FILE NAME: Pyramid-slips-element_1.dft	
			SCALE:	WEIGHT:
			SHEET 1 OF 1	

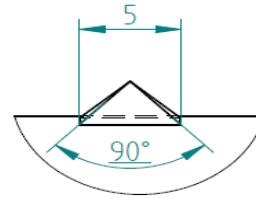
SOLID EDGE ACADEMIC COPY

Title	Master Thesis Spring 2013 Johannes Ohnstad	Page 114
-------	---	----------

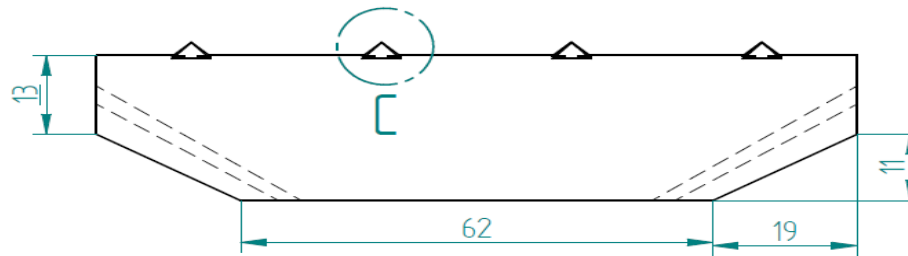
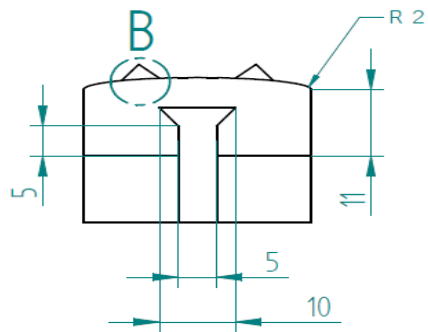
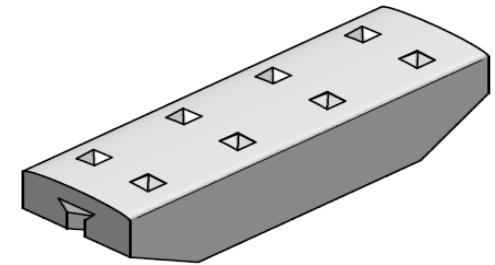
REVISION HISTORY			
REV	DESCRIPTION	DATE	APPROVED
	AISI 4140-steel slips element-pyramid profiles heat treated to 50-51HRc		



DETAIL B



DETAIL C



Unspecified tolerances are according to ISO 2768-m

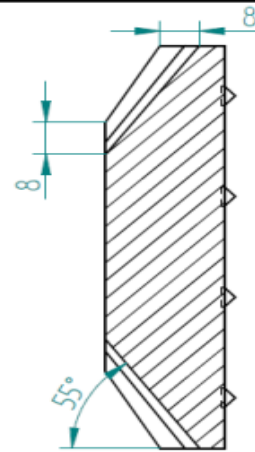
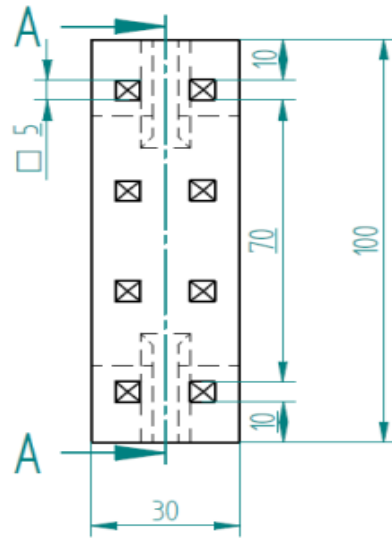
	NAME	DATE	UiS, Dept. of Mechanical & Structural Engineering	
DRAWN	215366	06/06/13	TITLE	
CHECKED			Pyramid slips element	
ENG APPR			SIZE	DWG NO
MGR APPR			A3	REV
UNLESS OTHERWISE SPECIFIED DIMENSIONS ARE IN MILLIMETERS ANGLES ±XX°			FILE NAME: Pyramid-slips-element_2.dft	
2 PL ±XXX 3 PL ±XXXX			SCALE:	WEIGHT: SHEET 1 OF 1

SOLID EDGE ACADEMIC COPY

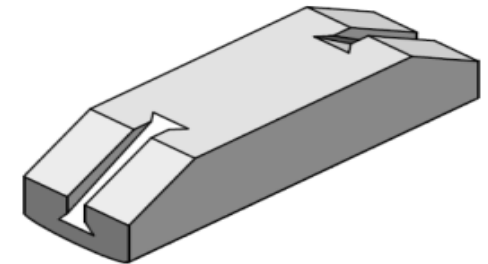
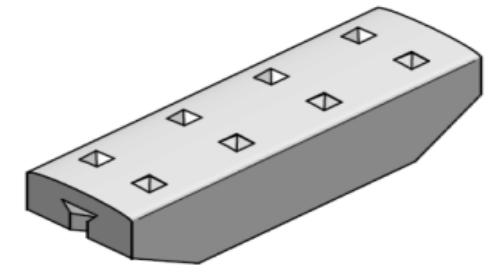
Title	Master Thesis Spring 2013 Johannes Ohnstad	Page 115
-------	---	----------

REVISION HISTORY

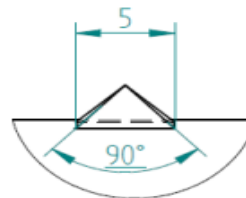
REV	DESCRIPTION	DATE	APPROVED
	AISI 4140-steel slips element-pyramid profiles heat treated to 50-51HRc		



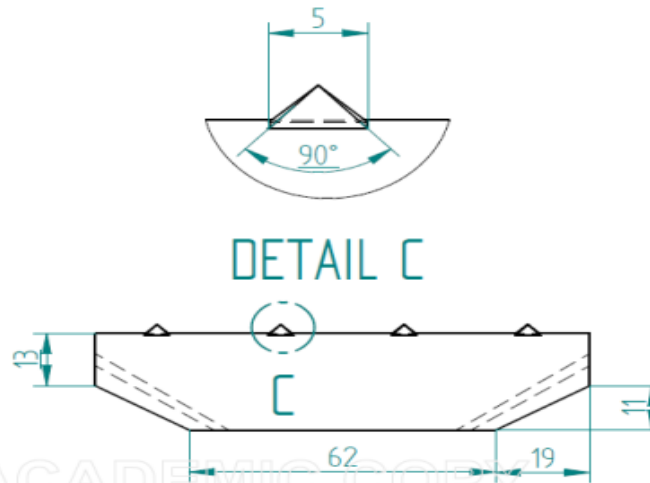
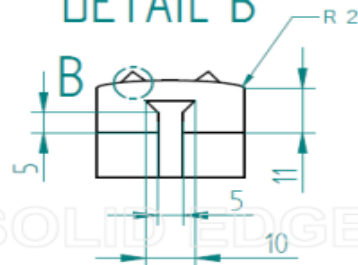
SECTION A-A



DETAIL B



DETAIL C



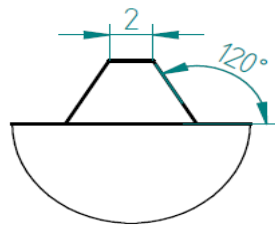
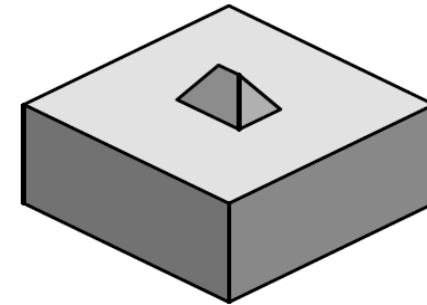
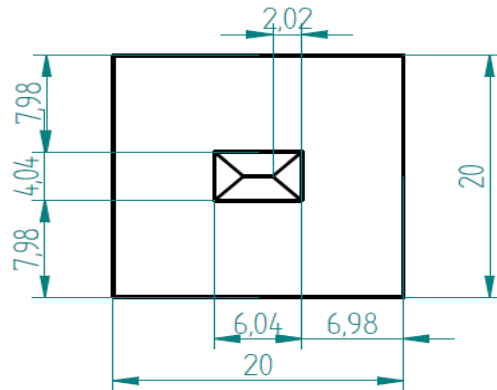
Unspecified tolerances are according to ISO 2768-m

	NAME	DATE	UIS, Dept. of Mechanical & Structural Engineering	
DRAWN	215366	06/06/13	TITLE	
CHECKED			Pyramid slips element	
ENG APPR			SIZE	DWG NO
MGR APPR			A3	REV
UNLESS OTHERWISE SPECIFIED DIMENSIONS ARE IN MILLIMETERS ANGLES =XX°			FILE NAME: Pyramid-slips-element.dft	
2 PL *XXX 3 PL *XXXX			SCALE:	WEIGHT: SHEET 1 OF 1

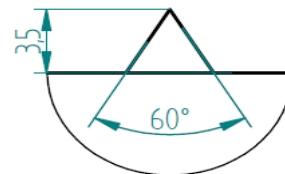
SOLID EDGE ACADEMIC COPY

Title	Master Thesis Spring 2013 Johannes Ohnstad	Page 116
-------	---	----------

REVISION HISTORY			
REV	DESCRIPTION	DATE	APPROVED
	AISI 4140 50-51HRC		

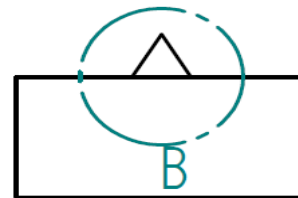


DETAIL A



DETAIL B

Unspecified tolerances are according to ISO 2768-m



	NAME	DATE	UiS, Dept. of Mechanical & Structural Engineering	
DRAWN	215366	06/06/13	TITLE	
CHECKED			Modified Wedge 60	
ENG APPR			SIZE	DWG NO
MGR APPR			A4	REV
UNLESS OTHERWISE SPECIFIED DIMENSIONS ARE IN MILLIMETERS ANGLES ±X.X° 2 PL ±X.XX 3 PL ±X.XXX			FILE NAME: Wedge60-modifisert.dft	
			SCALE:	WEIGHT:
			SHEET 1 OF 1	

SOLID EDGE ACADEMIC COPY

Title	Master Thesis Spring 2013 Johannes Ohnstad	Page 117
-------	---	----------

Indentation pressure

$$p = 3,446 \cdot Y_f = 3,446 \cdot 586,3 \frac{N}{mm^2} = 2020,4 \frac{N}{mm^2}$$

Load:

$$L = 1000kg$$

Surface area:

$$A_s = \frac{L \cdot g}{p} = \frac{1000 \cdot 9,81}{2020,4} = 4,855mm^2$$

Diagonal length:

$$d = \sqrt{4,855 \cdot 2 \cdot \sin 45} = 2,6203mm$$

Depth of penetration:

$$h = \frac{2,603}{2 \cdot \tan 55} = 0,9173mm$$

APPENDIX H. LOAD CELL DATA AND MEASUREMENT PHOTOS

Due to the large amount of load cell data and measurement photos produced, load cell data and measurement photos has been stored on the attached CD for practical reasons.

APPENDIX I. PRE-STUDY REPORT

Title	Master Thesis Spring 2013 Johannes Ohnstad	Page 118
-------	---	----------